

**UNIVERSITA' DEGLI STUDI
DI PADOVA**

Dipartimento di Fisica e Astronomia

Dipartimento di Ingegneria Industriale

**ISTITUTO NAZIONALE
DI FISICA NUCLEARE (INFN)**

Laboratori Nazionali di Legnaro

Under the Auspice of the TESLA TECHNOLOGY COLLABORATION

MASTER THESIS

in

“Surface Treatments for Industrial Applications”

**Purification technique of 6 GHz Tesla type superconducting
Nb cavities: A new approach for improving RF performances**

Supervisor: Prof. V. PALMIERI

Co-Supervisor: Dr. A. A. ROSSI

Student: Dr.rer.nat. Ram-Krishna THAKUR

N. Matr.: 1064844

Academic Year 2012-2013

Abstract:

The lowest possible surface resistivity and higher accelerating field are the paramount considerations, hence are obligatory for accelerating cavities. Since, superconducting materials are used to make radio-frequency cavities for future accelerators. In the case of rf cavities, superconductors are being used in order to minimize the power dissipated and increase the figures of merit of a radio-frequency cavity, such as the quality factor and accelerating gradient. Hence, these could be achieved by improving surface treatment to the cavity, and processing techniques must be analyzed in order to optimize these figures of merit.

The research work reported in this dissertation mainly carried out on tesla type seamless 6GHz Nb and Cu cavities. We have developed two innovative techniques: firstly, for mechanical polishing of cavities, and secondly for purification of these cavities at atmospheric pressure under cover of ⁴Helium gas (for protection) and at ultra-high vacuum (UHV) system. These cavities are fabricated by spinning technology to create seamless cavities.

The main advantages of 6 GHz bulk-Nb cavities are saving cost, materials and time to collect statistics of surface treatments and RF test in a very short time scale. Cavities are RF tested before and after high temperature treatment under atmospheric pressure (under cover of inert gas atmosphere to protect inner and outer surface of cavity) inside transparent quartz tube, and under UHV conditions. Induction heating method is used to anneal the cavity at temperatures higher than 2000°C and close to the melting point of Nb for less than a minute while few seconds at maximum temperature. Before RF test and UHV annealing, the surface treatment processes like tumbling, chemical, electro-chemical (such as BCP and EP), ultrasonic cleaning and high pressure rinsing (HPR) have been employed. High temperature treatment for few minutes at atmospheric pressure allow to reduce hydrogen, oxygen and other elemental impurities, which effects on cavity Q-factor degradation, hence recovers rf performances of these cavities. This research work will address these problems and illustrate the importance of surface treatments.

Key Words: Bulk Nb, SRF cavity, surface treatment, Atmospheric Pressure Annealing, Induction heating, RF test

Content

	Pages
Abstract	i
1. Foundation	1-3
1.1 Insight of Cavity research	1
1.2 Outline of the Dissertation	3
2. Theoretical Concept	4-28
2.1 Historical foundations of SCRF cavity	4
2.2 Essential features of superconductivity	5
2.2.1 Superconductivity: An overview	5
2.2.2 Meissner-Ochsenfeld effect	6
2.2.3 Coherence length in SC	7
2.2.4 London penetration depth	7
2.2.5 Microwave skin effect in normal metals	9
2.3 Salient characteristics of a SCRF cavity technology for accelerator	10
2.3.1 Acceleration of cavity	10
2.3.2 Quality (Q_0) factor	10
2.3.3 Accelerating Gradient	11
2.3.4 Surface resistance	11
2.3.4.1 BCS resistance	
2.3.4.2 Residual resistance	
2.3.5 Loss due to Hydrogen (Q- disease)	13
2.3.6 Geometrical factor	13
2.3.7 Shunt Impedance	14
2.3.8 RF critical magnetic field	15
2.3.9 Peak electric field	16
2.3.10 Cryogenics	16
2.4 SRF edge factors: Cavity loss mechanisms	18
2.4.1 Thermal breakdown (Quench)	18
2.4.2 Field emission	19
2.4.3 Multipacting	19
2.4.4 Diagnostic methods for SC cavities: Temperature mapping	20
2.5 Why 6GHz cavities?	21
2.5.1 Cavity fabrication techniques	22
2.5.2 Why Niobium?	24
2.5.3 RRR value	25
2.5.4 Properties of Nb	26
2.5.5 Promising new materials to bulk Nb for SRF application	27
3. State of the art of the surface treatments of cavity: A Review	29-44
3.1 Mechanical Polishing Techniques	30

3.1.1	Centrifugal Barrel Polishing (CBP) vs Vibrator: A new approach for Tumbling Process, Optical Inspection	30	
3.1.2	Results: Mechanical polishing	36	
3.2	Chemical treatment	36	
3.2.1	Light BCP	37	
3.2.2	Long BCP	38	
3.2.3	Electro-Polishing (EP), Optical Inspection	39	
3.3	Cleaning methods: Ultrasonic process and High Pressure Rinsing (HPR)	42	
4.	Thermal Treatment: Induction heating system		45-62
4.1	Induction heating	46	
4.2	Atmospheric pressure annealing	52	
4.2.1	Basic idea	52	
4.2.2	Experimental setup	53	
4.2.3	Efficiency	55	
4.3	Annealing under UHV system	56	
4.3.1	Basic idea	56	
4.3.2	Experimental UHV setup: Induction heating	56	
4.3.3	Efficiency	60	
4.4	Previous techniques of purification methods: External furnaces	61	
5	Experimental: RF cavity test		63-85
5.1	Experimental Setup/Techniques: A Review	63	
5.2	Preparation of cavity	65	
5.3	Clean room procedure	65	
5.4	Cryo cool down process	67	
5.5	RF cavity measurement system	70	
6	RF cavity results		86-116
6.1	Purification	88	
6.1.1	Atmospheric pressure treatment	88	
6.1.1.1	Thermal treatment and RF test results	88	
6.1.2	UHV treatment	100	
6.1.2.1	Thermal treatment and RF test results	100	
6.1.3	Comparison: ATM vs UHV treatment	113	
6.2	Conclusion	115	
7	Summary and Future Outlook		117-119
	References		120-122
	Acronyms		123-124
	Acknowledgement		125

Chapter 1

Foundation

Overall success of science, engineering and technology help to understand how unsuccessful we are in context of appropriate understanding of the natural behaviour of the universe. Hence, it inspires for further course of action without loss of enthusiasm. In principle, it is well agreed that international scientific community understood hardly 10% of natural behaviour of the matter and energy composing the universe so far, and rest of 90% is either less known or under the process. Though scientist are putting continuous and untiring effort and enthusiasm to understand materials behaviour even at nano-scale in more rigorous way. Researchers are developing ideas, machines and testing them with trial and error methods leading to continuous improvement to understand and explore these 90%, which is somehow, less analysed mysterious fact so called ace-known land of dark energy and dark matter. In other words, we are warming up the engine properly before putting the leg on accelerator!

1.1 Insight of Cavity research

The discovery of superconductivity has crossed 102 years. Since then theoretical and experimental advances have been made continually. Nevertheless, there are still much to learn about superconductivity and the uses of SC materials. At INFN/LNL, research and development is being done in order to understand the properties and uses of various superconducting materials to advance the fields of accelerator technology. The superconducting materials are used to fabricate radio-frequency cavities for future accelerators. Superconductors are being used in order to minimize the power dissipated and increase the figures of merit of a radio-frequency cavity, such as accelerating gradient and quality factor. Superconducting processing techniques must be analyzed in order to optimize these figures of merit.

A superconducting property of high-purity niobium makes it the preferred material for many accelerator projects using superconducting technology. Superconductors based on Nb possesses very intriguing physical and mechanical properties not only the highest superconducting transition temperature, T_c of 9.28 K, and the highest superheating field of 0.23 T among all available superconducting pure metals but also excellent ductility, which enables machining to be done relatively easily. Furthermore, the demand for high-purity niobium material is steadily growing. It is therefore important to consider different manufacturers and different fabrication methods of the superconducting cavity material. In addition, the high cavity accelerating gradient (E_{acc}) and quality factor (Q_0) are fundamental parameters as they affect the overall cost of the accelerator in a direct way. The accelerating gradient of the superconducting niobium cavities has been raised remarkably in the past decades with an advance of the cavity fabrication technology.

RF superconducting cavities have been in use for nearly five decades to accelerate the ion beam to ever increasing higher energies in a particle accelerator. Cavities used to-date are made of niobium- either in bulk or Nb coated on copper cavities. These cavities are operated between 1.5 and 1.8 K where the BCS component of the surface resistance is reduced to minimum and the cavity is operated in the residual resistivity regime. Operating temperature can be increased if we switch over to higher T_c superconductor. Researchers are developing machines that run continuous-wave beams, as contrasted with pulsed beams, for future accelerators such as Berkeley Laboratory's Next-Generation Light Source, also in light

sources at ESS Sweden and Fermilab's proposed Project. CW accelerators require a good deal of power. With increased Q, cavities use less power and therefore require less refrigeration, helping save financial resources. By putting the cavity through a particular polishing and baking regime, scientists achieved a lower surface resistance at 1.6 K than previously observed. This lower surface resistance increase the cavities' Q.

The technology of SRF involves the application of superconducting materials for radio frequency devices, where the ultra-low electrical resistivity allows obtaining high Q-factor in RF resonator, which means that the resonator stores energy with very low loss and narrow bandwidth. For example, in case of 1.3 GHz niobium cavity that obtained a Q-factor of 5×10^{10} at temperature 1.8 K [1].

A critical key for the competitiveness as well as technological and economical success of this new technology are reliable, efficient and low-cost cooling systems. This new approach will be useful in particle accelerators application that uses Superconducting Nb for various R&D projects.

The research work reported in this dissertation mainly carried out on seamless 6 GHz tesla type bulk-Nb cavities. We have developed two new techniques: firstly, for mechanical polishing of cavities, and secondly for purification of these cavities at atmospheric pressure under cover of ^4He gas and at UHV condition. Such cavities are fabricated by spinning technology to create seamless cavities. Several cavities are measured before and after high temperature annealing at atmospheric pressure as well as high vacuum conditions. Surface treatment processes like tumbling, electro-chemical processes (such as BCP and EP), and high temperature annealing, ultrasonic cleaning and High Pressure Rinsing (HPR) have been employed. Such processes are cost effective (low cost) in comparison to the real big accelerating cavities, fast and simple (i.e., very easy to operate). In order to prepare the niobium cavities, firstly it is polished with centrifugal tumbling and /or vibrator then with Buffered chemical polishing (BCP) and /or Electro-polishing (EP) and finally rinsed with ultra pure high pressure water (HPR). Thereafter, cavities are placed inside inducting heating (IH) under the influence of the voltage, time, sample position, temperature, and pressure of pure ^4He and Ar gas used for protection. We have investigated whether further increase of the E_{acc} and Q_0 -values could be achieved for cavities made from niobium with significantly higher purity. Thereafter, it was decided to perform purification in UHV chamber in order to increase the overall efficiency by reducing environmental contaminations rapidly (i.e., residual gases which are degassed from the cavity during high temperature treatment). So far, atmospheric purification and UHV purification have been done. The next step is planned for UHV purification by introducing cryogenic residual gas condensation, where the liquid nitrogen cooling will be used to trap residual gases produced by the cavity during the first few seconds.

Most significantly, instead of 1,5 GHz resonant structure we have used 6 GHz cavities in order to simulate the real condition with new superconducting materials. Such processes have been done at low cost due to reduction of energy in thermal treatments and fast cryogenic measurement. A spinning technology is used to create seamless Bulk-Nb cavity [2]. The main advantages of these 6 GHz bulk-Nb cavities over a 1.3 or 1.5 GHz SRF cavity are saving time, cost, and materials. One can fabricate such small 4-6 cavities out of the rest Nb sheet material which was used to prepare just one big (i.e., 1.3 or 1.5 GHz) SRF cavity with the same technology, and collecting all statistics of treatments like mechanical tumbling, chemical, electro-chemical process, heat treatment, and RF test data are simpler and in short time, say in a couple of week. However, for a big cavity which is about one meter long requires several months to collect same experimental statistics. So, what we have developed is a 6 GHz bulk-Nb SRF cavity that after all the above mentioned treatments in a couple of week like such a short time duration we get about 3 order of magnitude improvement in terms

of Q-factor, and hence reduction of surface resistivity. Results of purification technique seem to be one of the most promising for the cavities of high performance that could be used for the investigations in particle accelerators.

1.2 Outline of the Dissertation

This thesis covers all aspects of surface treatments, and focus on the physics and technology of Induction heating effects on tesla type cavities which improve the rf performance of resonators. The measurements of the gain are taken and compared under different conditions for obtaining the lowest surface resistance.

Chapter 1: The dissertation starts with a brief introduction describing the scientific context in which the technologic research was developed and also includes the reasons, motivating this development.

Chapter 2: Basics of superconducting radiofrequency cavities and theory of superconductivity together with the state of art in the production of cavities with emphases on some newly emerged techniques in the fabrication process aiming at reducing the production costs and increasing the throughput of high quality Nb SRF cavities are mentioned. The advantage and disadvantages of this technology with respect to the production of cavities are also presented.

Chapter 3: A review on the state of the art of surface treatments of a 6 GHz cavity is presented. Starting from mechanical polishing, (electro-) chemical processes alongwith cavity cleaning process have been mentioned respectively.

Chapter 4: An innovative technique to purify tesla type cavity at high temperature (by means of Induction heating) under atmospheric condition as well as UHV condition as a final treatment to improve rf performances of these cavity have been mentioned in a regorous was. Starting from theoretical concept, motivation, working principle, applications and efficiency, advantage and disadvantages of this technology are mentioned.

Chapter 5: A review on principle of cavity characterization for the new set up designed for testing these cavities are mentioned. Also the automation procedures that are implemented which makes measurement easier and faster has been explained.

Chapter 6: Illustrates the obtained results and the experience in the surface treatments to the 6GHz resonators are discussed.

Chapter 7: Presents a summary and a very brief perspective of future activities in this field.

-----*****-----

Chapter 2: Theoretical Concept

Fundamental physics and technology of SRF cavities and its influence over Superconducting RF cavity and material properties are mentioned. An spinning techniques in the fabrication process steps of SRF Nb cavities with emphasis at reducing the production costs, and R&D on exploring the requirements in mechanical, chemical, electro-chemical process are discussed that could increase performance of high quality Nb SRF cavities. Also progress in R&D in last five decades alongwith difficulties and challenges are mentioned in this chapter.

2.1 Historical foundations of Superconducting RF cavity

RF superconducting cavities have been in use for nearly five decades to accelerate the ion beam to ever increasing higher energies in a particle accelerator. The credential goes to High Energy Physics Laboratory (HEPL) at Stanford University, USA for being pioneer laboratory in the exploration of SRF for its application to accelerators. Hence, exploration of RF superconductivity for particle accelerators begun there in 1965 with the acceleration of electrons in a lead plated cavity [3]. In principle, particle accelerators are used for two different type of particle accelerating structures, which depends on the velocity (v) of the particle to be accelerated. Usually, a parameter β that is defined as v/c where C is the velocity of light is used to separate the two types. When $0.5 < \beta < 1$, this is typical for accelerating electrons with kinetic energy of a few MeV and protons with 100 MeV. Figure 2.1 is shows a typical Nb Superconducting RF cavity for this group of particle accelerating structures where a chain of five coupled RF cells are resonating in the transverse magnet (TM010) mode.

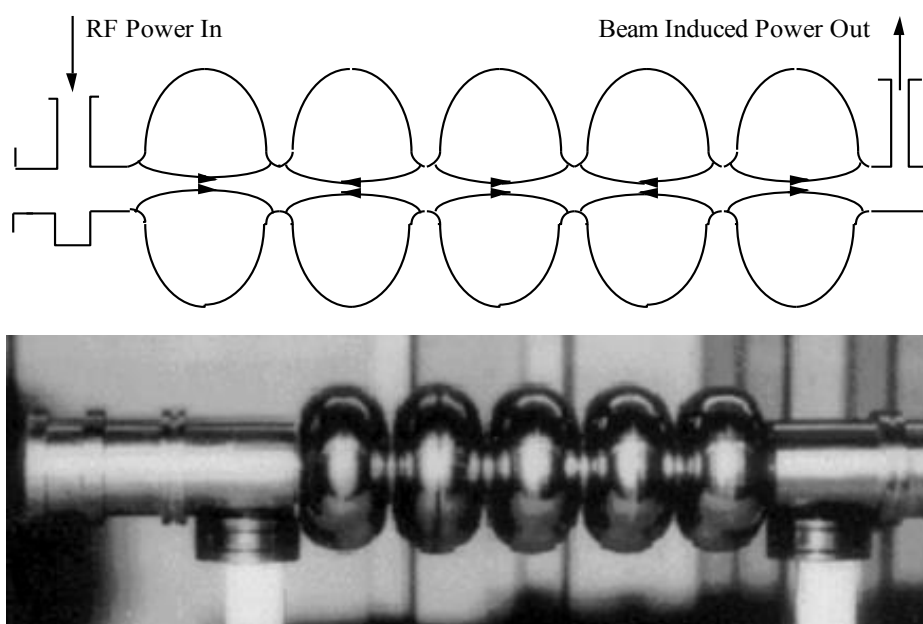


Figure 2.1: The typical Nb SRF accelerating structure consists of a chain of cavities and its side view. The cavity is fabricated from bulk Nb, and cooled in a bath of liquid He at temperature 4.2K (Courtesy of ACCEL)

In this field configuration, the longitudinal electric field is maximized along the axis of the cavity and the RF phase between adjacent cells is 180° as schematically illustrated in the upper part of Figure 2.1. In this way, a particle with velocity close to the speed of light will experience the maximum acceleration in each cell of the cavity.

In case, when $\beta < 0.5$, it is the typical for accelerating ions from helium to uranium with kinetic energies ranging from a few to 20 MeV per nucleon. For this group, a variety of different accelerating structures may exist, for example, such as; coils, helix, spoke, and crab shapes cavities. It is known from the earlier experience that the major consumption of Nb is from the first previous group of accelerators where $0.5 < \beta < 1$.

It is essential to operate Nb-cavities at below 2 K to obtain high accelerating gradient combined with high 'Q' factor. Liquid helium below 2 K is a superfluid with extremely high thermal conductivity and is thus an excellent coolant. Nb-cavities are accordingly operated at between 1.5 and 1.8 K. Generally, the performance of a SRF cavity is characterized by an excitation curve where the quality factor Q_0 is plotted as a function of the accelerating gradient E_{acc} . Therefore, we need to define first several fundamental physical parameters widely used in SRF technology for accelerators.

2.2 Essential features of superconductivity

2.2.1 Superconductivity: An overview

H. Kamerlingh Onnes became the first who succeeded in liquefying helium on July 10th, 1908 [4]. The discovery extended available temperature range below liquid hydrogen temperatures. One of experiments, which were carried out with newly acquired liquid helium, was designed to test a then-modern theory of resistance of metals at low temperatures. Contrary to expectations they found out that resistance of pure metals such as gold and platinum decreases as a function of temperature down to 1.5K. A greater surprise lay ahead in experiments with mercury. They failed to measure the resistance of mercury at temperatures below 4.2 K! These measurements led Kamerlingh Onnes in Leiden discover superconductivity in 1913. It was found for mercury below a certain temperature ($T = 4.2$ K) no ohmic resistance could be measured [5]. His striking discovery that on cooling mercury to near the absolute zero of temperature, the electrical resistance became vanishingly small, but this disappearance "did not take place gradually but abruptly." It is shown in Figure 2.2 below. He said, "Thus, mercury at 4.2 K has entered a new state which owing to its particular electrical properties can be called the state of superconductivity." He found this state could be destroyed by applying a sufficiently strong magnetic field, now called the critical field H_c . The temperature, at which resistance becomes immeasurable, is called critical temperature of superconductor, T_c .

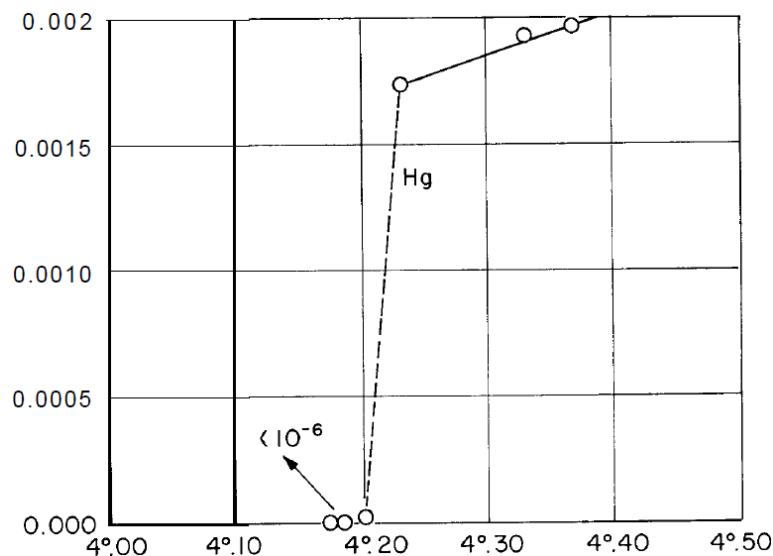


Figure 2.2: The original plot by H. Kamerlingh Onnes shows absence of resistance below 4.2 K.

In 1933 W. Meissner and R. Ochsenfeld performed an experiment, that triggered development of theories of superconductivity [6]. In their experimental investigation, it was focussed on a magnetic field distribution near two cylinders that were cooled down below T_c . After Meissner and Ochsenfeld's discovery it was realized that superconducting state is a thermodynamic state, i.e. the state of a superconductor is determined by external parameters and does not depend on history. Shortly after C.J.Gorter and H.Casimir put forward a theory that accounted for some superconducting phenomena, which presented a clear picture of superconductivity.

It was suggested that upon superconducting transition a number of electrons turn "super" and these, now "super" electrons, can carry a big current without losses. As the temperature goes closer to absolute zero the number of "super" electrons increases and the number of normal electrons decreases. In order to explain experimental results, C.J.Gorter and H.Casimir argued that the free energy of the electrons gas in the superconductor takes a rather peculiar form [7].

By now, a large number of elements and compounds (mainly alloys and ceramics) have been found showing SC behavior. For superconducting cavities, niobium shows the most interesting properties. Some of the paramount considerations of superconductivity are described in this section.

2.2.2 Meissner-Ochsenfeld effect

In the framework of the Gorter-Casimir theory, H. London and F. London introduced two equations for "superelectrons" in order to explain the Meissner effect. Since "superelectrons" move without friction through the material. There are two different types of superconductors were discovered. They have certain common features, but differ also in some important ways. When the material is cooled below the critical temperature T_c , the ohmic resistance vanishes below the measurement limit. In addition, any external magnetic field up to a critical field $B < B_{crit}$ is expelled. This magnetic field expulsion is called the Meissner-Ochsenfeld effect. Such behavior significantly differs from the properties of an ideal conductor where the field would be trapped inside the material. Even if the field is switched off, an ideal conductor would keep the magnetic field and become a permanent magnet, as the currents induced by the field will continue to flow. From a thermodynamical point of view, one can define the thermodynamical critical field B_c

$$G_n - G_s = \frac{1}{2\mu_0} V B_c^2 \quad (2.1)$$

There is difference of the free enthalpy G in the normal and SC state respectively. Experimentally, B_c can be determined from the area below the magnetization curve of the material. If the field exceeds a critical value B_c in a superconductors of type I the superconductivity breaks down and the normal conducting state is restored. This critical field depends on the critical temperature:

$$B_c(T) = B_0(T) \left[1 - \left(\frac{T}{T_c} \right)^2 \right] \quad (2.2)$$

Magnetic field will start to penetrate the material above the lower critical field B_{c1} for the II-type of SC. Magnetic fluxons enter the material and their number increases with increasing field. If the field is raised further to a value of B_{c2} , the material becomes normal conducting. The temperature dependence of the critical magnetic fields B_{c1} and B_{c2} is the same as for the B_c of a I-type SC.

2.2.3 Coherence length in SC

A very successful microscopic theory was developed by Bardeen, Cooper and Schrieffer, well known as BCS theory for classical superconductors like lead or tin, [8]. They assumed that electrons below T_c begin to condense as pair of electrons, so-called Cooper pairs. The two electrons in a pair have opposite momentum and spin. They experience an attractive force mediated via quantized lattice vibrations called phonons. Such bound state of the two electrons is energetically favorable. As the overall spin of these two-paired electrons is zero, many of these pairs can co-exist coherently, just like other bosons. The coherence length describes the distance over which the electrons are correlated. It is given by:

$$\xi = \frac{\hbar v_F}{\Delta} \quad (2.3)$$

where v_F denotes the velocity of the electrons near the Fermi level and 2Δ is the energy necessary to break up a Cooper pair. Typical values for the coherence length in niobium is reported $39 \pm 1.5 \text{ nm}$ [9]. Hence the Ginzburg-Landau parameter is very close to unity. For ultra high monocrystal niobium samples ($\text{RRR}=34000$) the Ginzburg-Landau parameter is 0.702, very close to magic number $\frac{1}{\sqrt{2}}$ [10], which separates type I and type II superconductors. If coherence length is interpreted as the size of a Cooper pair, one can observed that it spans over many lattice constants. The energy gap can be calculated using BCS theory as;

$$\Delta = 1.76 k_B T_C \quad (2.4)$$

The exact value of factor (1.76) in the relation of the energy gap and the critical temperature is material dependent and for niobium one finds higher values of $\Delta = 1.9 k_B T_C$. The number of Cooper pairs $n_{\text{cooper}} = n_s/2$ is temperature dependent and only at $T=0 \text{ K}$ all conduction electrons are condensed into Cooper pairs. The superconducting electrons co-exist with their normal conducting counterparts. The number of normal conducting electrons, n_n is given by the Boltzmann factor:

$$n_n(T \rightarrow 0) \approx n_s(0) \exp\left(-\frac{\Delta(T)}{k_B T}\right) \quad (2.5)$$

Where, k_B is Boltzmann Constant, and T is experimental temperature

2.2.4 London penetration depth

Type I superconductors exclude DC magnetic fields up to a lower critical field H_c , after which magnetic flux will penetrate the material and cause an abrupt transition to the normal conducting state. For type II superconductors, the surface energy of the normal-superconducting interface becomes negative when the applied magnetic field reaches the lower critical field H_{c1} . Above H_{c1} it is energetically favorable for flux to enter and the superconductor breaks up into finely divided superconducting and normal conducting regions (mixed state). The magnetic flux in the form of fluxoids will increase penetrating into the material until their normal conducting cores start to overlap, which happens at another higher field called upper critical field H_{c2} [11]. In otherwords, the magnetic field is not completely expelled even in a type I superconductor, but penetrates into the material over a small distance, as otherwise the shielding current density would have to be infinitely large. London penetration depth is given by the characteristic length of the exponential decay of the magnetic field x as,

$$B(x) = B(0) e^{-\frac{x}{\lambda_L}} \quad (2.6)$$

Its value is,

$$\lambda_L = \sqrt{\frac{m}{\mu_0 n_s C^2}} \quad (2.7)$$

where e is the charge of an electron, m its mass and n_s the number of superconducting charge carriers per unit volume. A typical value for the penetration depth in niobium is 32 nm at $T=0K$. The theory did not allow for impurities in the material or for a temperature dependence of the penetration depth. Gorter and Casimir introduced the two-fluid model where a coexistence of a normal- and superconducting fluid of charge carriers is postulated, and given as

$$n_C = n_n + n_s \quad (2.8)$$

They suggested a temperature dependence of the superconducting charge carriers:

$$n_s(T) = n_s(0) \left(1 - \left(\frac{T}{T_C}\right)^4\right) \quad (2.9)$$

Nevertheless, the two-fluid model is still used, the temperature dependence is not correct. The model will give good prediction of the n_s with the correct exponential T-dependence. Combining equations 2.7 and 2.9, the penetration depends on the n ratio.

Ginzburg and Landau (1950) have developed on a thermodynamic basis of an alternate method of treating the coherence of the superconducting wave functions. The Ginzburg-Landau parameter is defined as:

$$\kappa = \frac{\lambda_L}{\xi_0} \quad (2.10)$$

κ distinguishes between the two types of superconductors, namely

$$\kappa < \frac{1}{\sqrt{2}} \text{ Superconductor Type - I} \quad (2.11)$$

$$\kappa > \frac{1}{\sqrt{2}} \text{ Superconductor Type - II} \quad (2.12)$$

Niobium has $\kappa \approx 1$ and is a weak type-II superconductor. The role of impurities was studied by Pippard [12], that was based on the evidence that the penetration depth depends on the mean free path of the electrons ℓ in the material. The dependence of ξ on the mean free path is given by:

$$\frac{1}{\xi} = \frac{1}{\xi_0} + \frac{1}{\ell} \quad (2.13)$$

Pippard introduced an effective penetration depth:

$$\lambda_{\text{eff}} = \lambda_L + \frac{\xi_0}{\xi} \quad (2.14)$$

Here again ξ_0 is the characteristic coherence length of the superconductor. The relation reflects that the superconducting penetration depth increases with a reduction of the mean free path [13]. For pure ("clean") superconductor ($\ell \rightarrow \infty$) one has $\xi = \xi_0$. However, in the limit of "dirty" superconductors where $\ell \ll \xi_0$, the relation becomes

$$\xi = \ell \quad (2.15)$$

This means, R_s is minimum when the mean free path is comparable to the coherence length. Figure 2.3 shows R_{BCS} plotted against the mean free path for Nb at 4.2 K and at a frequency of 1.5 GHz [14]. The second term, R_{res} , of the BCS surface resistance expression is the so called residual resistivity and is temperature independent. The mean free path in the niobium

is strongly influenced by interstitial impurities like oxygen, nitrogen and carbon, as well as residual tantalum impurities.

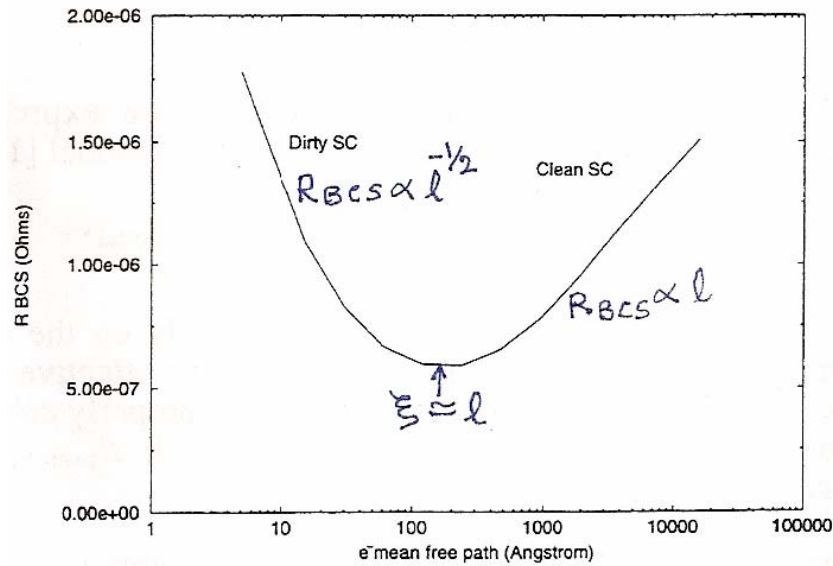


Figure 2.3: BCS surface resistance vs mean free path of electron is plotted. If the mean free path is comparable with the coherence length then the BCS surface resistance is found to be minimum as shown in figure.

2.2.5 Microwave skin effect in normal metals

The shielding mechanism of a static magnetic field in a superconductor is analogous to the shielding of a microwave field in a normal metal. If a microwave of frequency ω is incident on a metal surface one can show that the field is decaying over a characteristic distance, the skin depth δ . In case where the frequency is much lower than plasma frequency ($\omega \ll \omega_{\text{plasma}}$) and the mean free path of the electrons ℓ is smaller than the penetration depth (or skin depth) δ could be as,

$$\delta = \sqrt{\frac{2}{\sigma \mu_0 \omega}} \quad (2.16)$$

Where, σ is the conductivity of the metal. It is the regime of the normal skin effect. And the surface resistance could be calculated as,

$$R_{\text{Surf}} = \frac{1}{\sigma \delta} = \frac{\rho}{\delta} \quad (2.17)$$

According to this equation, a strong reduction of the surface resistance is expected at cryogenic temperature because σ grows for $T \rightarrow 0$. Unfortunately, for pure metals and at low temperatures ℓ may become larger than δ , which leads to the anomalous skin effect. Then the electrons are not only scattered by phonons, but also by impurities in the metal lattice. In the limit ($\ell \rightarrow \infty$), the surface resistance becomes [11]:

$$R_{\text{Surf}} = \left[\sqrt{3} \left(\frac{\mu_0}{4\pi} \right)^2 \right]^{\frac{1}{3}} \omega^{\frac{2}{3}} \left(\frac{\rho}{\sigma} \right)^{\frac{1}{3}} \quad (2.18)$$

2.3 Salient characteristics of a SRF cavity technology for accelerators

The physics of SRF could be extremely complex and lengthy. A few simple approximations derived from the complex theories, though can serve to provide some of the important parameters of SRF cavities for accelerators. By way of background, some of the pertinent parameters of RF cavities are itemized. Below mentioned are some basic fundamental physical parameters employed in Superconducting RF technology.

2.3.1 Acceleration of cavity

Accelerating cavities are used to increase the energy of a charged particle beam [15]. Hence, the cavity is a structure that stores most efficiently the electromagnetic energy when excited at the resonant frequency at one of its resonant modes. At resonance, the energy of the electric and magnetic fields are equal and is exchanged between the two ways at resonant frequency, and configuration of electric and magnetic field is defined and the field values oscillate periodically with time at the same frequency. Due to the low surface resistance, SC cavities can convert much more efficiently the RF input power in stored energy than the normal conducting cavities. Nevertheless, some other factors can limit their sustainable fields or their efficiency to transfer the electromagnetic energy to the beam. Therefore, these factors are very important to be considered.

2.3.2 Quality (Q_0) factor

A resonating circuit stores energy. A cavity's quality factor, Q_0 for short, is a measure of how efficiently energy is stored in the cavity. The energy stored in the cavity helps accelerate particle beams, which travel down the cavity's axis. A resonator's quality factor is defined as the ratio of stored energy (U) in the cavity to the dissipated power (P) through the cavity walls, Q is an efficiency so it is dimensionless, and is given as;

$$Q_0 = \omega \frac{U}{P} \quad (2.19)$$

Where, $\omega = 2\pi f$, and f is freq. of stored RF power, P is the power dissipated in the inner surface of the cavity. And U is the energy stored in the electromagnetic field in cavity, and is given as,

$$U = \frac{1}{2} \mu_0 \int_V H^2 dV \quad (2.20)$$

Moreover, an standard procedure to determine the quality factor is to measure the bandwidth of the resonance curve,

$$Q = \frac{f}{\delta f} \quad (2.21)$$

where f is the resonance frequency and δf the full width at half power points.

Superconducting cavities have quality factors in the range of 10^{10} . The equivalent bandwidth is less than 1 Hz. Therefore, it is more convenient to measure the quality factor by the decrement method,

$$Q = \omega \tau \quad (2.22)$$

Where τ is the decay time constant of the stored energy.

The accelerating voltage V_{acc} is the line integral of the electric field along the axis of the resonator. The stored energy U is proportional to the volume integral of the square of the electric (or magnetic) field in the resonator. These fields are determined by Maxwell's equations and depend on the shape of the resonator and not on the conductivity of the wall material.

2.3.3 Accelerating Gradient (E_{acc})

The energy gain per unit length is an important parameter of accelerating cavities. This is conveniently derived from the accelerating voltage to which a particle with charge e is subjected while traversing the cavity:

$$V_{acc} = \left| \frac{1}{e} \times \text{energy gain during transit} \right| \quad (2.23)$$

For particles travelling with the velocity of light c on the symmetry axis in z -direction ($\rho = 0$) and an accelerating mode with eigenfrequency ω that gives:

$$V_{acc} = \left| \int_0^d E_z(z) e^{\frac{i\omega z}{c}} dz \right| \quad (2.24)$$

The accelerating electric field, E_{acc} could be defined as the max energy gain for a charged particle when travelling through a cavity divided by the electron charge and by the cavity length (gap of accelerating cavity). It is conventionally given as

$$E_{acc} = \frac{V_{acc}}{d} \quad (2.25)$$

Where d is the path length. In otherwords,

$$E_{acc} \propto (PQ_0)^{1/2} \quad (2.26)$$

In general, E_{acc} is proportional to E_0 , which is proportional to H_{pk} . Therefore the higher the magnetic field a superconducting cavity can sustain the more energy can be delivered to charged particles for the same cavity length.

Further, cryogenic loss in the SC cavity wall is an important parameter. In order to sustain the RF fields in the cavity, an alternating current is flowing in the cavity walls. This current dissipates power in the wall as it experiences a surface resistance. Such power dissipated is given by the integral of resistive wall losses over its surface, and is given as,

$$P_d = \frac{R_s}{2} \int |\overline{H_s}|^2 dS \quad (2.27)$$

Here H_s denotes the magnetic field amplitude at the surface.

2.3.4 Microwave Surface Resistance R_s

2.3.4.1 BCS resistance

Condensation of charge carriers into cooper pairs at low temperature are the most intriguing properties of superconductivity. All the charge carriers are condensate at temperature, $T=0K$. Such pairs move frictionlessly. Whilst, at high temperatures, some carriers are unpaired. These fraction of unpaired carriers increase exponentially with temperature untill none of carriers are paired above T_c . Surface resistance R_s of the wall material of a SRF cavity is related to the power dissipation P through equation (2.27).

For direct current or low frequency alternating currents, the superconducting electrons shield the normal conducting electrons from the electromagnetic field so that no power is dissipated. For alternating currents at microwave frequencies, this is not true anymore. The inertia of the Cooper pairs prohibit them to follow the changing electromagnetic fields immediately, hence the shielding is not perfect anymore. The normal conducting electrons start to flow and dissipate power. It gives rise to a resistance, which depends on the number of normal conducting electrons and the frequency of the alternating current. For T_c temperatures $T < T_c / 2$ and energy of the microwave photons of $\hbar\omega \ll \Delta$ the surface resistance can be approximated by:

$$R_{BCS}(T, \omega) = A \frac{\omega^2}{T} \exp\left(-\frac{\Delta}{k_B T}\right) \quad (2.28)$$

The factor A depends on material parameters like coherence length, electron mean free path, and Fermi velocity and penetration depth. For niobium, the factor A is about $9 \times 10^{-5} \Omega \text{K} / (\text{GHz})$.

The result derived for RBCS from the two-fluid model will give,

$$R_{BCS}(T, \omega) = C \cdot \sigma_{nc} \cdot \lambda_{eff}^3 \frac{\omega^2}{T} \exp\left(-\frac{\Delta}{k_B T}\right) \quad (2.29)$$

Where, C is a constant, which does not depend on the material properties. σ_{nc} is the conductivity in the normal conducting state. Therefore, the dependence of RBCS on the mean free path:

$$R_{BCS}(\ell) \propto \left(1 + \frac{\xi_0}{\ell}\right)^{\frac{3}{2}} \cdot \ell \quad (2.30)$$

Here we see it exists a minimum of RBCS on the mean free path ℓ . A detailed calculation of the BCS theory shows that the two-fluid model gives a good approximation for $\ell < 500 \text{nm}$.

The following should be noticed:

- the surface resistance drops exponentially with decreasing temperature.
- the surface resistance increases with the square of the frequency.

2.3.4.2 Residual Resistance

As for the operation of the cavity one has to look at the BCS surface resistance. For Nb the surface resistance say for 1.3 GHz is about 800 n Ω at 4.2 K and drops to 15 n Ω at 2 K. It is essential to operate Nb-cavities at below 2 K to obtain high accelerating gradient combined with high 'Q' factor. Liquid helium below 2 K is a superfluid with extremely high thermal conductivity and is thus an excellent coolant. Nb-cavity are accordingly operated at between 1.5 and 1.8 K.

The second component of the surface resistance, the temperature independent residual resistance is minimized by producing clean surface, avoiding frozen-in-flux and by removing metallurgical defects. Yet one more criteria to have low surface resistance is, as discussed in section on surface resistance, is that the BCS surface resistance is minimum where the mean free path is comparable to the coherence length ($\ell = \xi$). One has therefore to go to optimum purity and not to very high purity. Nb with an RRR of 300 is normally used for cavity fabrication.

Surface resistance R_s of the wall material of a SRF cavity is related to the power dissipation P. It is an experimental finding that at very low temperatures the measured surface resistance in the superconducting state no longer decreases but approaches a constant value. Therefore,

the measured surface resistance R_s is described for a superconductor such as Nb at a temperature below the superconducting transition temperature (T_c), R_s can be expressed as

$$R_s = R_{\text{BCS}} + R_{\text{res}} \quad (2.31)$$

Where R_{BCS} is called the Bardeen-Cooper-Schrieffer (BCS) resistance and R_{res} is called the residual resistance.

Noted here that unlike R_{BCS} that is temperature dependent R_{res} is not. Ideally, R_{res} should be zero. But we know that it is impossible in the real world. Various defects and imperfections on the surface in a depth of the λ contribute to R_{res} . Empirically, R_{res} is found to be proportional to the square root of the normal state conductivity of the material.

2.3.5 Loss due to Hydrogen (Q- disease)

In this context, at first a peculiar loss mechanism so called niobium hydrides (also known as Q-disease or Hydrogen-disease) had been observed and reported in reference [16]. Cavities showed enhanced losses, depending on cool down conditions. The first observations were performed at accelerator installations, whereas laboratory measurements in vertical cryostats seemed not to be affected. After intensive investigations at several laboratories the effect could be identified as segregation of niobium hydride on the surface [17]. This is caused by the formation of harmful η and ν phases of niobium hydrides termed as Q disease. The harmful niobium hydrides can only form when the concentration of hydrogen in Niobium exceeds 100-200 ppm. Beyond all other consideration, such a dangerous level of Hydrogen concentration reaches due to following two reasons. Firstly, the mobility of Hydrogen atoms can reach 5 μm /minute at temperatures between 100 and 150 K. Hydrogen is dissolved in the bulk niobium and has a high mobility at room temperature. Around 100 K the hydrogen will segregate as niobium hydride; a slow cooling process through this temperature region will allow hydrogen to migrate and gather into Niobium. Its lattice constant is larger than that of niobium, and therefore it will segregate preferably at dislocations or on the surface. Niobium hydride is a normal conductor and thus will produce radiofrequency losses. If a niobium cavity stays for some time (several hours) at a temperature around 100 K, niobium hydride will be formed preferably at the surface because the mobility of hydrogen is still high enough in order to diffuse to the surface. In the case of a fast cool down to 4 K the amount of niobium hydride on the surface will be small. After warm up to room temperature, the niobium hydride is dissolved again. Hence, at some localized regions the hydrogen concentration can exceed 100-200ppm so that the harmful phases can be formed. Secondly, various cavity fabrication steps, during handling and treatments, such as, for examples, machining, tumbling, chemistry and surface polishing can result in an uptake of Hydrogen to Niobium that leads to an increase in Hydrogen concentration in Niobium. More specifically, It is well known that atomic hydrogen is produced during electro-polishing, so that the hydrogen content in the bulk niobium will be considerably enhanced after this cleaning procedure. Less intensive loading of niobium with hydrogen was measured after chemical polishing. A heating of the niobium at 800 C under vacuum will effectively 'de-gas' the bulk niobium from hydrogen and thus 'avoid the radiofrequency loss of the 'hydrogen disease'. Here a fast cool down is the only remedy against the 'hydrogen disease'.

2.3.6 Geometrical Factor

Geometry Factor is known as the one of important RF cavity parameter which ranks the cavity's effectiveness of providing accelerating electric field due to the influence of its shape alone, which excludes specific material wall loss. In other words, surface resistance and the

quality factor are related via the geometrical constant G which depends only on the geometry of a cavity and field distribution of the excited mode, but not on the resistivity of the material. In principle, the Geometry Factor is expressed by ,

$$G = \frac{\omega \mu_0 \oint_V H^2 dV}{\oint_A H^2 dA} \quad (2.32)$$

Hence above equation gives,

$$Q_0 = \frac{\omega \mu_0 \oint_V H^2 dV}{R_{\text{Surf}} \oint_A H^2 dA} \quad (2.33)$$

Since Q_0 is inversely proportional to the R_s of the wall material. By introduction of the mean surface resistance and geometrical factor of the cavity the quality factor of the cavity can be reduced to;

$$Q_0 = \frac{G}{R_{\text{surf}}} \quad (2.34)$$

Where G is called Geometrical constant.

We assume that surface resistance of the wall material is homogenous over the whole interior surface of the cavity. Therefore, the geometry factor is quoted for cavity designs to allow comparison to other designs independent of wall loss, since wall loss for SRF cavities can vary substantially depending on material preparation, cryogenic bath temperature, electromagnetic field level, and other highly variable parameters. The Geometry Factor is constant as a cavity shape is scaled to change its frequency, and independent of cavity size.

For example of the above parameters, a typical 9-cell SRF cavity for the International Linear Collider [18] would have $G=270 \Omega$ and $R_s=10 \text{ n}\Omega$, giving $Q_0=2.7 \times 10^{10}$. However, in our 6 GHz tesla type monocell cavity, Geometrical factor, $G=286 \Omega$ and $R_s=100 \text{ n}\Omega$, giving $Q_0=3 \times 10^9$.

It is worthwhile to understand that the efficiency by which a particle beam can be accelerated in a RF cavity depends on the surface resistance. The smaller the resistance, i.e., the lower the power dissipated in the cavity walls, the higher the RF power available for the particle beam. This is the fundamental advantage of superconducting cavities as their surface resistance is much lower and outweighs the power needed to cool the cavities to liquid helium temperatures.

2.3.7 Shunt Impedance

The power dissipation is related to the accelerating field through the shunt impedance R_{sh} of the accelerating structure. Therefore, the shunt impedance R_{sh} is a principal Figure of Merit of an accelerating system and depends upon the geometry of the system and inversely proportional to surface resistance, R_s of the interior walls.

The voltage drop across a resistor and its dissipated power is given by Ohm's law:

$$V^2 = 2.R.P \quad (2.35)$$

where V is the peak voltage across a resistor R and P the power dissipated in the resistor R by an alternating current.

Ohm's law can be defined for a RF accelerating structure, accordingly;

$$U^2 = 2.R.P \quad (2.36)$$

where U is the peak accelerating voltage seen by a particle when passing through the structure, P is the dissipated RF power in the structure to establish the voltage U , and R is the ‘shunt impedance’ of the accelerating structure.

In this definition the shunt impedance is the proportionality factor between the voltage squared and the dissipated power. It is a figure of merit, because it defines the power needed to establish the accelerating voltage U .

In order to sustain the radio-frequency fields in the cavity, an alternating current (AC) flows in the cavity walls. This current dissipates power in the wall as it experiences a surface resistance. In other words, there are tangential magnetic fields at the cavity wall due to the field distribution of the TM_{010} monopole mode. Following Maxwell’s equation, $\nabla \times B = \mu J + \mu E \frac{\partial E}{\partial t}$ current must

flow which results in power dissipation P_{diss} because of the surface resistance. Hence, the power which is dissipated in the cavity P_{diss} , that define the global surface resistance R_{surf} , is given as;

$$P_{\text{diss}} = \frac{1}{2} \oint_A R_{\text{Surf}} H_{\text{Surf}}^2 dA = \frac{1}{2} R_{\text{Surf}} \oint_A H_{\text{Surf}}^2 dA \quad (2.37)$$

Here H_{surf} denotes the magnetic field amplitude.

The shunt impedance is defined as $R_{\text{sh}} = \frac{(V_{\text{acc}})^2}{P_{\text{diss}}} = \frac{1}{R_{\text{surf}}} \quad (2.38)$

R_{sh} depends on the shape, the oscillating mode and the surface resistance of the cavity. For SC structure it is necessary to keep in mind that the shape which leads the best shunt impedance is not usually the one that optimize other parameters that severely contribute to the power quantity spent to yield the electromagnetic field. For example, field emission is enhanced by high electrical surface fields. This is the reason that the quality factor of cavity as a function of accelerating field is generally used for describing the cavity performance. In normal conducting copper cavities the only way to increase R_{sh} is to optimize the cavity shape, that minimizes the power consumption.

2.3.8 RF critical magnetic field

Meissner–Ochsenfeld effect explains, under ideal conditions there is no magnetic field inside the superconductor. There are two experimental ways to reach this state.

- The material is cooled below the critical temperature and then the external magnetic field is raised. Under these conditions, the displacement of the magnetic field could be explained just by shielding currents. They are induced by the time-varying magnetic field when being switched on and will flow in the ‘ideal conductor’ without loss. The external magnetic field is compensated according to the ‘Lentz’ law.
- The external magnetic field was applied before cooling below the critical temperature. Because there is no induction in the superconducting state, a material with zero resistance cannot expel the external field. However, it is the finding of the Meissner–Ochsenfeld experiment that the external magnetic field is expelled as well. This experiment demonstrates that a ‘superconductor’ cannot be explained by zero resistivity alone, but that superconductivity is a new phase of the material.

The superconducting state will be destroyed by an external magnetic field above the so-called critical value H_c . The value depends on the material and the temperature. The superconducting state is permitted only when the intensity of a static magnetic field is lower than the critical value, which is material and temperature dependent. If the magnetic field is

oscillating, a stronger H is permitted (superheating field). In fact it is necessary for $T < T_c$, to support the latent heat connected to the transition from the Normal Conducting (NC) to the Super Conducting (SC) state. Naturally, the level of the magnetic field must be anywhere less than the critical field both in operation and especially during the conditioning. One must consider that the surface resistance increases with H , is convenient to minimize the ratio H_p/E_a . For type I superconductors (e.g. lead), rf fields up to H_c have been reached. Niobium is the most commonly used type II superconductor. A maximum surface magnetic field of 170 mT has been reached in a Nb resonator. This is near to $\mu_0 H_{c1}(0) = 180 \text{ mT}$ of very clean niobium, but lower than $\mu_0 H_{c1}(0) = 200 \text{ mT}$. It is believed that H_{c1} presents no fundamental limit for radiofrequency fields. Furthermore, it is predicted that due to the fast varying radiofrequency field the phase transition is shifted to a value above H_c , the so-called superheated field H_{sh} . In the case of niobium, $\mu_0 H_{sh}(0)$ is calculated to be 240 mT [19].

2.3.9 Peak electric field

High surface electrical fields can lead to the field emission process in which electrons are pulled out from the surface and accelerated by the electrical field. These electrons lose their energy hitting the walls (phonon excitation, bremsstrahlung). Usually field emission is the main serious limit to the cavity performance and so particular care must be taken reducing to minimum value the peak surface electrical field (ratio E_p/E_a) and in the surface preparation (the presence of dielectric material on the S.C. surface lowers the threshold and increases the intensity of the process.) The threshold of the field emission can be shifted to higher field values by treating the cavity with the He conditioning. In this process pulsed high RF power is applied to the cavity where He gas at the pressure of 5×10^{-5} mbar is introduced. He atoms, ionized by the electrons, are accelerated by the electric field and hit the emitting site dumping, on time, the emission phenomenon.

2.3.10 Cryogenics

One of the most significant and intriguing part of SRF technology is Cryogenic engineering. SRF cavities tend to be thin-walled structures immersed directly in a bath of liquid helium in the range of temperatures 1.5K to 4.2K. Careful engineering is then required to insulate the helium bath from the room-temperature external environment. This is accomplished by:

- A vacuum chamber surrounding the cold components to eliminate convective heat transfer by gases.
- Multi-layer insulation wrapped around cold components. This insulation is composed of dozens of alternating layers of aluminized mylar and thin fiberglass sheet, which reflects infrared radiation that shines through the vacuum insulation from the 300 K exterior walls.
- Low thermal conductivity mechanical connections between the cold mass and the room temperature vacuum vessel. These connections are required, for example, to support the mass of the helium vessel inside the vacuum vessel and to connect the apertures in the SRF cavity to the accelerator beamline. Both types of connections transition from internal cryogenic temperatures to room temperature at the vacuum vessel boundary. The thermal conductivity of these parts is minimized by having small cross sectional area and being composed of low thermal conductivity material, such as stainless steel for the vacuum beampipe and fiber reinforced epoxies for mechanical support. The vacuum beampipe also requires good electrical conductivity on its interior surface to propagate the image currents of the beam, which is accomplished by about 100 μm of copper plating on the interior surface.

The major cryogenic engineering challenge is the refrigeration plant for the liquid helium. The small power that is dissipated in an SRF cavity and the heat leak to the vacuum vessel are both heat loads at very low temperature. The refrigerator must replenish this loss with an inherent poor efficiency, given by the product of the Carnot efficiency η_C and a "practical" efficiency η_p . The Carnot efficiency derives from the second law of thermodynamics and can be quite low. It is given by

$$\eta_C = \begin{cases} \frac{T_{cold}}{T_{warm} - T_{cold}}, & \text{if } T_{cold} < T_{warm} - T_{cold} \\ 1, & \text{otherwise} \end{cases} \quad (2.39)$$

Where, T_{cold} is the temperature of the cold load, which is the helium vessel in this case, and T_{warm} is the temperature of the refrigeration heat sink, usually room temperature.

In most cases $T_{warm} = 300$ K, so for $T_{cold} \geq 150$ K the Carnot efficiency is unity. The practical efficiency is a catch-all term that accounts for the many mechanical non-idealities that come into play in a refrigeration system aside from the fundamental physics of the Carnot efficiency. For a large refrigeration installation there is some economy of scale, and it is possible to achieve η_p in the range of 0.2–0.3. The wall-plug power consumed by the refrigerator is then

$$P_{warm} = \frac{P_{cold}}{\eta_C \eta_p}, \quad (2.40)$$

where, P_{cold} is the power dissipated at temperature T_{cold} .

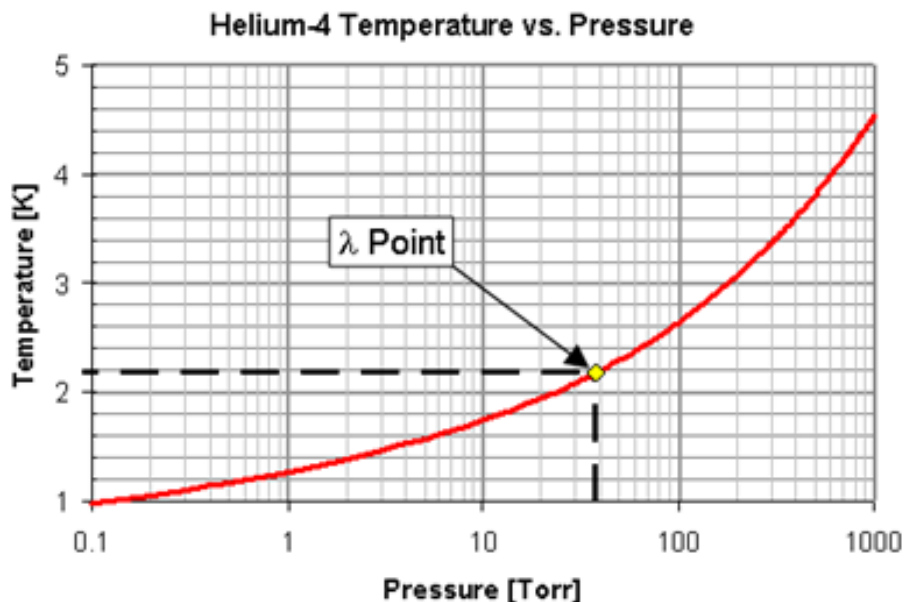


Figure 2.4: ⁴Helium temperature vs. Pressure is plotted in this graph, indicating the superfluid λ point (2.17K).

The temperature of operation of an SRF cavity is typically selected as a minimization of wall-plug power for the entire SRF system. Mostly SRF systems either operate at atmospheric pressure, 4.2 K, or below the λ point at a system efficiency optimum usually around 1.8 K.

2.4 SRF edge factors due to the accelerating gradient: Cavity loss mechanisms

In this section, an overview of limitations of superconducting cavity performance are described. Also research and development efforts towards understanding and curing these effects are discussed.

2.4.1 Thermal breakdown (Quench)

Thermal instability or thermal breakdown is among one of the typical limitation of the maximum field in a superconducting cavity. The name quench is commonly used to describe the breakdown of superconductivity in magnets. Here a critical value of the magnetic field is surpassed. In radiofrequency cavities, however, the critical temperature T_c is reached by a heating process. Therefore, the name ‘thermal instability’ is more appropriate. Nevertheless, the word ‘quench’ is often used when describing a breakdown in cavities.

The experimental observation of a thermal instability is as follows. The cavity is operated with constant radiofrequency power. At the end of the filling process an equilibrium condition is reached. The stored energy in the cavity stabilizes to such a value that the superconducting radiofrequency loss equals the transferred generator power. Above a critical value the stored energy decays to nearly zero in a short time, much faster than the time constant of the superconducting cavity. Diagnostic measurements with temperature sensors at the outer cavity wall have clearly indicated that some parts of the cavity exceed the critical temperature of the superconductor. Therefore, it is assumed that the cavity becomes partially normal conducting, the radiofrequency dissipation is dramatically enhanced and the stored energy is decreased accordingly. The breakdown of radiofrequency superconductivity is explained by a model of thermal instability [11]. The BCS part of the superconducting surface resistance has an exponential dependency on temperature (see also equation BCS)

$$R_{BCS} \propto \exp\left(\frac{\Delta}{k_B T}\right) \quad (2.41)$$

where R_{BCS} is the superconducting surface resistance, Δ the energy gap, k_B the Boltzmann constant and T is the experimental temperature.

Under steady-state conditions the temperature at the inner cavity surface is enhanced by ΔT as compared to that of the liquid helium at the outer cavity wall:

$$\Delta T = q \left(\frac{d}{\lambda} + R_k \right) \quad (2.42)$$

where ΔT is the temperature difference between the inner cavity surface and the liquid helium, q is the heat flux, d the thickness of the cavity wall, R_k the thermal resistance between the outer cavity wall and the cooling helium (Kapitza resistance) and λ the thermal conductivity of the cavity wall.

It is assumed that there is a small normal conducting spot (defect) on the inner cavity surface. It will produce loss according to Ohm’s laws and thus raise the heat flux. Hereby the temperature of the inner cavity surface increases and finally results in an enhanced BCS surface resistance.

There is a critical value of the heat flux at which a thermal runaway is launched (because of the exponential increase of the surface resistance with temperature [6] and large parts of the cavity surface will be driven to normal conductivity. Analytic models as well as numerical simulations can describe such an avalanche effect. Parameters of the calculations are the thermal conductivity of the superconductor, the size and resistance of the normal conducting spot and the Kapitza resistance. The thermal conductivity as well as the Kapitza resistance

can be measured, whereas the size and the resistance of the normal conductor are subject of fit parameters. There are two obvious ways to reduce the probability of a thermal instability:

- avoiding the normal conducting defect by extreme care in preparing and cleaning the cavity surface;
- increase of the thermal conductivity of the superconducting material.
- use thin film technology.
- use a different material with higher T_c and higher critical magnetic fields.

Progress has been achieved in both areas over the last ten years. Best Field level values around 40 MV m^{-1} in single cells have been measured. This is about a factor of two increase over the last two decades.

2.4.2 Field emission

Field emission is the another typical limitation from reaching its maximum high-gradient superconducting cavities. When the surface electrical field is strong enough for that small area, the electrons will start to tunnel out of the metal surface to form a steady current. The field emission current increase rapidly as the field is increased. It absorbs a great amount of RF power (just like the multipacting phenomenon), depositing the heat whersoever electrons hit. Some of the heating is strong enough that lead the resonant cavity to destroy the superconducting state.

The experimental observation is as follows:

- radiation is observed outside the cryostat
- the quality factor Q drops (the rf loss grows) with increasing slope for increasing field levels
- finally the maximum field is limited by too high rf power dissipation (low Q), sometimes also a thermal instability is observed.

The observation of radiation is a clear indication for electrons which are accelerated by the rf field and produce radiation when impacting the wall of the resonator.

There is experimental evidence that small dust particles on the cavity surface play A crucial role in initiating field emission. Therefore, careful cleaning of the cavity surface is the most important remedy against field emission. However, other surface conditions, like cryo absorption of gases, determine the field emission process and need adequate care. Superconducting cavities in an accelerator should not be operated above the onset of field emission. The first reason is to avoid the additional heat by impacting electrons. The second is that dark current will spoil the reading of beam monitors and might actually deteriorate the beam quality.

2.4.3 Multipacting

Multipacting (multiple impact electron amplification) is observed in radiofrequency components which are operated under vacuum. It is a phenomenon of resonant multiplication of electrons under the influence of radiofrequency fields. In RF resonant cavities, stray electrons can hit the cavity surface, creating secondary electrons, i.e., Secondary electrons can be created by a primary electron impinging on a metal surface. The secondary electrons, which in turn, can be accelerated by RF fields, absorb the RF energy and hit the wall surface to create more secondary electrons. When these secondary electrons happen to hit the same area, the absorbed RF energy heats the surface, thus creating a local hot spot. All that factors not only limit the accelerating gradient, but also create more rf surface loss, even leading to a

possible thermal quench. MP is usually enhanced for not very well cleaned surface condition. The experimental signature of multipacting is as follows.

- There is a threshold of the field strength in the radiofrequency component. Above this threshold the radiofrequency power can be raised but it has no effect on the stored energy.
- The threshold is of sharp nature. The component can be operated below without any sign of unusual behaviour.
- The likelihood of multipacting differs for different metals and surface conditions.
- Sometimes sparking is observed when operating in the multipacting regime and damage of the component might thereby result.

The most successful remedy against this one-point multipacting is the change of the cavity cross section from a cylindrical to a spherical shape. The magnetic resonance is destroyed by the presence of the strong electric surface field in the spherical shape [20]. Eventually multipacting can be overcome by conditioning. This means that the component behaves normally again after being operated for some time under conditions of multipacting. By adjusting the resonant cavity shape, the multipacting can be reduced but it cannot be totally eliminated.

2.4.4 Diagnostic methods for SC cavities: Temperature mapping.

Temperature mapping system is the most significant diagnostic tool in analysing the behaviour of a SC cavity¹. The good reproducibility of the cavity performance allows to clearly identify loss mechanisms with advanced diagnostic techniques. The temperature maps allow to distinguish between localised hot spots due to foreign particle inclusions or multipacting, traces of field emitters or global heating effects. To do this, temperature sensors are placed at the outer wall of the cavity and register the temperature distribution. From these data, information about the location and physical nature of spots with enhanced losses can be gained, such as: the scaling of losses with the cavity field, field emissions, the location of quenches, the time development of defects or the creation and processing of loss mechanisms. Carbon resistors have proved to be sensitive and cheap temperature sensors. They are selected to have maximum sensitivity at the operating temperature. Nominal 50 Ω resistors are widely used for the temperature range from 4.2 K to 1.8 K. The outer plastic housing of the resistor might be ground off to reach good thermal contact between the cavity wall and the sensitive carbon layer. Mainly there are two different arrangements in scientific operation.

- I. Fixed temperature mapping: A large number of resistors (typically more than 500) is mounted on assembly boards which are attached to the cavity. The resistors are pressed by a spring against the outer cavity wall, the typical distance between adjacent resistors is 10 mm. The thermal contact is improved by using grease with good heat conductivity between resistor and cavity wall.
- II. Rotating temperature mapping: A smaller number of temperature sensors is attached to a movable arm. It rotates stepwise around the cavity axis.

In addition to the temperature sensors, small radiation detectors (diodes) are also placed around the cavity wall, being assembled on the same boards. They allow one to trace the trajectory of field emitted electrons by localizing the γ -radiation when impinging the inner cavity surface. Temperature mapping is a suitable tool for localizing heating spots. However,

¹ Some of most important temperature measurement tools are described in [H. Padamsee et al. 1998]

some helpful information can be gained by pure RF measurements, avoiding any mechanical effort for diagnostics. In the case of multicell cavities it might be helpful to know which cell is troublesome, or if there is more than one possible quench location.

2.5 Why 6GHz cavities?

Advantages of SRF cavities for accelerators are well known and widely documented in last five decades. At present, Nb resonators in accelerators are operated at gradients considerably below the physical limitation of the superconductor. The main limitations are thermal instabilities (quench) and field emission. Research and development is being undertaken to explore the reason for these limits and to search for improvements. Material samples are being investigated to examine the effect of different fabrication, treatment and handling procedures. However, finally, these results must be confirmed in measurements of full size cavities under radiofrequency operations. Single-cell resonators are an appropriate test vehicle for this purpose. They allow a fast turn-around time and they sample enough surface area under realistic radiofrequency conditions. Multicell resonators with auxiliary components for accelerator application are more difficult to handle and will lag behind in performance. Nevertheless, the hope is that multicell cavities will come close to the performance of single-cell resonators.

These small cavities are fabricated by spinning technology to create seamless structure [V. palmieri]. A schematic diagram of 6 GHz tesla type Nb mono cell SRF cavity is shown in Figure 2.5. The main advantages of these 6GHz bulk-Nb cavities over a 1.3 or 1.5GHz SRF cavity are saving time, cost, and materials. One can fabricate such small 4-6 cavities out of the rest Nb sheet material which was used to prepare just one big (i.e., 1.3 or 1.5GHz) SRF cavity with the same technology, and collecting all statistics of treatments like mechanical tumbling, chemical, electro-chemical process, heat treatment, and RF test data are simple and in short time, say in a couple of week.

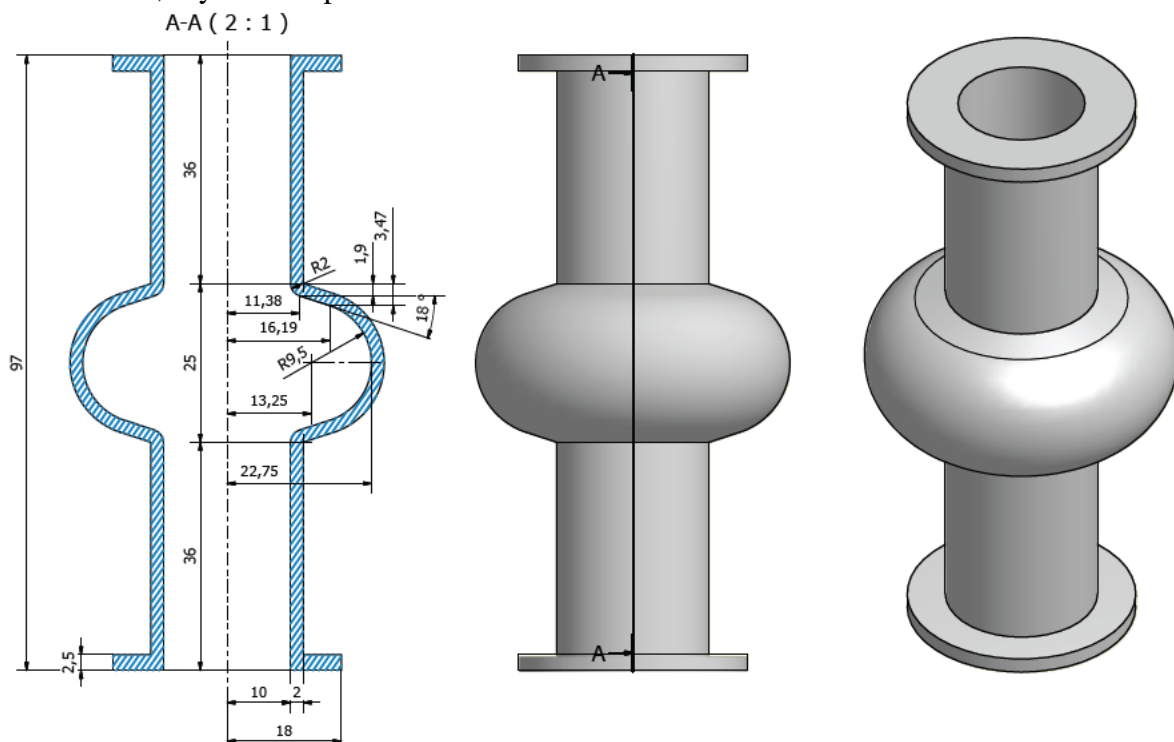


Figure 2.5: A schematic diagram of 6 GHz tesla type Nb mono cell SRF cavity.

2.5.1 Cavity Fabrication techniques

Ultra high pure (UHP) bulk Niobium (Nb) is used for the fabrication of Superconducting (SC) RF cavities to achieve high accelerating fields [3, 15]. Accelerating radiofrequency structures can be realized in different ways. There are several methods to fabricate SRF cavities². Most widely used fabrication technique is given below. However, this thesis research work mainly concerns with tesla type seamless cavities. Therefore, only spinning technique is explained in the frame work of this research.

- Hydroforming of multi-cells (W.Singer, DESY): REAL CAVITY
- Use of composite material Nb-Cu: REAL CAVITY
- Thin film coating of Cu cavities: REAL CAVITY
- Spinning of single/multi cells (V. Palmieri, INFN): : REAL+6 GHz CAVITY; *These cavities have no welded joints by electron beam welding under UHV system*

Spinning of single/multi cells seamless SRF cavities: An Innovative Techniques for Fabricating SRF Cavities: Classical industrial process used for cavity fabrication is the Electron Beam Welding (EBW). However, it is very expensive, complicated and manufacturing damage induced at equator. Current is maximum at equator while electric field is maximum at iris. Therefore, in order to reduce cost and avoid EBW, an innovative technique has been discovered so called spinning³ technique [2]. This technique has potential to produce tesla type complete cavities (including all frequency range) that has no seams which would greatly reduce not only huge welding costs, but also eliminates any possibility of weld errors. Pure Niobium sheets of thickness 2 mm have been used to fabricate seamless 6 GHz SRF Cavities for the present experimental investigation. These sheets were purchased from Heraeus superconducting company. The RRR of these sheets were approximately 170. The total length of mono cell cavities are about 100mm while diameter of apertures are 20mm, at euqator 50mm and thickness of cavities are 2mm and 1mm, and initial grain size is about 50-70 μm .

It was demonstrated by V. Palmieri that single cell and multi-cell Nb and Cu seamless cavities could also be fabricated by spinning. Figure 2.6 shows various progressive steps during the fabrication of a tesla type copper monocell cavity by this technique. Seamless Nb SRF cavities are also fabricated in the same way.

After spinning, cavity has to be tumbled and mechanically grinded for at least 100 μm to remove surface manufacturing defects before any further chemical treatment. Several single cell cavities reach an accelerating gradient of 40 MV/m with a Q_0 about 2×10^{10} . In Figure 2.7 a collection of 6GHz Nb and Cu cavities are shown, while Figure 2.8 shows the first nine-cell Nb cavity manufactured by the spinning technique. Although there are still many technical problems waiting to be resolved for the seamless cavity formation techniques, nevertheless, the exclusion of welding steps from cavity fabrication process is a very significant progress.

² A very good explanation about SRF cavity fabrication techniques are given in book RF supercond for accelerators (H. Padamsee, J. Knobloch, T. Heys)

³ A very good discription of manufacturing procees of spinning technology for seamless cavities is given by V. Palmieri, Seamless cavities: the most creative topic in RF superconductivity, Proceedings of the 8th workshop on RF superconductivity (1997)

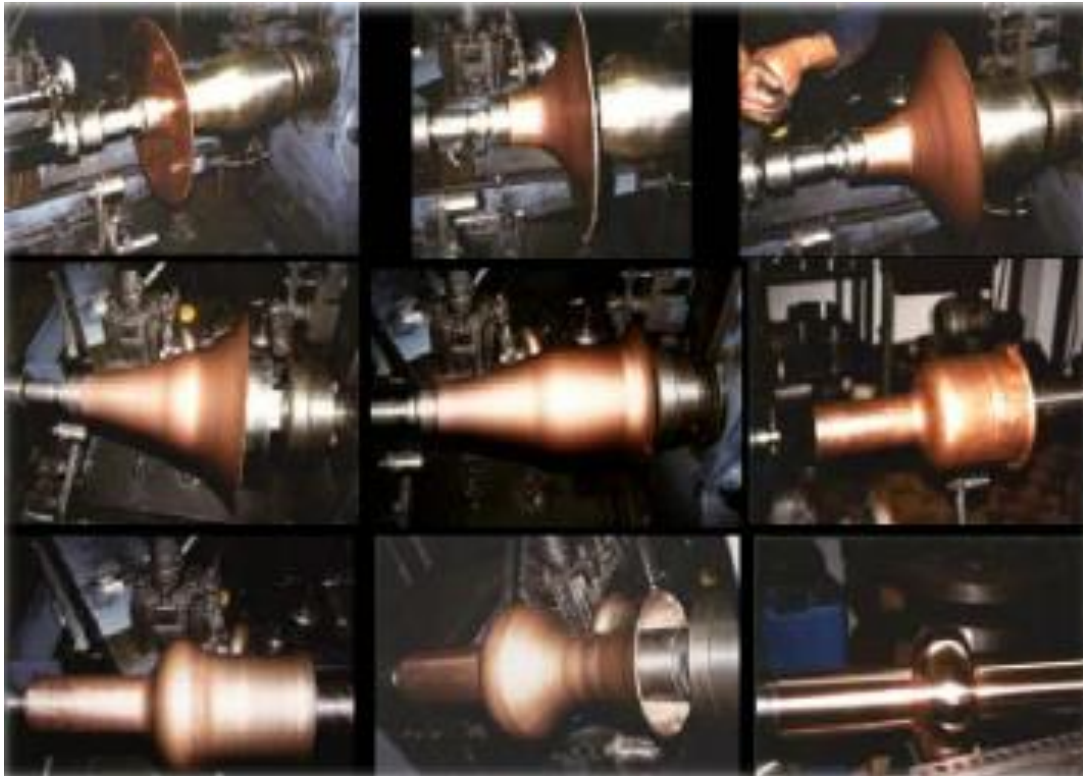


Figure 2.6: various steps during the fabrication of a 1.5 GHz copper monocell cavity by spinning (circular blank).

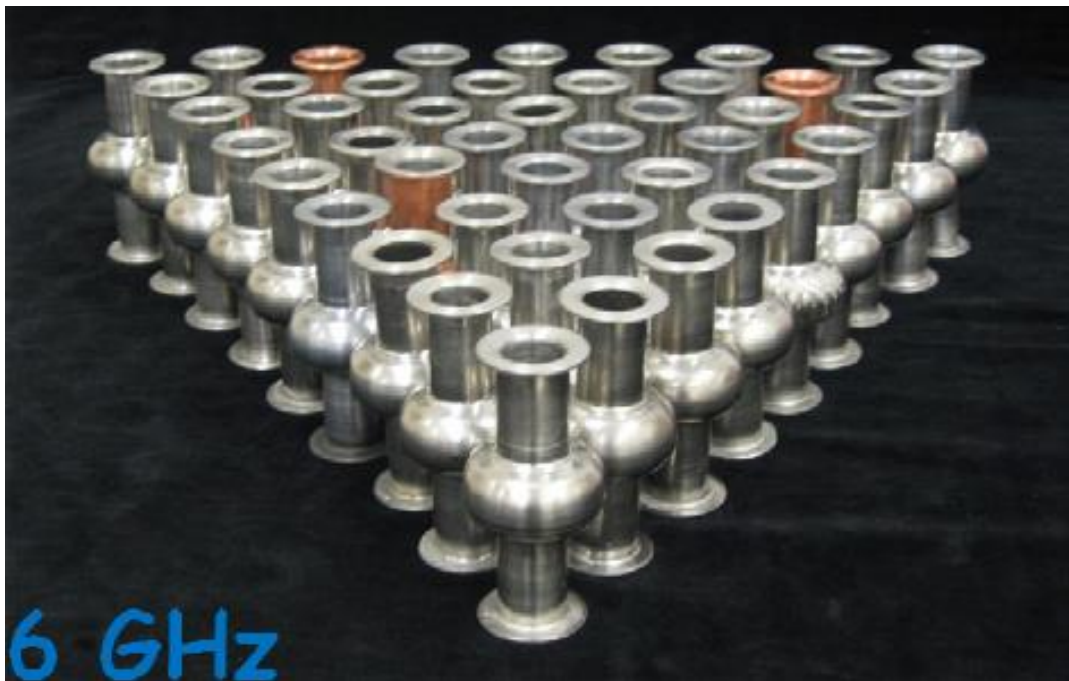


Figure2.7: A collection of 6 GHz monocell seamless Nb and Cu cavities

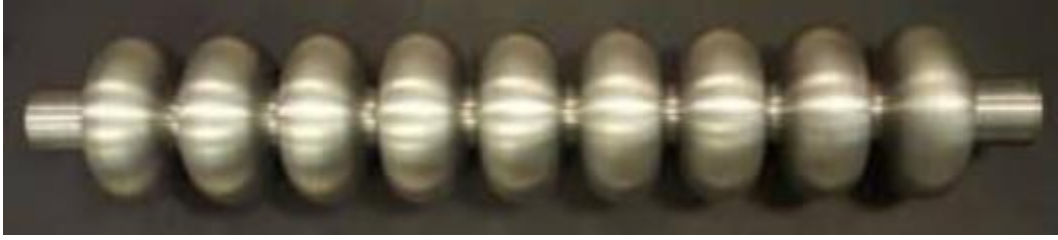


Figure 2.8: First 9 cell tesla type Nb SRF cavity fabricated by spinning technique. A spinning technology (seamless) is used to form bulk-Nb cavity .

2.5.2 Why Niobium?

For any particle accelerators, cavities have to be superconducting due to the operation cost which is one of the paramount consideration. Besides some historical significance, the first natural reason is the Nb has the highest critical temperature, T_c of 9.25 K among all available elements in the period table. Some significant properties of Nb are listed in section 2.5.4. Nb is the most investigated and well documented material for SRF applications and the major material used in particle accelerators based on SRF technology.

Therefore, Nb has been selected as the major material for constructing SRF cavities. This makes the requirement for cooling the cavities down to a temperature below T_c a relatively easy task. Choice of superconducting cavities over normal conducting cavities as the accelerating structure of an accelerator could save huge amount of the operation cost, which is true for accelerators in a continuous wave (cw) mode. If copper cavities are considered as an example. For cw operation, the power dissipation through the walls of a copper cavity is huge. This is due to the fact that the dissipated power per unit length of an accelerating structure is given by the following formula:

$$\frac{P}{L} = \frac{E_{acc}^2}{\frac{r_a}{Q_0} Q_0} \quad (2.43)$$

Where r_a/Q_0 is the geometric shunt impedance in Ω/m , it depends primarily on the geometry of the accelerating structure. The resistance of copper is approximately 5 orders of magnitude higher than that of a microwave surface resistance of a superconductor, and Quality factor (Q_0 value) is typically 5 orders of magnitude lower. Some simple calculations can show that if Cu cavities are operated at cw mode, the dissipated power for each cavity could have been some hundreds of kW, exceeding the 100 kW power dissipation limit for a Cu cavity. This already exceeds the 100 kW power dissipation limit for a copper cavity. Also, above which the surface temperature of a Cu cavity will exceed 100 C, which will invite several unwanted effects. For examples, such as: stresses in the Cu, vacuum degradation, metal fatigue due to thermal expansion. Therefore, for Cu cavities, high accelerating gradients larger than 50 MV/m can only be produced for a period less than a few microseconds before the RF power needed becomes prohibitive. In contrast, Nb cavity could dissipate power of only a few watts. However, it is necessary to consider the cost of cooling a superconducting material down to a temperature below T_c and normally the efficiency of refrigerators that are used to cool down the material is low.

Besides the general advantages of reduced RF capital and associated operation costs, superconductivity offers certain special advantages that stem from the low cavity wall losses. Because of superconductivity, one can afford to have a relatively larger beam holes in superconducting cavities than for normal ones. This significantly reduces the sensitivity of the accelerator to mechanical tolerances and the excitation of parasitic modes. Also larger beam holes reduce linac component activation due to beam losses. Superconducting cavities

are intrinsically more stable than normal conductor cavities. Therefore the energy stability and the energy spread of the beam are better.

Moreover, E_{acc} is proportional to the peak electric field (E_{pk}) and peak magnetic field (H_{pk}) on the surface of a cavity, one has to be sure that the material that is used to make the cavity can sustain large surface fields before causing significant increase in surface resistance or a catastrophic breakdown of superconductivity (known as quench). The ultimate limit to accelerating gradient is the theoretical RF critical magnetic field that is called the superheating field H_{sh} . Nb has the highest H_{sh} of 0.23 T among the all available metal elements.

Another advantage of Nb is that it is relatively easy to be shaped into different structures due to its outstanding ductility and the fact that it is relatively soft. Nb can be cold-worked to a degree more than 90% before annealing becomes necessary. This property is responsible for the recent new developments on fabricating seamless Nb SRF cavities by hydroforming and spinning as described in above section (2.5.1).

2.5.3 The Residual Resistivity Ratio (RRR)

The Residual Resistivity Ratio, RRR is a parameter that can be used to quantify the general impurity content of a material. For a relatively impure Nb, the d.c. resistivity ($\rho \approx \sigma$) drops by a factor of 30 from its room temperature value of $1.4 \cdot 10^{-8} \Omega \text{ m}^{-1}$ in the normal state, to its residual value. The factor by which resistivity drops to the residual value is called the residual resistance ratio, RRR. The higher is the RRR, the lower is the impurity content of the material. It is important to point out here that there are background contributions to RRR value from phonons and grain boundaries. The RRR is defined as the ratio of the electrical resistivity at two temperatures: 300 K and 4.2 K.

$$\text{RRR} = \frac{\text{resistivity at 300K}}{\text{residual resistivity at low temperature (normal State)}}$$

The value of RRR indicates the purity and the low-temperature thermal conductivity of a material, and is often used as a material specification for superconductors. For Nb, this is usually done either by the measurement at a temperature just before the superconducting transition temperature T_c and extrapolation to 4.2 K or at a specific temperature below T_c where an external magnetic field is applied just enough (a homogeneous magnetic field up to 1 Tesla parallel to sample) to drive Nb to lose its superconductivity at 4.2 K. For pure Nb used in radio-frequency cavities of linear accelerators, the low temperature resistivity is defined as the normal-state value extrapolated to 4.2 K, but this value doesn't differ much from the 10K value.

In a sputtered cavity, the grain size and the purity of the thin film are such that the mean free path is very small (10-100 nm). Nevertheless, the Q_0 of such a cavity is twice that of a cavity made from high RRR bulk niobium. Experimental results show that surface resistance depends on the ratio ξ_0/ℓ . When both $\xi_0/\ell \ll 1$ and $\xi_0/\ell \gg 1$, then the surface resistance is relatively high. For $\xi_0/\ell > 1$, the surface resistance reaches a minimum and this corresponds to RRR values between 12 and 17.

RRR values serve as a convenient measure of the purity of the metal. High-purity niobium has higher RRR values. Calculated theoretical limit for RRR for Nb is 35000 and is

determined by scattering of electrons by lattice vibration [21]. In practice, the highest RRR ever achieved for Nb is 33000 [22]

2.5.4 Properties of Nb

Niobium is the main topic of this dissertation. Niobium is a chemical element having symbol Nb and atomic number 41. It is a transition metal belongs to group V in fifth period of the Periodic table. It is a ductile transition metal, soft, gray in appearance, and is found in pyrochlore and columbite. It was first discovered in the latter mineral and so was initially named columbium. Now the mineral is also called "niobite", which is well used not only for scientific research but also for commercial purpose. For examples, such as: in special steel alloys, in welding, electronics, optics, nuclear industries, and jewelries.

Table 2.1: List of the niobium properties

Atomic number	41
Atomic weight	92,9 g/mol
Atomic radius	2.08
Density	8570 kg m ⁻³
Crystal structure	Body centered cubic (b.c.c.)
Space group	Im3m
Electrical conductivity typical	@0°C 152 nΩ.m
Electrical resistivity (300K)	14.9 μΩ•cm
Thermal conductivity (300K) (0K)	53.7 W m ⁻¹ K ⁻¹ 52.3
Debye Temperature	275K
Melting Temperature Boiling Temperature	2741K (2468 °C) 4927 °C
Critical temperature	9.26K
Superheating field	0.23 Tesla
Covalent radius	1.64±6 Å
Lattice constant at 20 °C	3.294Å

Among all existing superconducting elements, it has the highest critical SC transition temperature. The research group led by W. Meissner reported the discovery of superconductivity in niobium at T_c=9.2K [23] in 1930. Niobium is the pure element with the

highest T_c under normal conditions. The critical temperature measured in monocrystal high purity niobium (RRR=5000) was reported to be 9.2877K [24]. The critical field H_c measured in monocrystal high purity niobium (RRR=4000) was reported to be 2061 Gauss [25]. In 1933 W. Meissner and R. Ochsenfeld performed an experiment that triggered development of theories of superconductivity [26]. Some important and useful information and constants of Nb (properties) are listed in table 2.1

2.5.5 Promising new materials to bulk Nb for SRF application

A critical key for the competitiveness as well as technological and economical success of this new technology are reliable, efficient and low-cost cooling systems. The INFN Superconducting and Surface treatments laboratory gives the opportunity to exchange ideas and experiences between International research laboratories.

Nb is the most researched and well documented material for SRF applications and the major material used so far in particle accelerators based on SRF technology. Although there are other superconducting compounds that have higher T_c or higher H_{sh} . Research effort has been going on over other superconductors such as NbN ($T_c=16.2$ K), NbTiN ($T_c=17.5$ K), Nb₃Sn ($T_c=18.3$ K), V₃Si ($T_c=17$ K), Mo₃Re ($T_c=15$ K), and MgB₂ ($T_c=39$ K) compounds (presently about 40) are being investigated, and are under investigation at several laboratories [27]. YBaCuO compound is the most popular one due to high T_c . These compounds promise operation at the temperature of liquid nitrogen (77 K) instead of 4.2 K with liquid helium. The measured residual surface resistance of these films is rather high. The maximum magnetic surface field on small samples corresponds to accelerating gradients below 5 MV m⁻¹. These limitations are explained by imperfections in the film morphology, which could be cured by proper substrate preparation and coating technique. However, at present, these materials are not applicable for accelerator technology.

Table 2.2: Critical temperature values for different materials.

Material	T_c [K]
Niobium (Nb)	9,28
Lead (Pb)	7.1
Tantalum (Ta)	4.4
Mercury (Hg)	4.1
Tin (Sn)	3.7
Indium (In)	3.4
V ₃ Si	17
Nb ₃ Sn	18.3
Nb-Ge	23
YBa ₂ Cu ₃ O ₇	90
TlBaCaCuO	125

Many possible applications of planar microwave components have been identified which use epitaxial thin films of high-temperature superconductors [28]. Coating of cavities for accelerator application, however, results in polycrystalline and textured layers. The radiofrequency surface resistance and the maximum surface fields are determined by loss mechanisms in the grain boundaries (granular superconductor). With the present knowledge of film coating, the performance of a high-temperature superconductor is far below the needs in accelerator application. There are several research groups [29] have started to revisit the Nb on Cu as an alternative for making SRF cavities by taking the advantages of the good superconducting properties of Nb and good thermal conductivity and cheap Cu substrates. Table 2.2 gives the list of all classes of superconductors known to-date. For one reason or the other we have just a handful of systems and the superconductors which can be considered for RF cavity application. The summary of various class of superconductors⁴ [30] for cavity application is placed here. Cavities used to-date are made of niobium- either in bulk or Nb coated on copper cavities. These cavities are operated between 1.5 and 1.8 K where the BCS component of the surface resistance is reduced to minimum and the cavity is operated in the residual resistivity regime. Operating temperature can be increased if we switch over to higher T_c superconductor. The oxide superconductors which once looked most attractive with T_c above 77 k, however, proved disastrous because of weak superconductivity at the intergrain boundaries. Therefore, A-15 superconductors as the possible materials for RF cavities are appropriate. Out of a total of more than 50 known A-15 superconductors only Nb₃Sn, Nb₃Ge, Nb₃Al, V₃Ga, V₃Si and Mo₃Re with high T_c are the possible candidates for being considered as the replacement of Nb for accelerator technology.

-----*****-----

⁴ A deatail discussion about the merits of various class of superconductors for cavity application has been given by V. Palmieri [30].

Chapter 3

State of the art of surface treatments of cavity:A Review

The complete set of techniques for the cavity purification method have been tested via several systematic steps by applying a certain surface treatments to the cavity. The accumulated know-how of several research institutes shall be exploited to further improve the quality of the SRF accelerator cavities by pushing further the detailed diagnostics tools and the surface treatment of the cavities. Therefore, highest accelerator performance requires optimised production, surface treatments, and diagnostics of the accelerating structures. The knowledge and mastering skills of these technologies become even more important since large scale production involves in industry.

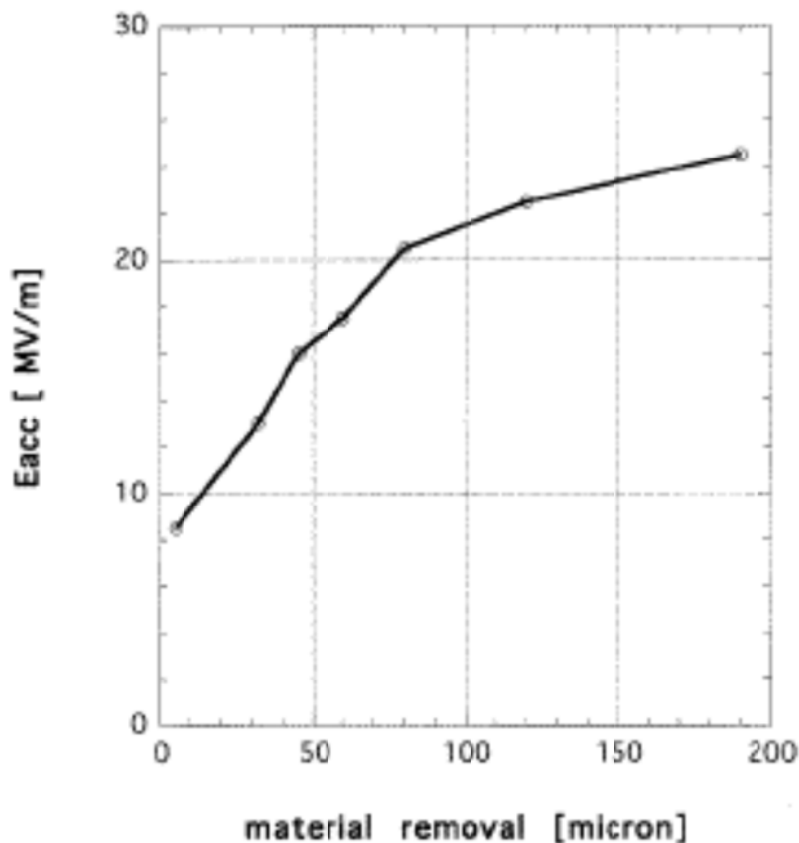


Figure 3.1: Accelerating gradient vs material erosion from the inner surface of cavity is plotted in this figure, showing a damage layer of about 150 μm must be removed until a clean surface can be prepared for the superconducting cavities. Increase of quench threshold by successive removal of Nb from the inner cavity surface [31]. Most likely the quench is initiated by local impurities in the bulk niobium due to contaminations during the rolling process of the Nb sheet production.

For the material investigations, it is well established that a layer of about 150 μm of Nb must be removed after cavity fabrication to reach high fields and high quality factors which lead low radiofrequency loss. The damaged layer contains dirt, inclusions and other impurities which will produce radiofrequency losses or initiate a quench. Figure3.1 shows the quality factor and quench field of a single-cell resonator after successive material removal [31]. A

low surface resistance can be reached after only 50 μm etching, whereas the quench limit still improves after 300 μm total removal rate. The radiofrequency loss of a single, small normal conducting defect will not be noticeable in the integral measurement of the quality factor but can initiate a thermal instability. There is the suspicion that dust, dirt or other foreign material is pressed into the Nb during forging and rolling of the sheets. The handling mistakes can be detected by careful visual inspection of the surface, by a discoloration at defects after anodizing the Nb sheets or by a rust-test (immersing the sheets into water and searching for traces of rust due to iron particles). These quality controls are essential but are only sensitive to surface defects. They cannot detect buried defects which will be uncovered after the next chemical etching process. Therefore, a scanning apparatus with an eddy current has been developed [32]. The eddy current measurement is sensitive to changes of the bulk electric conductivity. Therefore, inclusions of foreign material as well as mechanical defects. In this context, mechanical grinding is a powerful method to remove surface defects. Therefore, first of all, resonators were treated in order to remove damaged surface layer and to polish the internal surface.

3.1 Mechanical polishing (MP) technique

Advantages of SRF cavities for accelerators are well known and widely documented. Ultra high pure (UHP) bulk Niobium (Nb) is used for the fabrication of Superconducting (SC) RF cavities to achieve high accelerating fields [1-2]. Classical industrial process used for cavity fabrication is the Electron Beam Welding (EBW). However, it is very expensive, complicated and manufacturing damage induced at equator. Therefore, in order to reduce cost and avoid EBW, an innovative technique has been discovered so called spinning technique [3], but this technique has also some draw back like contamination, surface damage in internal part due to Mandrel line. For this reason it is very important to do mechanical finishing to the cavity which reduces contamination and manufacturing scratches.

In this section, we discuss the new tumbling technique of 6 GHz bulk Nb SRF cavity, giving special attention to important new developments that enable easy and quick to study surface erosion of defected materials. Purposes to use such cavity are less treatment time and cost effective. Mechanical Treatment Method is described under Experimental Procedure

3.1.1 Centrifugal Barrel Polishing (CBP) vs Vibrator: A new approach for tumbling processes:

Two different approach of mechanical polishing as an alternating method of materials removal have been discussed. Namely, centrifugal barrel polishing and polishing using a small vibrator.

Mechanical treatment (centrifugal barrel polishing-CBP): Mechanical treatment is performed by means of the centrifugal tumbling. Centrifugal tumbling system and for multiple 6 GHz cavities, and a compact tumbling system for a single cavity are shown in Figure 3.2. A complete process to assemble cavities for tumbling/mechanical finishing are shown in Figure 3.3.

There are various materials available for mechanical polishing, such as: Silicon Carbide, Yttria stabilized Zirconium oxide (5 mm sphere), and flakes of Al_2O_3 , SiO_2 powder embedded in a polyester matrix. We have mainly used mixture of Silicon Carbide (SiC) and Yttria stabilized Zirconium oxide ($\text{ZrO}_2\text{-Y}$) balls, and also and flakes of Al_2O_3 , SiO_2 as an abrasive agent pieces so called medium for tumbling these bulk Nb cavities. It is shown in Figure 3.4. The resonators are half filled with the medium, deionized water added below the neck with a drop of liquid soap then plugged up and fixed to the tumbler-machine. The tumbler makes the cavity rotate at 300 rpm for more than 16 hours in each cycle. The abrasive agent pieces could

erode the inner metal surface in a uniform way. Abrasive media reduces to small size after tumbling, which is shown in Figure 3.5. Hence the treatment reduced fabrication scratches and other defects. The advantage is less chemistry needed. However, during the process, hydrogen is dissolved in the Niobium (Q-disease). And such a harmful Hydrogen concentration needs to be removed and avoided by high temperature treatment and quick cooling-warming up process at temperatures 100-150 K.

After tumbling process, cavities are cleaned in ultrasonic bath with detergent (RODACLEAN having pH=12) and ultra-pure DI water (Resistivity = 18 MΩcm, Filtration < 0.2μm) to remove residual SiC+ZrO₂-Y-residuals from the inner surface of cavity. Table 1 details the tumbling performance during 3 or 4 cycles of the process.



Figure 3.2: Left fig: Centrifugal tumbling system for multiple 6 GHz cavities. One can tumble 6 cavities at a time. Right fig: A compact tumbling system for a single cavity, cavity is tumbled in zig-zag motion.



Figure 3.3: Left fig: 6 GHz cavity, plastic flange with viton O-ring is shown. In next figures: Cavity enclosed with abrasive media fastened at post inside the box, 3 cavities fastened in a box, and closed box (extreme right fig), which in turn placed inside metal box of centrifugal tumbling system is shown respectively. Two box, each contains 3 cavities can be tumbled at a time.

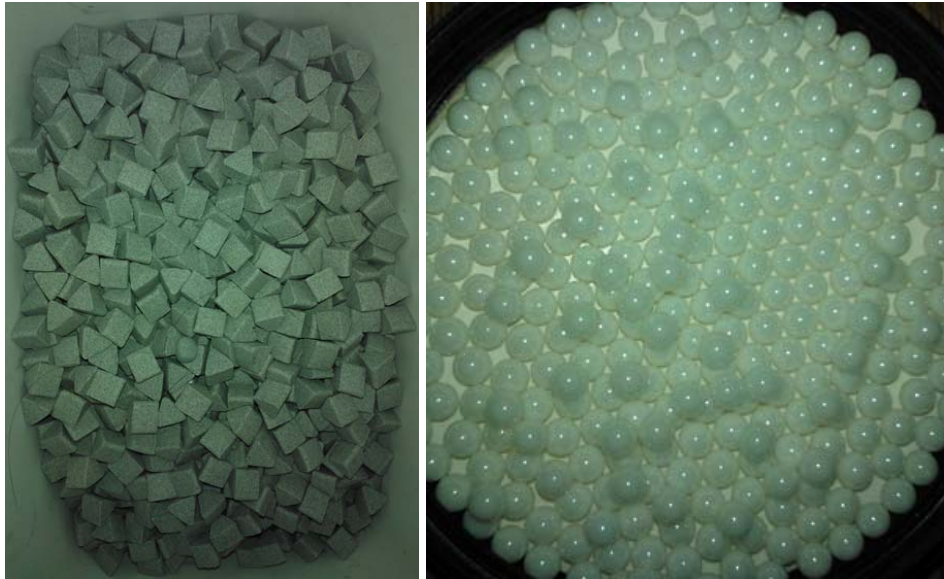


Figure 3.4: An abrasive agent pieces SiC and ZrO₂-Y, mixture of both media are used to polish internal surface at initial stage. For final stage of finishing we used small pieces of SiC (already used in previous cycle) or Al₂O₃+SiO₂ or small wooden pieces are used alongwith water and a drop of surfactant in all cycle of tumbling . **Left fig:** Silicon Carbide (SiC). **Right fig:** Yttria stabilized Zirconium oxide (ZrO₂-Y) balls.



Figure 3.5: An abrasive agent pieces reduced in small size after 4 hours of tumbling process. **Left fig:** Silicon Carbide (SiC) and Yttria stabilized Zirconium oxide (ZrO₂-Y) balls. **Right fig:** after final finishing residuals of media; SiC, ZrO₂-Y, Al₂O₃+SiO₂

Mechanical finishing/Polishing with Vibrator:

Vibrators are used in many different industrial applications both as components and as individual pieces of equipment. Vibratory feeders and vibrating hoppers are used extensively in the food, pharmaceutical, and chemical industries to move and position bulk material or small component parts; Vibrating screens are used to separate bulk materials in a mixture of different sized particles. For example sand, gravel, river rock and crushed rock, and other aggregates are often separated by size using vibrating screens; Vibrating compactors are used for soil compaction especially in foundations for roads, railways, and buildings; Concrete vibrators consolidate freshly poured concrete so that trapped air and excess water are released

and the concrete settles firmly in place in the formwork; Vibrating tables or shake tables are sometimes used to test products to determine or demonstrate their ability to withstand vibration. Testing of this type is commonly done in the automotive, aerospace, and defense industries; Vibrating tables can also be used in the packaging process in material handling industries to shake or settle a container so it can hold more product.

There is no experimental information available till date in context of tumbling process using Such small vibrator. Therefore, an idea has been received to fix the vibrator and mount the cavity on it via a plastic or steel board for connection between them, hang them up through both the upper and lower spring, and rotate the cavity by a motor when vibrating. The vibrating frequency can be changed by an inventor, in this way, we can find out the highest erosion rate at resonance frequency.

We can vibrate one cavity for 3~4 hours at each time, and get the maximum erosion rate of 300~400 grams/hour. Or, vibrating multi-cavities putting them on a larger board in one process, which may give us a higher efficiency.

In this context, an ingenious source is discovered for tumbling process and performed the preliminary tests to study a various parameters in order to erode internal surface of mono cell cavity. This project is based on the tumbling process of cavity using a small vibrator. Hence internal defected layer of cavity could be eroding uniformly leaving a very smooth inner surface. These cavities could be used for the development of an accelerator. To do this, it was required to develop a tumbling platform, a vibrator and a test cavity. Firstly, the methodology provides to use various types of abrasive materials [e.g., Silicon Carbide (SiC), Yttria stabilized Zirconium oxide balls (ZrO₂-Y)], water level in side cavity in order to observe the erosion rate and uniformity. The preliminary results are focused on adjusting various parameters to achieve best result. The erosion rate measurement has been done using single cavity tumbling, two cavities and also three cavities simultaneously on a vibrator. Efficiency of abrasive media like number of filled SiC as a function of most effective time (in hours) has been tested to see differences in erosion rate. All the parameters are taken into consideration, guidelines and results from previous measurements using vibrator, improving the design and position of the tumbling plate of vibrator, frequency of vibrator with the research on abrasive material performance in order to determine maximum erosion rate and the uniformity inside the cavity.

Mechanical Finishing Process: Mechanical grinding is a powerful method to remove manufacturing defects of internal surface. Resonator is treated in order to remove damaged surface layer and to polish the internal surface which arose due to spinning process. For the purpose, mechanical treatment was performed by means of Vibrator. The vibrator is purchased from Italvibras g. silingradi, Fiorano (MO), Italy. Type: MVS1 15/35-S02, Series: AA, power 3 kW, operating temperature is up to 120 °C, and working frequency is between 180 to 220 Hz. A complete set up of cavity tumbling process on vibrator is shown in Figure 3.6 (top figure) while lay out of vibrator is shown in bottom figure.

Highest performance requires optimized procedure. The knowledge and mastering skills of these technologies become even more important since large scale production involves in industry. In this sense, a complete set of technique for the cavity tumbling method has been tested via several systematic steps by applying a certain configuration to the cavity and measuring final weight as a function of most effective tumbling time. A Cavity during tumbling in inclined position on tumbling stand is shown in Figure 3.7.

Several cavities are tumbled to corroborate this technique. It is found that cavities are defect less after removing about 10 grams of inner surface. We have used mixture of Silicon Carbide (SiC) and Yttria stabilized Zirconium oxide (ZrO₂-Y) balls as an abrasive agent pieces so called medium for tumbling these bulk Nb, Cu and Fe cavities. However, most of the time SiC has been used as an abrasive agent pieces along with DI water and a drop of detergent.

SiC erodes defected inner surface while ZrO₂-Y polishes internal surface. The resonators are filled with the abrasive agent pieces up to the neck of cavity, also deionized water added with a drop of surfactant then plugged up and fixed to the tumbler-machine. The tumbler makes the cavity vibrate and rotate slowly for more than 3 hours so that the abrasive agent pieces could erode the metal surface in a uniform way. Hence the treatment reduced fabrication scratches and contaminations. The advantage is less chemical process required.

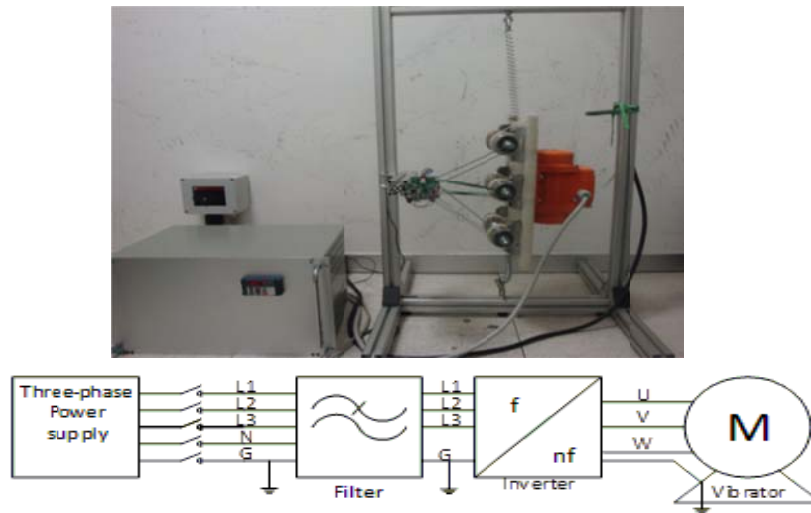


Figure.3.6. Top figure: Cavity mounted on plate and attached to vibrator is shown in top. Bottom figure: lay out of vibrator is shown.

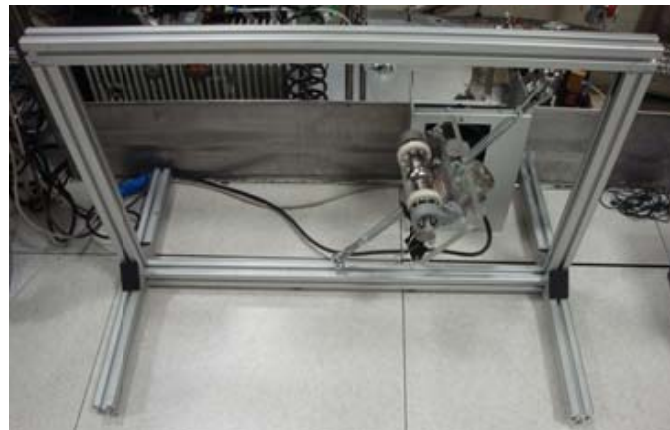


Figure 3.7: 6 GHz cavity during the process on tumbling stand

After tumbling, cavities are cleaned in ultrasonic bath about 1 hour (each cycle is of 30 minutes). Firstly with detergent (RODACLEAN having pH=12) and later on using DI water to remove residual SiC+ZrO₂-Y-residuals from the inner surface of cavity. Then flushed with ethanol and dried using N₂ gas. Finally cavity is weighed. Hence, removed defected inner materials are calculated by subtracting the initial weight.

Overall systematic procedures in each cycle of tumbling are as follows;

1. Ultrasonic cleaning for 1 hour (each cycle is of 30 minutes). Firstly with detergent then in DI water. Then rinse with ethanol and dry with N₂. Weigh the cavity. Optical Inspection of inner surface of cavity.

2. Fill abrasives in resonators, add DI water and a drop of detergent then plugged up and fixed to the tumbler-plate.
3. Start tumbling on vibrator for about 3 hours which is the most effecting time we have observed so far.
4. Clean in ultrasonic bath for 1 hour (two cycles, each 30 minutes) then rinsed with DI water and ethanol and dry with N_2 gas.
5. Measure the cavity and calculate weight lost.
6. Optical Inspection of inner surface to observe smoothness of surface.
7. Repeat the process for next set of tumbling cavity until required layer of defected surface will be removed.

Optical Inspection:

Before starting tumbling an inner surface picture has been taken to compare surface smoothness after final set of tumbling. A set up for optical inspection is shown in figure 3.8. Our goal is to remove about 10 grams of inner materials. Hence after removing 10 gram we took picture and found that inner surface is defect less, all manufacturing scratches and contaminations are removed, and provides very smooth surface. It is shown in figure 3.9 for one cavity (Number 132). In left figure extremely rough surface and several scratches and Mandrel lines are seen clearly inside red circle and in red dots while in right figure all the scratches removed after several cycles of tumbling living very smooth surface.



Figure3.8: An optical inspection set up for Inner surface of cavities is shown.

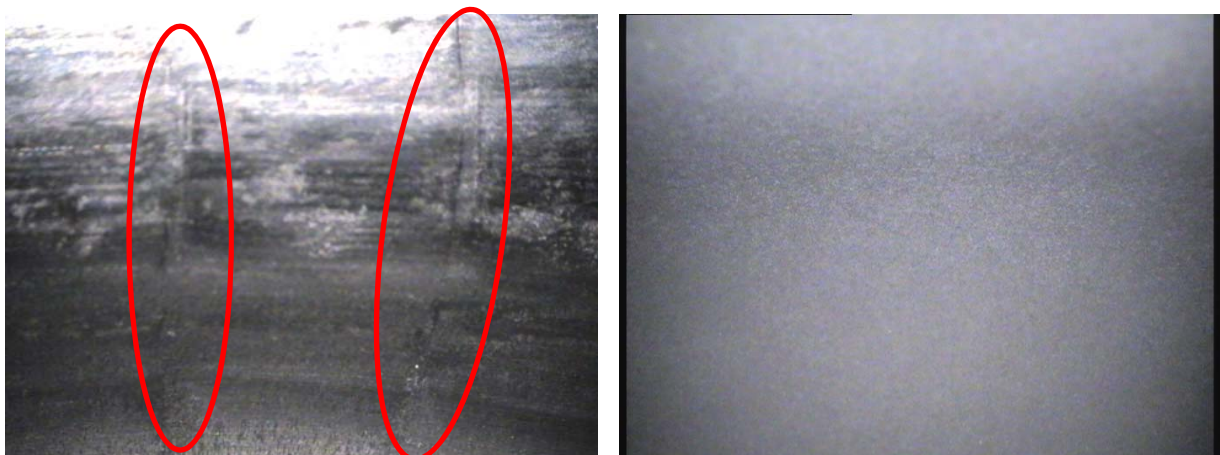


Figure3.9. Inner surface of cavity before tumbling (left fig.), and after tumbling which removed more than 10 grams of defected materials of cavity-number 132 (right figure) are shown. Fig. Nb 130: Image: 720*532 Pixels, Horz. Res: 72dpi, Vert. res.: 72dpi (3*3mm)

3.1.2 Result and Conclusion: Mechanical polishing

In total we have studied eight Nb and one Cu mono cell seamless cavities with different parameters to achieve best tumbling result till date. Series of tumbling process to successive removal of inner materials of cavities using vibrator has been done. However, mechanical finishing is going on for several Nb, Cu cavities. Tumbling results with best efficiency are shown in table 1.

Previously centrifugal tumbler has been used for mechanical finishing of cavities, which is heavy, expensive and dangerous as well. So the centrifugal tumbler could be substituted by Vibrator-tumbling technique, since all required process steps need not more than a week per cavity. Such a technique is simple, cost effective and fast. Results obtained from vibrator seem to indicate that this technique has considerable improvement to increase removal rate of defected inner materials and contaminations of the cavity hence reduces the chemical process.

Table1. Summary of the tumbling results after final set of tumbling, total weight removed from internal surface and the best efficiency achieved under influence of vibrating tumbler are shown in this table.

Cavity No.	Initial Wt. (gram)	Final Wt. (gram)	Total Wt removed (gram)	Max. Efficiency (mg/hr)
127	191,352	181,142	10,21	216
128	177,775	167,365	10,40	413
129	184,483	174,383	10,10	249
130	170,209	159,937	10,27	312
131	175,812	165,686	10,13	242
132	167,89	157,82	10,07	379
133	174,381	164,285	10,1	200
134	168,378	18,386	10,05	226

3.2 Chemical treatment

In this section chemical etching process [Buffered Chemical Polishing (BCP) and the electrolytic polishing (EP)] of niobium will be discussed, as EP allows to improve the accelerating gradients at which the breakdown occurs substantially. Results from previous experimental observations have revealed that there is damaged inner layer of cavities that occurs during various fabrication methods, mechanical deformation or during the mechanical polishing (grinding), which is in the order of approximately 150-200 μm . Such damaged layers must be removed from the inner surface of cavity in order to obtain good RF performance in the superconducting state. For example, Nb has a natural Nb_2O_5 -layer with a thickness of about 5 nm. Below this natural layer other oxides and suboxides can be found [33]. Nb_2O_5 is rather inert and can be dissolved only with hydrofluoric acid (HF). HF is an essential ingredient, in order to remove defects during the manufacturing process by dissolving either the defective material itself or the surrounding niobium. In this case, the most probable defects could be abrasive particles during mechanical finishing process, imprints from the mendral, niobium protrusions from scratches or dirt particles on the surface. Therefore, Cleaning the niobium surface with chemical or electro-chemical process is the most appropriate scientific way to achieve reproducible conditions of good RF performance on inner surfaces of TESLA cavities. These wet chemical processes can be applied safely to

niobium cavities, by obeying the security and environmental standards regarding HF-containing acid mixtures. Various gases, i.e., nitrous gases, oxygen and hydrogen can be produced during etching or electropolishing (EP)¹.

There are two techniques of chemical polishing (etching) empirically found to produce best results for the treatment of niobium cavities. Therefore, cleaning (ultrasonic) followed by few cycles of chemical and electro-chemical process have been done to the resonators. Chemical etching is done by using acid mixtures. A standard chemical treatments are performed in our laboratory is fast static BCP for about 5 minutes then either long BCP or EP process for about 3 to 5 hours, where the solution circulates in a closed circuit that removed inner defected layer thickness of cavities between 200 μm to 400 μm .

3.2.1 Light BCP

Buffered Chemical Polishing (BCP): Fast BCP is done for approximately 5 minutes to remove highly contaminated surface as a pre cleaning tool. Usually two up/down cycles are done, where each cycle takes about 2 to 3 minutes. A Nb cavity has to be chemically etched in order to remove most probable surface damage and residuals due to cavity fabrication and mechanical grinding process, or any other effects of previous treatments. There are two techniques of BCP (1:1:2) are implemented in our laboratory to produce best results to the cavities. Firstly, light BCP applied to all cavities, which consists of Hydrofluoric acid, HF (48%), Nitric acid, HNO_3 (65%) and Phosphoric Acid, H_3PO_4 (85%) acids solution in the volume ratios 1:1:2 respectively. Secondly, long (flux) BCP for 3 to 5 hours.

Chemical etching is done by using these mentioned acid mixtures. The cavity is fastened at top flange with Nb wire, and initially cavity is immersed inside acid solution bath. One has to hold the Nb wire and immerse cavity and pull out (push-pull vertically) from the bath of acid solution slowly and carefully for about 2-3 minutes, then change the orientation of cavity (by fastening Nb wire at other end of cavity) and do the same for 2-3 minutes in order to evacuate properly the contaminations, residuals and hydrogen that was produced during the previous process. In this system, inner and outer surface of cavity is completely immersed inside acid solution, hence cavity is cleaned from inside and outside as well. The essential component of this chemical solution is hydrofluoric acid, which is responsible for etching niobium pentoxide off the niobium surface. Since HF dissolves pure niobium very slowly. Therefore, a strong oxidising acid is added to the mixture, which re-oxidises the niobium [34]. The oxide will be dissolved by the HF again. The bare Nb surface oxidizes via reaction with NO_3 . The mixture solely of HF(48%), HNO_3 (65%) reacts with niobium at room temperature very strongly and heats up rapidly. In order to have better process control over the reaction, a buffer substance like H_3PO_4 with a concentration of 85% [35] is added to the solution, hence the solution is cooled to temperatures below 15 C which not only reduces the migration of hydrogen into the niobium material [36], but also dilutes solution. And viscosity of solution increases all that helps slowing down the reaction.

The reaction of niobium pentoxide with hydrofluoric acid is strongly exothermic, and the product of reaction depends on the concentration of the hydrofluoric acid. For solution with high concentration of hydrofluoric acid a heptafluoroniobic acid, H_2NbF_7 , is formed, for diluted solutions oxipentafluoroniobic acid, H_2NbOF_5 [38]. The most frequently used oxidising agent for niobium is nitric acid (HNO_3), during BCP treatment the niobium stripped of its oxide reacts with nitric acid, HNO_3 . The reaction is also strongly exothermic with brown gas, NO_2 , being released. It was found empirically that the temperature of solution must always be below 15 C, in order to avoid hydrogen contamination of Nb.

¹ A review including many references into the preparation of niobium cavities is given in [37].

In other words, Nitric acid is an oxidizing agent on niobium surface. Hydrofluoric acid reduces the niobium pentoxide into a salt that is soluble in water. Phosphoric acid acts as a moderator for the chemical reaction giving rise to a less turbulent and more controllable reaction. In this way, ultimately, the purity of the sample surface increases. Immediately after the BCP, cavities are rinsed with low pressure ultra-pure water then with High Pressure Rinsing (HPR) for 10-15 minutes then rinsing with acetone or ethanol and drying with nitrogen, and is weigh and proceed further step of chemical process, either long BCP or EP.

In this process, about 40-50 μm is removed. The removal rate is approximately 1 $\mu\text{m}/\text{min}$. The material removal rate is very high and is strongly depends on the contents of HF as well as the temperature of the acid mixture. The chemical etching is done without magnetic stirring and ice cooling.

Advantages of light BCP are: Inner and outer surface of cavity has less contaminations. In fact, at first sight, most of contaminations, defects and residuals from grinding materials like SiC are removed by this process. Hence, in clean environment less chemical or EP process required.

The cavities are rinsed with low pressure ultrapure water immediately after the chemical treatment.

3.2.2 Long BCP

The acid solution recipe for this type of chemical etching process is exactly similar as it is explained above under fast BCP process. However, polishing technique is different. During fast BCP, one has to immerse cavity inside the bath of acid solution and push-pull vertically by holding Nb wire for about 5 minutes, while in long BCP process the solution circulates inside cavity in a closed circuit. In the pulsed mode system, the acid flux is directed from the bottom to the top of the cavity. A simpler version for vertical BCP has been developed at INFN, Legnaro. The schematic of the setup is presented under EP section (figure 3.10). The only modification is needed for BCP is removal of electrodes, otherwise, same configuration continues. Using such type of set up saves lots of chemical, time, and reduces man power, danger risk, and data collection is rather much faster.

Therefore, after light BCP cavities are subjected to further chemical etching so called long BCP (or flux BCP) by using an acid mixtures which contains 1 part HF, 1 part HNO₃ and 2 parts H₃PO₄ in volume, where the solution circulates in a closed circuit chemical system for about 3 to 5 hours in order to remove few hundreds of defected inner layer along with contaminations of cavity. In this system, the acid is pumped from a storage tank through a cooling system, a filter then the cavity finally back to the storage tank. The gases produced are not released into the environment without prior neutralization and cleaning.

In this process, about 300 to 500 μm is removed. The removal rate is approximately 1 $\mu\text{m}/\text{min}$. The material removal rate is very high and is strongly depends on the contents of HF as well as the temperature of the acid mixture. A mixture of HF (40%) and HNO₃ (65%) removes 30 μm per minute [39]. As these reactions are strongly exothermic and large quantities of gases (hydrogen, nitrous gases, HF) are produced this mixture is not applicable to large surfaces. The chemical etching is done without magnetic stirring and ice cooling.

The drawback of BCP process could be explained, as the acid attacks preferentially at the grain boundaries and therefore the surfaces are not very smooth as they could be achieved with electropolishing (EP). There exists step height between adjacent grains which is roughly about 10 μm , while well EP treated has less than 1 μm [40].

Just after the BCP process, firstly, cavities are rinsed with low pressure ultra-pure water then with HPR for 10-15 minutes followed by rinsing with acetone or ethanol, flushed with nitrogen gas, weigh, sealed in a plastic bag and carried inside the cleanroom (class 100) in

order to assemble cavity on RF insert (ie, RF antennas are assembled on cavity flanges using Kapton^R as a gasket) for RF test.

3.2.3 Electro-polishing (EP), and Optical Inspection

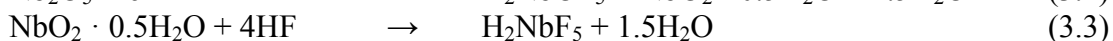
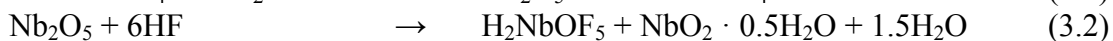
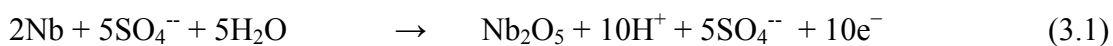
An Electro-polishing (EP) is an alternative technique. EP of Nb cavities has been known for more than 40 years. The most widely used electrolyte is a mixture of concentrated HF(48%), and concentrated H₂SO₄ (96%) in volume ratio of 1:9 [41]. Chemical etching investigation over niobium surface revealed that the surface of electro-polished samples is more smoother than that of BCP treated samples. A pulsed electric current is used in a vertical EP setup for superconducting niobium monocell cavities. During electro-polishing the oxidation of the niobium surface is enhanced by applying a positive potential to the cavity surface. Thus electropolishing can be considered as a continuous oxidation (anodizing) and HF etching. During the process, the material is removed in an acid mixture under flow of an electric current. Sharp edges and burrs are smoothed out and a very shiny, mirror like surface can be obtained. A complex horizontal electropolishing setup, in which the cavity is half-filled with acid and rotates during electropolishing, was developed by K. Saito [42]. A simpler version of vertical electropolishing was developed at INFN, Legnaro. The schematic of the setup is presented in Figure 3.10. Using such type of set up saves lots of chemical, time, and reduces man power, danger risk, and data collection is rather much faster. The EP parameters used for 6 GHz mono-cell cavities are presented in Table 3.2 .

The simplest idea is to assume that a current passing through the electrolyte experiences a higher viscosity and resistivity than the rest of the liquid. For a rough surface the thickness of the film varies. Above protrusions it is thinner and hence the resistivity lower. Therefore the current density becomes higher at these places and they dissolve faster. The time needed to form this layer is typically in the order of milliseconds.



Figure3.10: Chemical and electro-chemical layout for BCP and EP process at INFN/LNL

The chemical processes are summarized as follows [43], [44]:



In our laboratory, vertical EP system is used for 6 GHz mono cell Nb cavities. However, horizontal EP system is used widely for accelerating cavities, due to numerous advantages: most notably all produced gases (mainly hydrogen) can be kept away from the niobium surface [45]. This avoids concentration inhomogeneities in the viscous layer. Gas bubbles sticking on the surface would produce etching pits. In a vertical setup these bubbles would slowly move upwards along the upper half cell's surface and cause radial wells [46]. A disadvantage of the horizontal arrangement is that the cavity has to be rotated. It is not trivial to achieve a leaktight rotary sleeve for these acid mixture. Also, the speed of the removal is reduced by a factor of two as the surface is immersed only half of the time in the acid to allow the hydrogen gas to escape through the upper part of the beam tube.

Few international research group have convincingly demonstrated that EP raises the accelerating field by more than 7 MV/m with respect to BCP, while electropolished cavities suffer a clear degradation when they are subjected to a subsequent BCP [47]. Hence there is strong evidence that electropolishing is the superior surface treatment method. The typical steps between adjacent grains are less than 0.5 μm for electropolishing, and are about 10 μm for BCP treated samples. The major advantage of this method is a much improved control of the chemical reaction, as a further control parameter namely the electric voltage is introduced. The electrical field is high at protrusions, so that the niobium will be dissolved first. On the contrary in the grain boundaries the field is low and no material will be removed. The basic ingredient in all theories is a viscous layer of electrolyte forming near the anode [48] which is the basis for the smoothening effect.

Table 3.2 : EP parameters for 6 GHz mono-cell cavities at INFN/LNL

Acid Mixtures: HF(48%), H ₂ SO ₄ (96%)	10% 90%
Voltage	5-20 V
Current	3-7 A
Temperature of electrolyte	30-35 C
Acid flow	6 liters/min
Removal rate	0.5 $\mu\text{m}/\text{min}$

An overview of the working system / procedure and precautions: Very strong acid mixture is used during the EP, therefore, only a few materials are possible to use during the process. Especially for HF only fluoroplastics are applicable. All parts in contact with the acid should be either made from PFA (Polyperfluoroalkoxyethylene), PVDF(Polyvinylidene Fluoride) or PTFE (Polytetrafluoroethylene, also called Teflon®). The whole system has to be placed in a vented area where the exhaust gases are pumped through a neutralisation system to avoid any environmental hazards. The acid mixture should be used in a closed-circuit, as this is a much safer procedure. The electrolyte is stored in containers clad with Teflon which can be cooled via cold water flowing through Teflon-covered piping. The volume above the electrolyte can be covered with dry nitrogen to avoid a degradation due to water vapour absorption by the strongly hygroscopic H₂SO₄. The acid mixture is pumped with a membrane pump through a cooler and a filter with 1 μm pore size before it reaches the inlet of the

cathode. Then the electrolyte flows through the cathode to the center of the cell. The acid flows back to the storage tank via an overflow. After the cavity is installed vertically in the system with the cathode, the pump will be started to fill the cavity with electrolyte. The acid mixture attacks the niobium very slowly when no voltage is applied. Typically less than 1 nm per hour is removed without applied voltage. After the equilibrium filling level is reached, the rotation is switched on and a leak check is done. When the current is switched on, the current-voltage characteristic is measured quickly. The voltage applied is increased in steps of 1 V and the current is measured. After this preparation the voltage is set to the value where the current oscillations are at a maximum. The temperature has to be around 30 – 35 C during the EP. When the desired amount of material has been removed, the current is switched off. The rotation is stopped and the cavity is put into vertical position to empty the acid from the resonator. Then the cavity is dismounted along with the electrode and rinsed with ultra pure water then rinsed with HPR to remove remaining chemical residues. After the HPR rinsing the wet cavity is kept into a glovebox with nitrogen atmosphere. A rinsing with filtered butanol is applied to improve the drying process. The cavity is then carried inside the cleanroom (class 100) in order to assemble cavity on RF insert for the cryogenic test.

The niobium cavity is used as the anode and pure aluminium cathode is used in our system which is typically made from pure 1100 series of aluminum. Since a copper electrode has a disadvantage: While the current is flowing, the copper surface becomes passivated and is not attacked by the acid mixture. But when the current is switched off copper ions can be dissolved and can precipitate on the niobium. It was observed in a test that this leads to an increased residual resistance and to strong field emission level below 10 MV/m. Therefore a further rinsing step was introduced at CERN after the first low pressure water rinsing after EP. The cavities are now rinsed in sequence with concentrated HNO₃ (60 %), water, HF and water again. These steps are repeated twice. The HNO₃ removes the copper and oxidises the niobium. Hydrofluoric acid removes the oxide layer and several contaminants as indicated by surface studies [49].

Overall procedures are summarized below;

- washing with few drop of Rodaclean (pH 12) and ultrapure water in ultrasonic bath (60 min)
- washing with deionized water in ultrasonic bath (60 min)
- rinsed with low pressure ultra-pure water
- drying with nitrogen
- Static BCP for about 5 minutes
- EP flux to remove about 200 micro-meter (4-5 hrs) or BCP flux (3-5 hrs) in the acid solution: For EP: HF(48%), and H₂SO₄ (95%) , 1:9. For BCP: HF/HNO₃/H₃PO₄, 1:1:2
- rinsed with low pressure ultra-pure water
- Ultrasonic cleaning (1 Hr) and High pressure cleaning (15 min.)/
- drying with nitrogen inside class 10 clean room
- Mounting cavity on RF stand inside clean room (class 1000).

Soon after the Electro-polishing, cavities are rinsed with low pressure ultra-pure water then with HPR for 10-15 minutes followed by rinsing with acetone or ethanol, flushed with

nitrogen gas, weigh, sealed in a plastic bag and carried inside the cleanroom (class 100) in order to assemble cavity on RF insert (ie, RF antennas are assembled on cavity flanges using Kapton^R as a gasket) for RF test.

Due to the wet chemical processes and the several rinsing treatments, water sticks on the surface in abundance of the cavity. All that leads to the degradation of the quality factor at high accelerating fields, however, heating treatment plays an essential role to cure this degradation, which will be discussed in chapter 4 (Thermal treatment: An Induction method).

Optical Inspection

After the BCP or EP process we have done optical inspection of inner surface of cavities to observe smoothness of surface. And found very smooth mirror like shining surface after EP. It is shown in figure 3.11

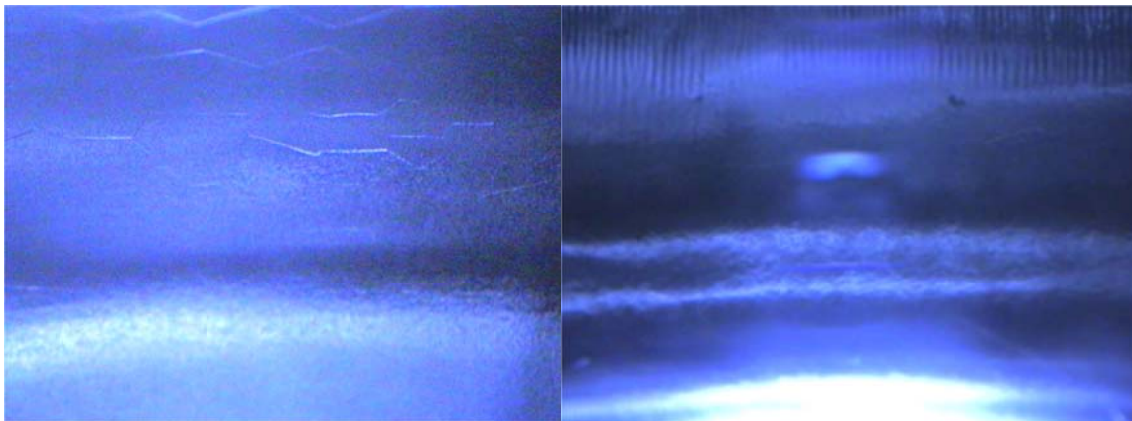


Figure 3.11: An optical inspection of inner surface of cavity has been done (cavity identification number Nb122) after EP. Left figure is at equator while right figure is captured near iris of cavity.

3.3 Cleaning methods: Ultrasonic process and High Pressure Rinsing (HPR)

Ultrasonic process

Ultrasonic process is the initial stage to clean residuals, contaminations from the inner surface of cavities that arose due to mechanical or (electro-) chemical treatments. Firstly, cleaning has been done with ultra-pure water and surfactant and then using ethanol or, in low pressure water jet followed by ultrasonic cleaning in ultrapure water. It is very important to clean polished surface carefully in order to obtain good RF performance. Chemical procedure for cleaning cavities, samples, or fine polished surface is discussed in terms of degassing and sonic process.

There are two steps to clean these components, Degassing and Sonic Process. *De-gassing process to the cleaning fluid medium (without emerging polished electrodes inside solution) must be done before Sonic Process.* So that many dissolved gasses, micro bubbles present in solution will be removed.

In absence of degassing process there are two incident occurs during the sonic process. First, the diffused air bubbles present in the solution will produce micro-explosion at the surface of electrode that could damage the surface of material. Second, the dissolved gasses absorb the ultrasonic energy, and hence reduce ultrasonic action.

Degassing Procedure: At first, the degassing process should be done for 5 minutes to the chemical (i.e., Ethanol, Propanol) which is supposed to use as cleaning fluid medium for the cavities or sample. Here, solution is without electrodes in the ultrasonic bath for 4-5 minutes

at degassing mode.

Sonic Procedure: In degassed solution, cavities or samples or any fine component could be cleaned at sonic mode for 10-60 minutes or more as per requirement at room temperature.

During the ultra-sonic process, operating frequency is about 40 kHz, so proper care should be taken to avoid the surface damages of the polished surface due to the vibration. Also, exhaust tube should be kept at the top of the bath to prevent the hazardous effect from the ethanol fumes. Once the cleaning time is over, turn OFF power supply of bath. Take out the cavity from the bath by wearing the *La-tex* gloves (powder-free) and rinse the inner surface of cavity or diamond turned face of the Electrode using absolute ethanol while the face of cavities or electrode must be upward. Place the cavity under the Laminar flow workstation for drying about 5-10 minutes. The ultrasonic system is integrated in a clean-room facility.

Overall cleaning procedure for polished surface is as follows:

- Before starting the cleaning process, Branson ultrasonic cleaner bath should be cleaned with ethanol by using tissue (WIPES- disposable bactericidal cleansing tissue sachets) papers.
- Initially bath should be filled either ultrapure water or with required liters of 96% purity of ethanol up to the operating level and place the cavity or electrodes vertically in the mesh basket (removable). The basket should be immersed in ethanol solution. Switch ON power to the bath.
- While cleaning the component, exhaust tube should be kept at the top of the ultrasonic cleaner to prevent the hazardous effect from the ethanol fumes.
- Once cleaning time is over, take out the oscillator from the bath. Rinse the cavity with absolute ethanol. Place it under Laminar flow workstation for drying about 5-10 minutes.
- Transfer used ethanol from the bath into the empty bottles (labeled them as *used ethanol*)
- Turn OFF power supply to ultrasonic bath.

High Pressure Rinsing (HPR)

One of the most effective process to remove residuals, micro-particle contaminations from the inner surface of cavities is high pressure rinsing (HPR) with ultra-pure water. The resistivity of the water should be close to the theoretically pure (ie, >18 MΩ-cm) and the water inlet should be filtered to eliminate particles > 0.2 μm. Such contaminations, usually lead to electron field emission and quench during rf test. Also, cleaning all the dust particles is still very important to reduce the residual loss that might cause and raise the quench field of the cavities. A special design for holding the cavity and samples alongwith a HPR SS nozzle head having small diameter 0.3mm orifice are developed for cleaning cavities and sample plates. HPR is carried out inside the clean room (class1000) to prevent recontamination.

Particles on the niobium surface cause field emission (explained later in Chapter 2). The effective way to remove dust particles from the cavity inner surface is to rinse the inner surface with ultra-pure de-ionized water under 80 up to 150 bar pressure. The cavity is placed on the holder of the high pressure rinsing set up, and fastened tightly. The cavity outer and inner (mostly) surface is rinsed with ultra-pure de-ionized water at 120 bar pressure. Usually two up/down cycles are done by changing orientation of cavity. Each cycle takes about 5-7 minutes, so that the water jets do not follow the same path on niobium surface. Hence, the potent jets of water are scanned across all parts of rf surface to dislodge and sweep away all microscopic contaminants. The cavity surface comes in contact with filtered air after the final

ultra-pure rinsing. The High pressure rinsing gun is shown in figure 3.12. Table 3.3 summarizes the HPR parameters for tesla type cavities.



Figure 3.12. High pressure rinsing (HPR gun) with a water jet

Table 3.3: HPR parameters for cleaning tesla type cavities

Pressure	80-150 bar
Water flow rate	5-20 liters/min
Filter pore size '0.2µm	0.2 µm
Nozzle diameter	0.3mm orifice
Treatment time	10-15 minutes for 6GHz cavity

After high pressure rinsing the cavity surface is normally left drying by filtered nitrogen gas through the cavity for some minutes inside clean room. After drying, all the cavity ports are sealed, and the cavity is attached cleanly to its test stand in the clean-room class 100 (the detail is given in chapter 5). Following assembly the pumping line to a roughing/turbo pump is connected to evacuate, and cavity is pumped down to $2 \cdot 10^{-8}$ bar as indicated by cold cathode gauge on the pump.

-----*****-----

Chapter 4

Thermal Treatment: Induction heating

Achieving very high quality factor value hence lowest possible surface resistivity and higher accelerating field are the paramount considerations in Accelerator technology. It is well known fact from previous research that higher fields are obligatory for accelerating cavities.

Therefore, further improvement toward the rf performances of resonator by means of high temperature post purification is required. A new technique for purification of bulk-Nb SRF cavities has been developed in order to optimize RF resonators for accelerator technology. Such purification has been accomplished either under cover of He or Ar gas (inert gas) atmosphere for protection or under UHV system. This is the most important goal of the research work reported in this dissertation.

In order to improve RF resonators, theoretical and experimental investigation of Nb properties were reported by several authors [50-62], and continuous effort have been made by numerous research scientist [63-66] after the creation of first SRF cavity. The purity of Nb is improved for the fabrication of SRF bulk Nb cavity under the influence of UHV annealing techniques. For example, purification of Nb have been accomplished by using either Yttrium (Y) or Titanium (Ti) as a solid state getter in reference [63, 64], by this technique a factor of 3-4 improvement in thermal conductivity of Nb have been observed. While in reference [65], Nb sample (two mm thick) has been thermally treated in Ultra-High Vacuum (UHV) to improve Residual Resistivity Ratio (RRR) using solid state gettering with Titanium (Ti). It was observed that the temperature and duration of purification by means of UHV annealing depends on evaporation rate of getter materials and diffusion rate of the impurities. By this technique authors have improved the RRR by the factor of 10. In reference [66] authors examined quality requirements and control process of pure Nb for SRF cavities, and showed that among all metallic impurities in Niobium, Tantalum (Ta) is found to be highly concentrated, typically around 500 ppm, which is due to the similar chemical properties of Nb and Ta and hence difficult to separate Ta from Nb. In this context, at first niobium hydrides cause Q-disease, had been reported in reference [32]. This is caused by the formation of harmful η and ν phases of niobium hydrides termed as Q disease. The harmful niobium hydrides can only form when the concentration of hydrogen in Niobium exceeds 100-200 at ppm. Beyond all other consideration, such a dangerous level of Hydrogen concentration reaches due to following two reasons. Firstly, the mobility of Hydrogen atoms can reach 5 μm /minute at temperatures between 100 and 150 K. A slow cooling process through this temperature region will allow hydrogen to migrate and gather into Niobium. Hence, at some localized regions the hydrogen concentration can exceed 100-200ppm so that the harmful phases can be formed. Secondly, various cavity fabrication steps, during handling and treatments, such as, for examples, machining, tumbling, chemistry and surface polishing can result in an uptake of Hydrogen to Niobium that leads to an increase in Hydrogen concentration in Niobium.

However, after all, there is no experimental information available till date in context of purification technique of SRF Nb cavity under atmospheric pressure at extremely high temperature. This new approach will be useful in particle accelerators application that uses Superconducting Nb for various R&D projects. Also, Purification processes has been done under ultra high vacuum condition, which lead evaporation of metallic impurities and degassing. Both the processes have been discussed. The main topic of this chapter is induction heating, which is a combination of electromagnetic induction, the skin effect, and the principle of heat transfer. In short, induction heating refers to the generation of heat energy by the

current, and eddy current created on the surface of a conductive object (according to Faraday's Law and the skin effect) when it is placed in the magnetic field, formed around a coil, where the AC current flows through (according to Ampere's Law). Detailed descriptions of induction heating system is presented here.

4.1 An Induction Heating (IH) System

Introduction: Induction heating (IH) applied systems are developed using electromagnetic induction which was discovered by a English physicist, one of the most influential scientists in history, Michael Faraday (22 September 1791– 25 August 1867) in 1831. Electromagnetic induction is a heating technique for any electrical conductive materials (for example metal, graphite, glass at high temperature). It is frequently applied in several thermal processes such as heating of metals. Induction heating is a non-contact heating process. It uses high frequency electricity to heat materials that are electrically conductive. Since it is non-contact, the heating process does not contaminate the material being heated. It is also very efficient since the heat is actually generated inside the workpiece. This can be contrasted with other heating methods where heat is generated in a flame or heating element, which is then applied to the workpiece. For these reasons Induction Heating lends itself to some unique applications in industry.

Induction heating is the process of heating an electrically conducting object (usually a metal) by electromagnetic induction, where eddy currents are generated within the metal and resistance leads to Joule heating of the metal. An induction heater (for any process) consists of an electromagnet, through which a high-frequency alternating current (AC) is passed. Heat may also be generated by magnetic hysteresis losses in materials that have significant relative permeability. The frequency of AC used depends on the object size, material type, coupling (between the work coil and the object to be heated) and the penetration depth.

Types of Electric Process Heating: Prior to describing induction heating in more regorous way, some types of electric process heating are mentioned below;

- Resistance Heating
- Conduction Heating
- Infrared Radiation Heating
- Induction Heating
- Dielectric Hysteresis Heating
- Electric Arc Heating
- Plasma Heating
- Electron Beam Heating
- Laser Heating

Here, only Induction heating method is explained which is the main part of this research work. It is an interesting device, allowing one to rapidly heat a metal object. With enough power, one can even melt metal. The induction heater works without the need for fossil fuels, and can anneal and heat objects of various shapes.

Theory: Induction heating is comprised of three basic factors: electromagnetic induction, the skin effect, and heat transfer. The fundamental theory of IH, however, is similar to that of a transformer. Figure 4.1 demonstrates a very basic Induction heating system, which consists of inductive heating coils and current, to explain electromagnetic induction and the skin effect.

Electromagnetic induction: It refers to the phenomenon by which electric current is generated in a closed circuit by the fluctuation of current in another circuit placed next to it. The basic principle of induction heating, which is an applied form of Faraday's discovery, is the fact that AC current flowing through a circuit affects the magnetic movement of a secondary circuit located near it. The fluctuation of current inside the primary circuit generates current in the

neighboring secondary circuit. Mathematically, it can be explained as, when the AC current enters a coil, a magnetic field is formed around the coil according to Ampere's Law.

$$\int Hdl = Ni = F \quad (4.1)$$

$$\Phi = \mu HA$$

When an object kept into the magnetic field causes a change in the velocity of the magnetic movement. The density of the magnetic field wanes as the object gets closer to the center from the surface. According to Faraday's Law, the current generated on the surface of a conductive object has an inverse relationship with the current on the inducting circuit as described in equation (4.2). The current on the surface of the object generates an eddy current.

$$E = \frac{d\lambda}{dt} = N \frac{d\phi}{dt} \quad (4.2)$$

As a result, the electric energy caused by the induced current and eddy current is converted to heat energy as mentioned in equation (4.3).

$$P = \frac{E^2}{R} = i^2 * R \quad (4.3)$$

Here, resistance is determined by the resistivity (ρ) and permeability (μ) of the conductive object. Current is determined by the intensity of the magnetic field. Heat energy is in an inverse relationship with skin depth which is described under Skin Depth below. If an object has conductive properties like iron, additional heat energy is generated due to magnetic hysteresis.

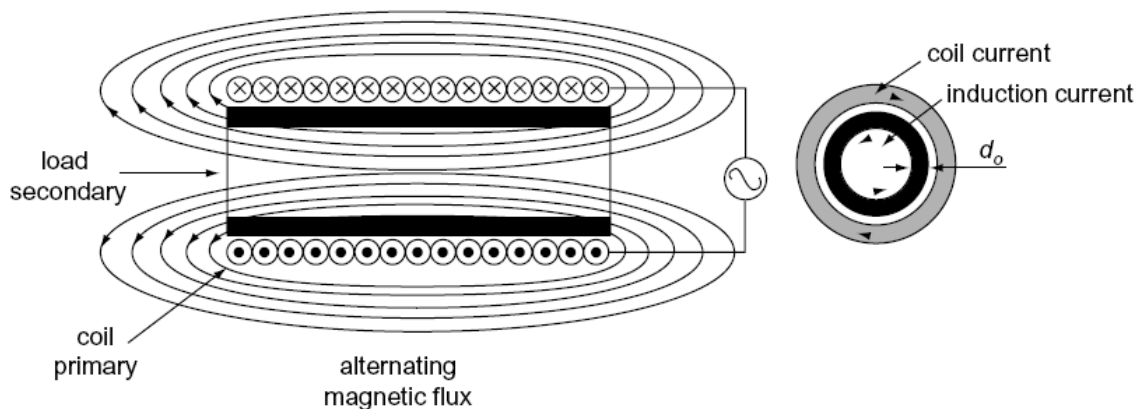


Figure 4.1: The figure demonstrates a very basic Induction heating system, consisting of inductive heating coils and current, to explain electromagnetic induction and the skin effect (d_o).

Moreover, Faraday's Law was followed by a series of more advanced discoveries such as Lenz's Law. This law explains the fact that inductive current flows inverse to the direction of changes in induction magnetic movement. Therefore, IH was first noted when it was found that heat was produced in transformer and motor windings. Accordingly, the theory of induction heating was studied so that motors and transformers could be built for maximum efficiency by minimizing heating losses. The development of high-frequency induction power supplies provided a means of using induction heating for surface hardening. Throughout the years the understanding of the basic principles has been expanded, extending currently into computer modeling of heating applications and processes. Knowledge of these basic theories of induction heating helps to understand the application of induction heating as applied to induction heat

treatment. Induction heating occurs due to electromagnetic force fields producing an electrical current in a part. The parts heat due to the resistance to the flow of this electric current.

All metals conduct electricity, while offering resistance to the flow of this electricity. The resistance to this flow of current causes losses in power that show up in the form of heat. This is because, according to the law of conservation of energy, energy is transformed from one form to another (not lost). The losses produced by resistance are based upon the basic power-electrical formula given in equation (4.3). Because the amount of loss is proportional to the square of the current, doubling the current significantly increases the losses (or heat) produced. Some metals, such as silver and copper, have very low resistance and, consequently, are very good conductors.

Induction heaters are used to provide alternating electric current to an electric coil (the induction coil). The induction coil becomes the electrical (heat) source that induces an electrical current into the metal part to be heated (called the workpiece). No contact is required between the workpiece and the induction coil as the heat source, and the heat is restricted to localized areas or surface zones immediately adjacent to the coil. This is because the alternating current (ac) in an induction coil has an invisible force field (electromagnetic, or flux) around it. When the induction coil is placed next to or around a workpiece, the lines of force concentrate in the air gap between the coil and the workpiece. The induction coil actually functions as a transformer primary, with the workpiece to be heated becoming the transformer secondary. The force field surrounding the induction coil induces an equal and opposing electric current in the workpiece, with the workpiece then heating due to the resistance to the flow of this induced electric current. The rate of heating of the workpiece is dependent on the frequency of the induced current, the intensity of the induced current, the specific heat of the material, the magnetic permeability of the material, and the resistance of the material to the flow of current. Induction heating system involves heating a workpiece from room temperature to a higher temperature, such as is required for induction tempering or induction austenitizing of stainless steel (S.S.). The rates and efficiencies of heating depend upon the physical properties of the workpieces as they are being heated. These properties are temperature dependent, and the specific heat, magnetic permeability, and resistivity of metals change with temperature. Steel has the ability to absorb more heat (i.e., high specific heat) as temperature increases. This means that more energy is required to heat steel when it is hot than when it is cold. At 760 °C steel exhibits an increase in resistivity of about ten times larger than when at room temperature. Finally, the magnetic permeability of steel is high at room temperature, but at the Curie temperature, just above 760°C, steels become nonmagnetic with the effect that the permeability becomes the same as air.

Hysteresis: Hysteresis losses occur only in magnetic materials such as steel, nickel, and a few other metals. As magnetic parts are being heated, such as those made from carbon steels, by induction from room temperature, the alternating magnetic flux field causes the magnetic dipoles of the material to oscillate as the magnetic poles change their polar orientation every cycle. This oscillation is called hysteresis, and a minor amount of heat is produced due to the friction produced when the dipoles oscillate. When steels are heated above Curie temperature they become nonmagnetic, and hysteresis ceases. Because the steel is nonmagnetic, no reversal of dipoles can occur.

Skin Effect and Reference Depth: The higher the frequency of the current administered to the coil, the more intensive is the induced current flowing around the surface of the load. The density of the induced current diminishes when flowing closer to the center as given in equation (4.4) and (4.5) respectively. This is called the skin effect or kelvin effect. From this effect, one can easily infer that the heat energy converted from electric energy is concentrated on the skin depth (i.e., surface of the object).

$$i_x = i_0 \exp^{-x/d_0} \quad (4.4)$$

where, i_x is the distance from the skin (surface) of the object, current density at x ; I_0 is the current density on skin depth ($x=0$); and d_0 is a constant determined by the frequency (current penetration depth or skin depth).

The skin thickness, d_0 is determined by the resistivity, permeability, and frequency of the object, which could be stated as,

$$d_0 = \sqrt{2\rho/\mu\omega} \quad (4.5)$$

where, ρ is resistivity, μ is permeability of the object, and ω is the frequency of the object.

For the induction heating process to be efficient and practical, certain relationships of the frequency of the electromagnetic field that produces the eddy currents, and the properties of the workpiece, must be satisfied. The basic nature of induction heating is that the eddy currents are produced on the outside of the workpiece in what is often referred to as “skin effect” heating. Because almost all of the heat is produced at the surface, the eddy currents flowing in a cylindrical workpiece will be most intense at the outer surface, while the currents at the center are negligible. The depth of heating depends on the frequency of the ac field, the electrical resistivity, and the relative magnetic permeability of the workpiece.

For practical purposes of understanding, the skin heating effect (reference depth) is defined as the depth at which approximately 86% of the heating due to resistance of the current flow occurs. The reference depths decrease with higher frequency and increase with higher temperature. The reference depth, as mentioned, becomes the theoretical minimum depth of heating that a given frequency will produce at a given power and workpiece temperature. The cross-sectional size of the workpiece being heated must be at four times the reference depth.

Magnetic materials: Due to hysteresis, magnetic materials are heated more readily than non-magnetic, resisting the alternating magnetic field within the induction coil. **Frequency:** The advanced technology senses and adapt to the resonant frequency of our configuration automatically, ensuring optimal power transfer to the workpiece. The higher the frequency, the shallower the heating in the workpiece. Since the relationship of the current flow in the workpiece and the distance between the workpiece and the coil is key, hence a close-coupling increases the flow of current, increasing the amount of heat produced in the workpiece.

Parameters to control: There are some important parameters need to control in order to get most efficient result, are summarized below.

- Voltage
- Time
- Sample position
- Pressure of gas
- Temperature
- Type of gas (in the environment)

Working of Induction Heating: A source of high frequency electricity is used to drive a large alternating current through a coil. This coil is known as the work coil. The passage of current through this coil generates a very intense and rapidly changing magnetic field in the space within the work coil. The workpiece to be heated is placed within this intense alternating magnetic field. Depending on the nature of the workpiece material, a number of physical processes takes place. The alternating magnetic field induces a current flow in the conductive workpiece. The arrangement of the work coil and the workpiece can be thought of as an

electrical transformer. The work coil is like the primary where electrical energy is fed in, and the workpiece is like a single turn secondary that is short-circuited. This causes tremendous currents to flow through the workpiece. These are known as eddy currents.

In addition to this, the high frequency used in induction heating applications gives rise to a phenomenon called skin effect (see formula 4.5). This skin effect forces the alternating current to flow in a thin layer towards the surface of the workpiece. The skin effect increases the effective resistance of the metal to the passage of the large current. Therefore it greatly increases the heating effect caused by the current induced in the workpiece. A schematic diagram of IH is shown in figure 4.2. In brief, working of IH can be explained as; in an inductor, an a.c. current, I_1 of suitable freq. flows and creates an alternating magnetic flux. The flux link with any ideal conducting path in the workpiece to be heated, induces an a.c. current I_k . The induced current I_k heat the work piece by Joule effect.

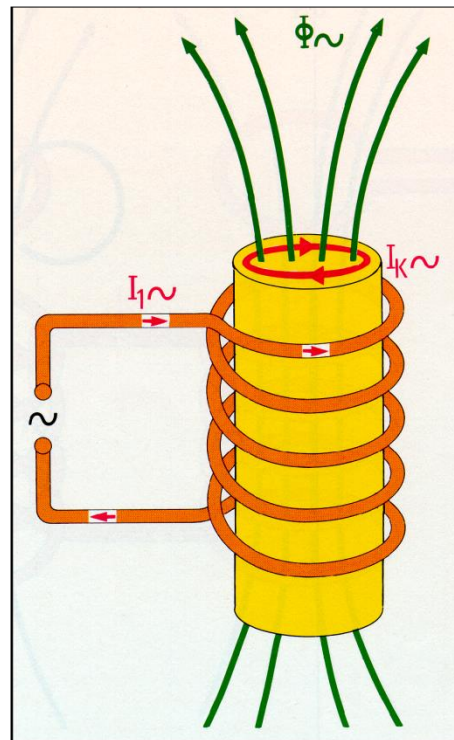


Figure 4.2: A sketch of an Induction Heating system is shown in this figure.

For ferrous metals like iron and some types of steel, there is an additional heating mechanism that takes place at the same time as the eddy currents mentioned above. The intense alternating magnetic field inside the work coil repeatedly magnetises and de-magnetises the iron crystals. This rapid flipping of the magnetic domains causes considerable friction and heating inside the material. Heating due to this mechanism is known as Hysteresis loss, and is greatest for materials that have a large area inside their B-H curve. This can be a large contributing factor to the heat generated during induction heating, but only takes place inside ferrous materials. For this reason ferrous materials lend themselves more easily to heating by induction than non-ferrous materials. It is interesting to note that steel loses its magnetic properties when heated above approximately 700°C. This temperature is known as the Curie temperature. This means that above 700°C there can be no heating of the material due to hysteresis losses. Any further heating of the material must be due to induced eddy currents alone. This makes heating steel above 700°C more of a challenge for the induction heating systems. The fact that copper and

Aluminium are both non-magnetic and very good electrical conductors, can also make these materials a challenge to heat efficiently.

IH equipments: Few things are essential to implement induction heating. In principle, an induction heating plant generally consists the following:

- i. A source of high frequency electrical power: A medium or high-frequency power source combining a frequency converter (generator or inverter)
- ii. A working coil to generate alternating magnetic field, inductor
- iii. An impedance matching network
- iv. An electrically conductive workpiece to be heated,
- v. A positioning and handling system for the part to be heated,
- vi. A water cooling system for the power source, the matching unit and possibly the inductor,
- vii. A plant control panel.

For example, an impedance matching network is often required between the High Frequency source and the work coil in order to ensure good power transfer. Water cooling systems are also common in high power induction heaters to remove waste heat from the work coil, its matching network and the power electronics. Finally some control electronics is usually employed to control the intensity of the heating action, and time the heating cycle to ensure consistent results. The control electronics also protects the system from being damaged by a number of adverse operating conditions.

Magnetic materials improve the induction heat process because of hysteresis. Materials with high permeability (100–500) are easier to heat with induction heating. Hysteresis heating occurs below the Curie temperature where materials lose their magnetic properties. High permeability below the Curie temperature in the workpiece is useful. Temperature difference, mass, and specific heat influence the workpiece heating. The energy transfer of induction heating is affected by the distance between the coil and the workpiece. Energy losses occur through heat conduction from workpiece to fixture, natural convection, and thermal radiation. The induction coil is usually made of copper tubing and fluid cooled. Diameter, shape, and number of turns influence the efficiency and field pattern.

Operating principle: Induction heating results from the direct application of two physical laws, the Lenz law and the Joule effect: any electrically conductive material placed in a variable magnetic field (generated by an exciting winding called inductor) is the site of induced electric currents, called eddy currents. Due to the Joule effect ($P = I^2 \cdot R$), these currents dissipate heat in the material in which they appeared. In order to transfer a maximum amount of energy to the part to be treated, the heat generated in the material implies a quick response and a high efficiency. Several parameters must be taken into consideration:

- The respective position of an inductor and a part to be treated (coupling, respective-lengths).
- The supply frequency and the skin effect which characterize the dispersion of the induced current throughout the part: the higher the frequency, the closer to the surface the induced currents will concentrate. This fundamental notion is determined by the penetration depth, also referred as skin thickness.
- The magnetic (relative permeability μ_r), electrical (resistivity ρ) and thermal (conductivity) properties of the parts to be heated, most of which vary in accordance with the temperature.
- The type of inductor (geometry and technology).

Advantages of IH: Induction heating offers several inherent advantages which explain not only its constant market development but also in scientific research in laboratory. The major advantage of this system are summarised below;

- Contactless heating: absence of pollution from the source of heating.
- High power densities in a wide range of frequency and consequent short heating times: heating speed linked to the possibility of obtaining very high power density, exact location of the heating effect thanks to the inductor design and an operating frequency perfectly adapted to the part to be heated,
- Bulk or surface heating
- Melting with stirring
- A process perfectly adapted to industrial medium-sized and mass production requirements
- Easy automation of equipment,
- Absence of thermal inertia (rapid start-up),
- Repeatability of operations carried out,

Applications of IH: Induction heating can be used for various applications of thermal treatment of an electrically conductive material in a clean, efficient and controlled manner. For example, such as; for sealing the anti-tamper seals that are stuck to the top of medicine and drinks bottles. It is also widely used as "getter firing" to remove contamination from evacuated tubes such as TV picture tubes, vacuum tubes, and various gas discharge lamps. The getter absorbs any last remaining traces of gas inside the vacuum tube and increases the purity of the vacuum. Another common application for induction heating is a process called Zone purification used in the semiconductor manufacturing industry. This is a process in which silicon is purified by means of a moving zone of molten material. Other applications include melting, welding and brazing of metals. Metal hardening of ammunition, gear teeth, saw blades and drive shafts are also common applications because the induction process heats the surface of the metal very rapidly. Therefore it can be used for surface hardening, and hardening of localised areas of metallic parts by "outrunning" the thermal conduction of heat deeper into the part or to surrounding areas. The non contact nature of induction heating also means that it can be used to heat materials in analytical applications without risk of contaminating the specimen. Similarly, metal medical instruments may be sterilised by heating them to high temperatures whilst they are still sealed inside a known sterile environment, in order to kill germs.

4.2 Atmospheric pressure annealing

The production of Nb (and another refractory metals) is complicated by the fact that, at elevated temperatures, it reacts with all gases (except the inert gases, such as helium and argon). A heat treatment of refractory metals must be carried out either in ultra high vacuum or under a pure inert gas @ atmospheric pressure (under a protective atmosphere). In this section atmospheric pressure treatment has been discussed.

4.2.1 Basic idea

Hydrogen contamination of the niobium generated during the EP or even BCP (if acid solution temperature too high) must be driven out by a furnace treatment. In this context, an atmospheric pressure purification has been done either under protection of He or Ar gas atmosphere to reduce the hydrogen concentration to below a few atomic ppm in the bulk. Also, the thermal treatment is generally believed to help relieve stresses and dislocations introduced by mechanically rolling and deep drawing of the sheet niobium metal.

Choosing the proper annealing conditions is important to produce the correct grain size near 100% recrystallization and keep the highest possible purity (RRR). Recrystallization of Nb. That means lattice has less defects and become less vulnerable to a new hydrogen contamination. One of the most significant characteristic of niobium is its ability to react actively with the gases H₂, N₂, O₂, H₂O, CO, CO₂. In the solid state, the elements H, N, O and C are dissolved interstitially in niobium. The maximum solubility of the interstitials is relatively large at elevated temperatures and decreases with according so that either precipitation of compounds occurs or the corresponding liquid enriched in gases at equilibrium with the α -solid solution is formed. For both the solid and the liquid, the concentration of the impurities at a given partial pressure decreases with increasing temperature.

In order to prepare the niobium cavities for thermal treatment, mechanical finishing has been done either with centrifugal barrel polishing or using vibrator then fast BCP treated followed by either flux BCP or EP and finally rinsed with ultrapure high pressure rinsing. Thereafter, the samples or cavities were placed inside inductor under the influence of the voltage, time, sample position, temperature, and pressure of pure ⁴He and Ar gas for protection.

4.2.2 Experimental setup (at atmospheric pressure):

Induction System: The seamless superconducting mono cell cavities were etched and RF tested before the first annealing process. In next step, to improve performance of RF superconducting resonators an induction heating method has been employed which allows direct heating either on samples or cavities that reaches temperatures higher than 2600°C. In UHV system contamination comes mainly from the sources of residual gas (i.e., leaks: real and virtual from atmosphere, bulk diffusion, desorption, back streaming from pump etc.). However, we cannot claim that quartz tube is completely clean and perfectly light system. Nevertheless, clean quartz tube has fewer contaminations than UHV chamber. The sketch of an experimental system is assembled for the induction heat treatments as shown in figure 4.3. Therefore, the induction system that consists of a Quartz tube of length 1 meter and diameter about 8 cm has been used.

Moreover, the system of quartz tube has several advantages in comparison to the other heating systems or infra-red heating in UHV system. For example, Clean quartz tube is transparent for IH, where contaminations are not found from chamber or alumina crucible, it takes short operation time of thermal treatment (few minutes or seconds), reaches very high temperature around 2700°C in short time, allows direct heating on samples or cavities reaching very high temperatures around 3000°C. On the contrary, the infra-red heating reaches no higher than 1100°C.

High temperature treatment procedure: At first, all components used during atmospheric treatments are cleaned in ultrasonic, dried with N₂ gas then assembled all components inside quartz tube. The cavity is centered against the induction coil but cavity is in static position (not rotating during heating), and electrically insulated. Induction coil is connected to the work head (Ameritherm model), an induction heating systems for 124-150 kHz range that provide reliable and repeatable solutions for high-speed heating of smaller parts. The work head connected with the power supply Eko Heat brand, where time and voltage are controlled, and approximately 15kW of maximum power allowed in the system. The chamber of Quartz tube is sealed with Viton O-ring to the aluminum flanges at top and bottom. The bottom part of quartz tube is fluxed with extra-pure helium gas or other inert gas few minute before heating and flushing continues even after power supply is switched off for about 5 minutes to cover cavity, hence to prevent oxidation by the atmospheric gases in the tube which protects the inner and outer surface of cavity before, during and after the thermal treatment. The water cooling system

turned on for cooling induction coil, work-head and power supply. Soon after power supply is switched on, and power to the coil increased manually starting from few watt up to 13 kW quickly (say in 30-40 seconds or few minutes, depends on treatment goal) which reach above 2000 °C. At maximum temperature cavity is left to heat for some seconds upto few minutes then power supply is switched off. Cavity needs relatively more time to approach maximum temperature due to the heat exchange at atmospheric pressure. Pyrometers (Pyrospot DG 10N and/or DS 10N model) are employed to read the temperatures between 250-1300°C and 900-3000°C respectively.

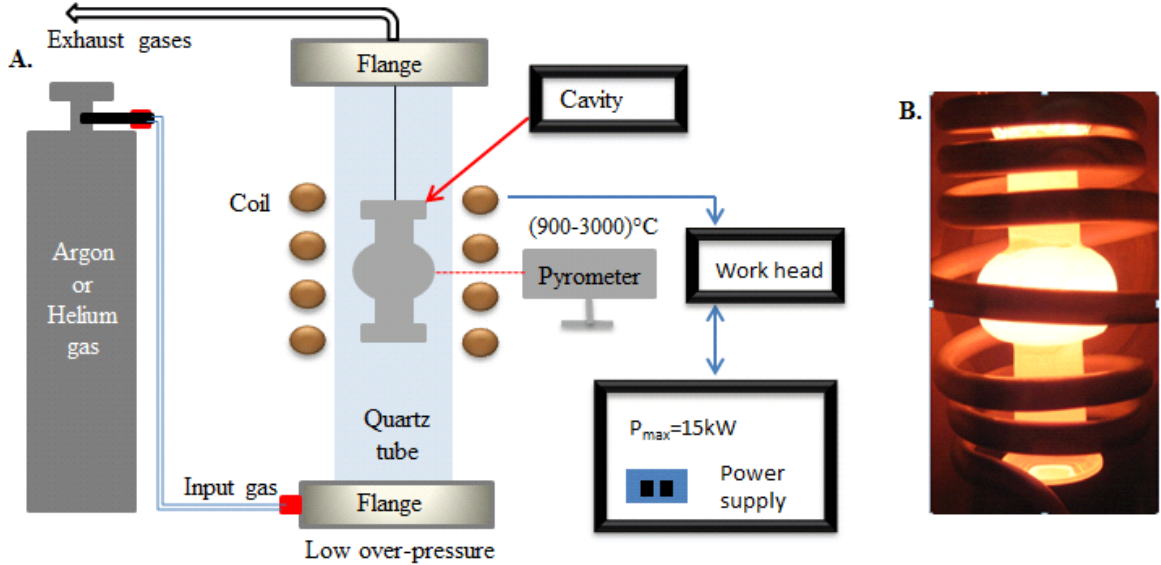


Figure4.3: Fig. A: Experimental Setup/ Sketch of the system: Induction heating at atmospheric pressure. **Fig. B:** Cavity during high temperature annealing inside induction coil and Quartz tube.

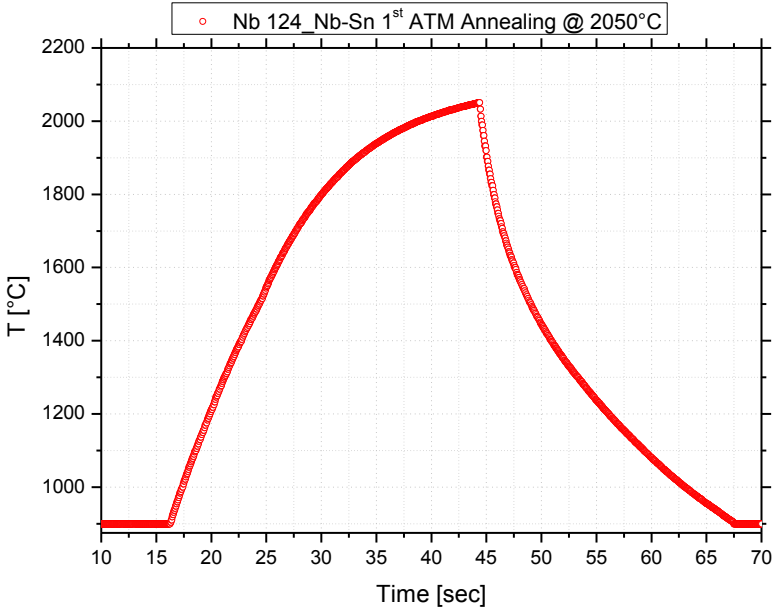


Figure 4.4: Graphical representation of annealing process

The heat treatment has been done at atmospheric pressure in He gas atmosphere at approximately 2bar. Cavities are heated between temperatures 2000°C–2350°C for 1 to 5 minutes. As for example, thermal treatment accomplished on Nb cavity is shown in figure 4.4. At this temperature, all dissolved gases diffuse out of the material and the Resistive Residual Ratio (RRR) increases by about a factor of 2 to values around 500. In order to capture the oxygen coming out of the Niobium and to prevent oxidation by the residual gas in the quartz tube, extra-pure 4He gas is used as a flux medium (few liters/sec.) to protect the inner and outer surface of cavity. After the heat treatment cavity is cleaned (HPR) and mounted on RF stand, pumped out and inserted in cryostat for RF test. The purpose is to observe improvement after thermal treatment at atmospheric pressure.

4.2.3 Efficiency

Induction heating is used for low frequency and conductive materials. With this method complete surface is heated. Efficiency of IH is low (40% to 50%) for highly conductive materials like, Au, Ag, Cu, Al etc. If we have special electro-heat process than efficiency will increase between 50% to 95%, and one can reach very high temperature, hence very high power density goes inside the work piece and consequently very short heating time. If power increase than the time decreases. Every work piece depending on its shape requires different Inductor geometry. Hence, one has to shape electro-mechanical geometry. Nb is low magnetic field materials, so it is easy to design coils for Nb cavity for induction heating for better power density distribution.

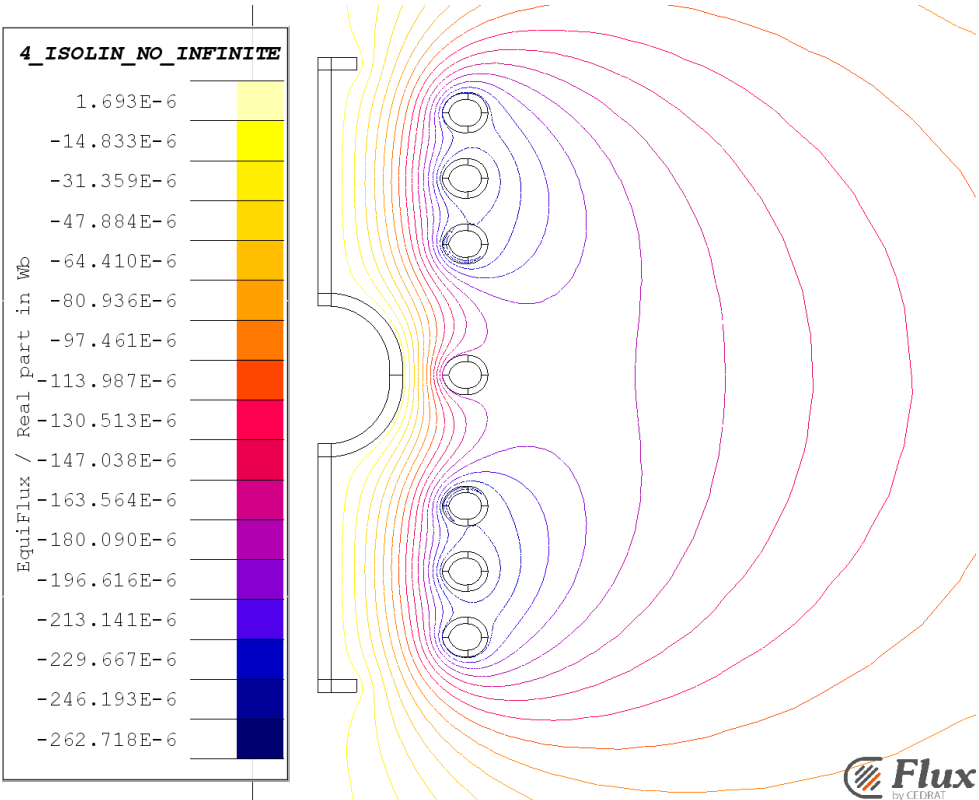


Figure 4.5: cavity simulation, Efficiency of IH during atmospheric pressure treatment inside quartz tube.

A cavity simulation has been done to calculate power density distribution during the treatment at atmospheric pressure taking in to account inducting heating system (i.e., coil geometry, quartz tube dimension, distance between coil and work-piece, cavity materials and dimension,

power, temperature, pressure of gas etc.). Efficiency of IH during atmospheric pressure treatment inside quartz tube is shown in figure 4.5. Calculation yield about 47-50% inductor power has been used to heat the cavity. Therefore, in order to increase efficiency, it is required to design inductor taking into account cavity geometry besides other parameter, such as, distance between inductor and cavity. Most significantly, it could be worth mention that rotating the work-piece meanwhile heating will increase efficiency. The reason is; the work-piece is never be centered perfectly inside the inductor, also induction coil is not absolutely circular. If the work-piece is static the heating by rf will never be uniform. The temperature map with and without rotation during the heating shows little different efficiency due to non-homogenous heating. This could also provide reasonable explanation regarding our A15 cavities that were corroded non uniformly.

In the course of atmospheric pressure purification, again RF test has been repeated to the cavity at cryogenic temperatures. The purpose is to observe improvement after thermal treatment at atmospheric pressure. Later on, thermal treatments has been performed in UHV condition as well, which is mentioned in next section.

4.3 Annealing under UHV system

4.2.1 Basic Idea

In next step, to improve performance of resonators an induction heating under UHV condition has been employed. Application of ultra-high vacuum technology increases the purity and lowers gas concentrations. During the Purification process evaporation of metallic impurities and degassing takes place which helps to improve SRF resonators. Few cavities are RF tested before and after high temperature annealing in UHV condition, and finally performance of both annealing process (i.e., at atmospheric pressure and UHV) have been compared by means of RF test.

4.2.2 Experimental UHV set up for Induction heating

The sketch of an experimental system is assembled for the induction heat treatments under high vacuum condition is depicted in figure 4.6. While the real experimental set up is shown in figure 4.7.

High temperature treatment procedure: At first, UHV system and all other components are cleaned in ultrasonic, dried with N₂ gas then assembled all components. The cavity is centered against the coil (but the cavity is in static position, not rotating during heating), and this in turn is connected to the work head (Ameritherm model), an induction heating systems for 50-150 kHz range that provide reliable and repeatable solutions for high-speed heating of smaller parts. The work head connected with the power supply Eko Heat brand, where time and voltage are controlled, and approximately 15kW of maximum power allowed in the system. The cavity is electrically insulated from the chamber, tested and finally chamber is closed with CF flange using Cu gasket. Chamber is pumped for some hours to achieve approximately 2×10^{-8} mbar pressure using a turbo molecular pump which is attached at two different face of CF flange of UHV chamber. For initial treatment to some cavities (Cavity identity number 115 upto 126) turbo molecular pump was connected between 3 chambers, hence the partial pressure in main chamber was high. However, for annealing cavities (Cavity identity number 127 upto 133) turbo molecular pump was connected directly at main chambers, hence the partial pressure was lower in main chamber.

Thereafter, chamber is backed at low temperature, approximately at 130 °C for 60 hours. For this, automatic backing panel is used where temperature and duration of time is set. After the backing vacuum is improved about one order of magnitude (ie, 5×10^{-9} mbar). Once the chamber is at room temperature, water cooling system turned on for cooling induction coil,

UHV chamber, work-head and power supply. Soon after power supply is switched on, and power to the coil increased manually starting from few watt up to 12 kW quickly (say in 30-40 seconds) which reach above 2000 °C. At maximum temperature cavity is left to heat for some seconds (ie, 10-60 sec.) then power supply is switched off. Pyrometers (Pyrospot DG 10N and/or DS 10N model) are employed to read the temperatures between 250-1300°C and 900-3000°C respectively. Water cooling system is also turned off after 20 minutes. Once the cavity is at room temperature, chamber is fluxed with extra-pure helium gas or other inert gas to prevent oxidation by the residual gas in the chamber which protects the inner and outer surface of cavity after the thermal treatment, and soon pumping system is switched off.

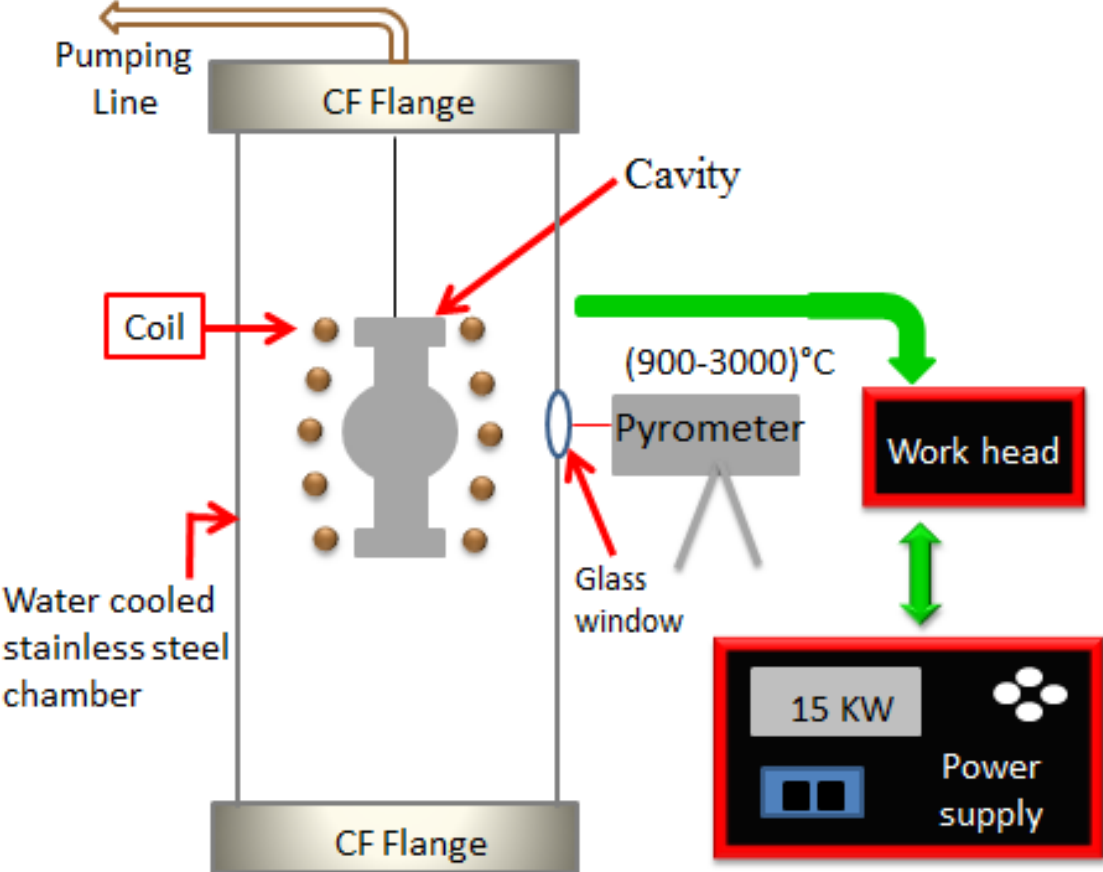


Figure 4.6: Sketch of UHV set up for Induction heating showing all other essential instruments.

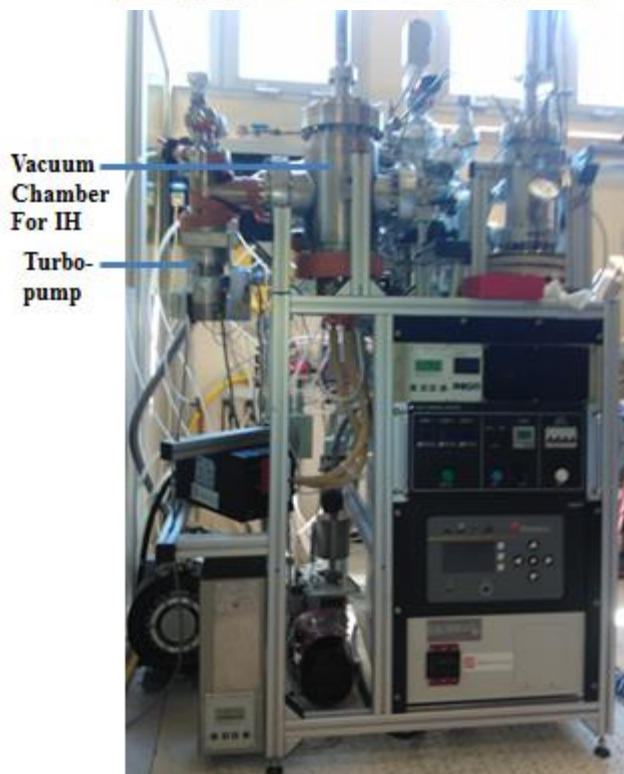
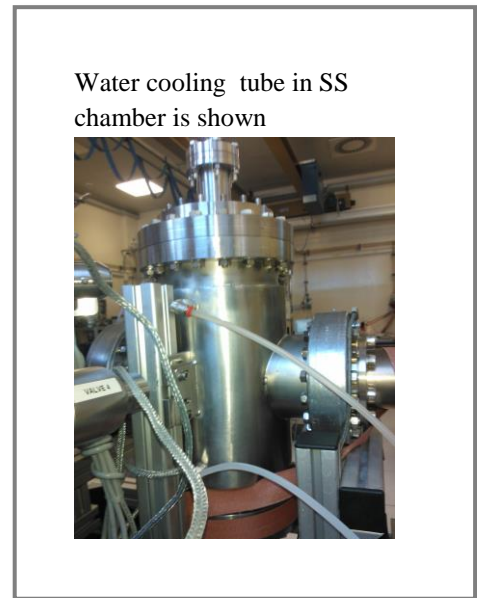
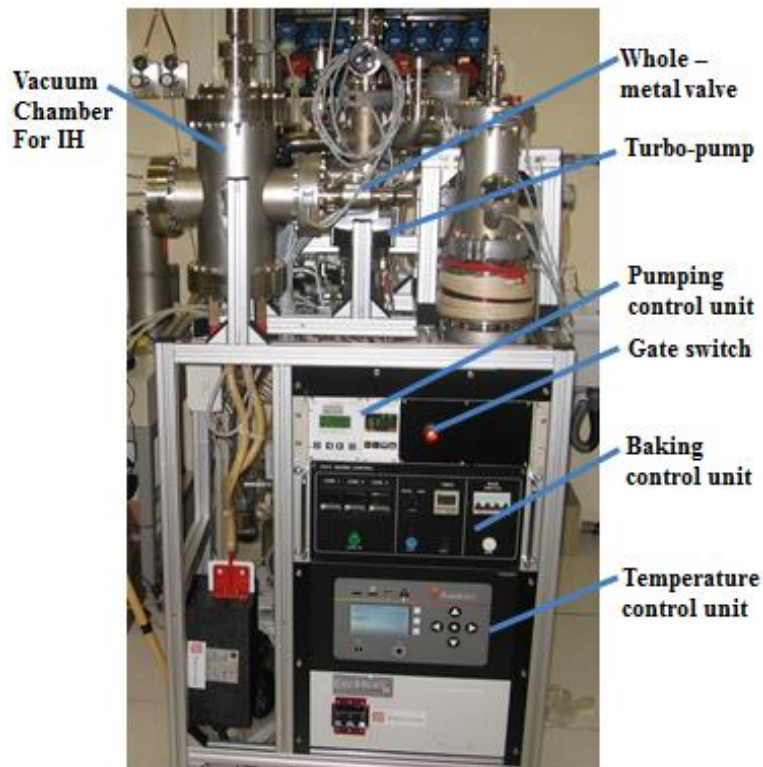
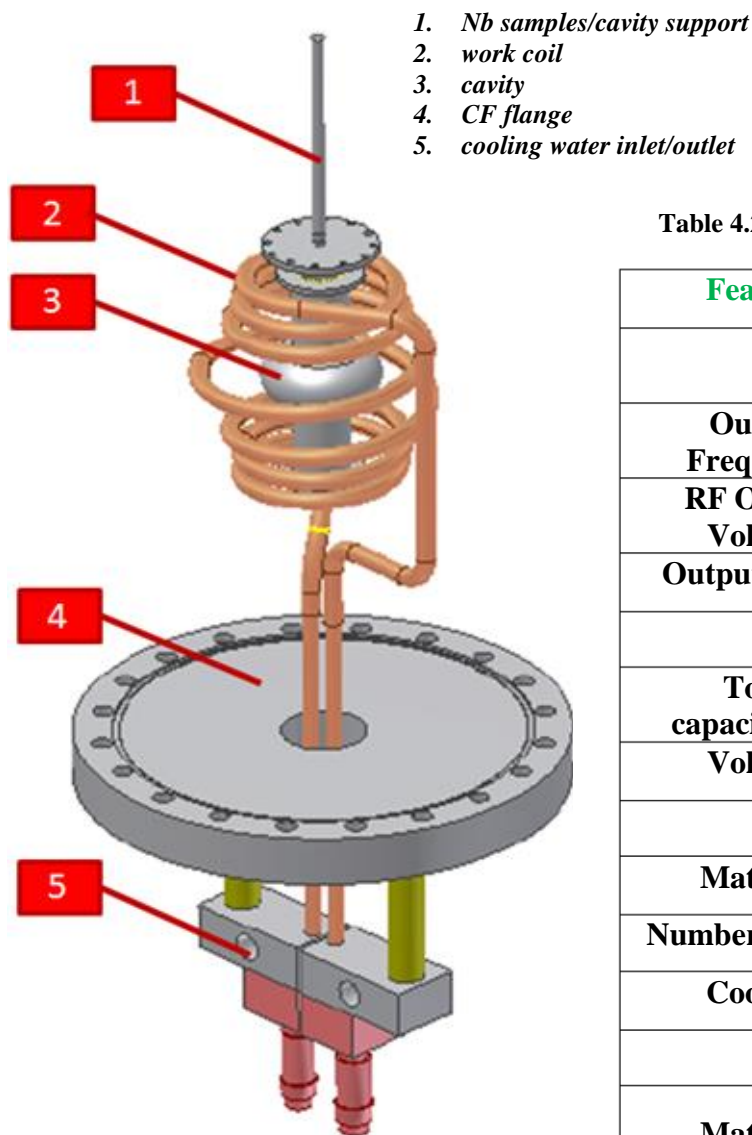


Figure 4.7: The real experimental set up for UHV test along with various parameter control unit is shown. In the course of annealing, there are two configuration for pumping the chamber is adopted. **Top-left Fig** shows 1st configuration, i.e., a turbo molecular pump was attached between 3 chambers, hence the partial pressure in main annealing chamber was high. **Bottom-left Fig.** shows 2nd configuration of annealing cavities (Cavity identity number 127 upto 133). Here, turbo molecular pump is connected directly at main chambers, hence the partial pressure was low in main chamber. **Top-right Fig.** shows water cooling system of main annealing chamber.



1. Nb samples/cavity support
2. work coil
3. cavity
4. CF flange
5. cooling water inlet/outlet

Table 4.2: Details of Induction heating system

Feature	Value	Units
	Power supply	
Output Frequency	50-150	kHz
RF Output Voltage	1020	V _{RMS} max
Output Power	12	kW max
	Work head	
Total capacitance*	2	μF
Voltage	1000	V _{RMS} max
	Work coil	
Material	copper	
Number of rings	7	
Cooling	water	
	Heating	
Material	Niobium cavity	
Material	Niobium cavity	
Final temperature	2200-2400	°C

*serial – parallel of 4 capacitors of 2uF

Figure 4.8: Induction coil connected to the water cooling tube of UHV CF flange, showing various essential component along with the work-piece (cavity) insided.

Previous research indicates that at very high temperature, all dissolved gases diffuse out of the material and the Resistive Residual Ratio increases by about a factor of 2 to values around 500. Soon after the heat treatment cavity is cleaned (HPR). Since High Pressure Rinsing at 100 bar reduces approximately 10 times in particle count. Thereafter, cavity is mounted on RF stand inside clean room, pumped out for several hours to achieve up to 2×10^{-8} mbar pressure using roughing/turbo molecular pump and placed inside cryostat for RF test at temperatures 4.2K up to 1.8K. The purpose is to observe improvement after thermal treatment at UHV condition.



Figure 4.9: Induction coil designed for heating 6 GHz tesla type cavities (top-left fig.); Nb cavity inside induction coil in UHV chamber (top-right fig.); Nb cavity during high temperature annealing inside UHV chamber (bottom-left fig.); Nb cavity after high temperature annealing (bottom-middle and right figures.)

4.1.4 Efficiency

Efficiency of IH will increase between 50% to 95%, and one can reach very high temperature, hence very high power density goes inside the work piece because the induction coil better match the cavity geometry (i.e., coil is much closer and in better shape), and consequently very short heating time. It is explained in the section 4.2.3. Nevertheless, in UHV system efficiency

is higher than the atmospheric pressure treatment inside quartz tube. Chamber was pumped few days, backed for 60 hours, hence residual gases are reduced.

In the course of annealing, there are two configuration for pumping the chamber is adopted, i.e., a turbo molecular pump was attached at two different face of CF flange of UHV chamber. In the beginning, a turbo molecular pump was attached between 3 chambers, hence the partial pressure in main annealing chamber was high. However, for 2nd configuration of annealing cavities (Cavity identity number 127 upto 133) turbo molecular pump was connected directly at main chambers, hence the partial pressure was lower in main chamber. Therefore, due to ultra-high vacuum (i.e., very low residual gases, contaminations) there is much less heat exchange with residual gases between work piece and heating system, hence most of the power density goes to the cavity. That also helps reduce time scale to approach maximum temperature.

Most significantly, efficiency will increase, if the work-piece will rotate inside coil during thermal treatment. The reason is; the work-piece is never be centered perfectly inside the inductor. If the work-piece is static the heating by rf will never be uniform. The temperature map with and without rotation during the heating shows little different efficiency.

After the UHV purification, again RF test has been repeated to the cavity at cryogenic temperatures. The purpose is to observe improvement after thermal treatment at atmospheric pressure.

4.4 Previous techniques of purification method: External furnaces

Nb has many uses in the manufacture of stainless steel alloys and superalloys for aerospace applications. Hence, its metallurgy has been extensively studied. After extraction from the ore, the most widely used method of consolidation and refinement for commercial high purity source is e-beam leaching in a furnace. In this method, the beam is arranged to hit the feedstock as well as the top of the ingot which is contained in a water-cooled copper sleeve. Hence, impurities are boiled out of the pool and pumped away. This procedure drives out all volatile impurities. The method is shown in Figure 4.10.

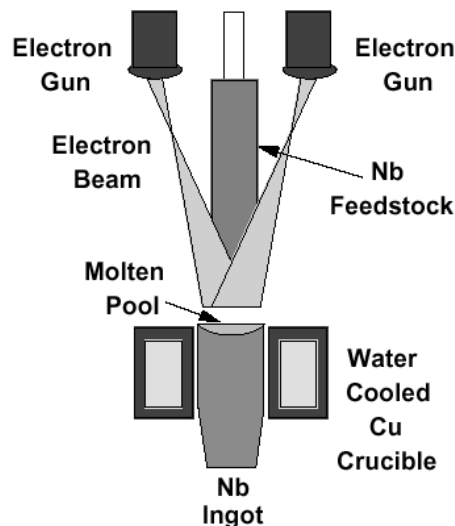


Figure 4.10: Purification technique to improve RRR of Ingot at vacuum furnace is shown

Moreover, higher field is desired for accelerating cavities. Therefore, a post purification steps has been used to improve thermal conductivity of Nb cavity. There were few methods employed in past to improve purity of cavities under the influence of UHV annealing techniques. For these type of purification of Nb have been accomplished using either Yttrium (Y) or Titanium (Ti) at high temperature as a solid state getter in reference [63, 64]. The

foreign material is vapour deposited on the Nb surface and in the same step, the high temperature decreases diffusion time of the oxygen in Nb. Over a few hours, oxygen collects in the deposited layer. With this technique, a factor of 3-4 improvement in thermal conductivity of Nb have been observed. While other researchers have used solid state gettering with Titanium [65], where the Nb sample (two mm thick) has been thermally treated in Ultra-High Vacuum (UHV) to improve Residual Resistivity Ratio (RRR). It was observed that the temperature and duration of purification by means of UHV annealing depends on evaporation rate of getter materials and diffusion rate of the impurities. Interstitials like O, N and C are the major impurities limiting Nb RRR. By this technique factor of 10 have improved the RRR value. This process leaves several micron of Ti or Y that has to be chemically removed. Experimental method for post purifying a complete cavity is shown in Figure 4.11. Now a day at J. Lab researchers do Hydrogen degassing at 600 C for 10 hours, while at KEK they do thermal treatment at 750 C for 3 hours, KEK.

Over all procedure for post purification process for cavity or half-cell is summarized as:

- Heat in vacuum furnace to ~ 1250 C (if Yttrium is used)
- Heat in vacuum furnace to ~ 1400 C (if Titanium is used)
- Evaporate Ti on cavity surface
- Use titanium as getter to capture impurities
- Later etch away the titanium
- Doubles the purity (RRR ~ 600 if originally RRR = 300)

However, this method is rather complicated. Furnace has to heat some hours before the sample, and after heating the sample furnace need several hours to cool down. Also, during the long procedure, there is high possibility to contaminate work piece.

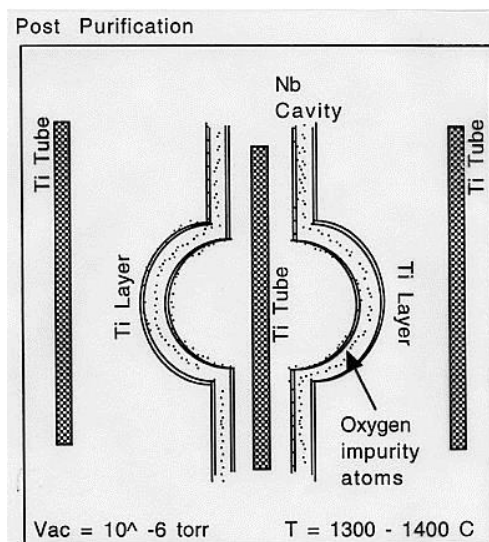


Figure 4.11: Purification technique to improve RRR of Nb using solid state gettering with Titanium is shown.

-----*****-----

Chapter 5

Experimental: RF cavity test- A Review

A complete procedure and principle of tesla type RF cavity characterization, new set up designed and built for testing these cavities have been explained in this chapter. Also, the automation procedures that were implemented and that made the measurement easier and faster are also mentioned.

5.1 Experimental Setup-Techniques:

The RF setup is designed to measure two important values for accelerator applications: quality factor (Q) of the cavity and accelerating field (E_{acc}) in the cavity. The schematic picture of RF setup is presented in Figure 5.1. A superconducting rf cavity is lowered vertically into a liquid helium bath (Figure 5.2). This bath is initially around 4.2K (at atmospheric pressure) when data is first taken. The testing starts with an RF generator.

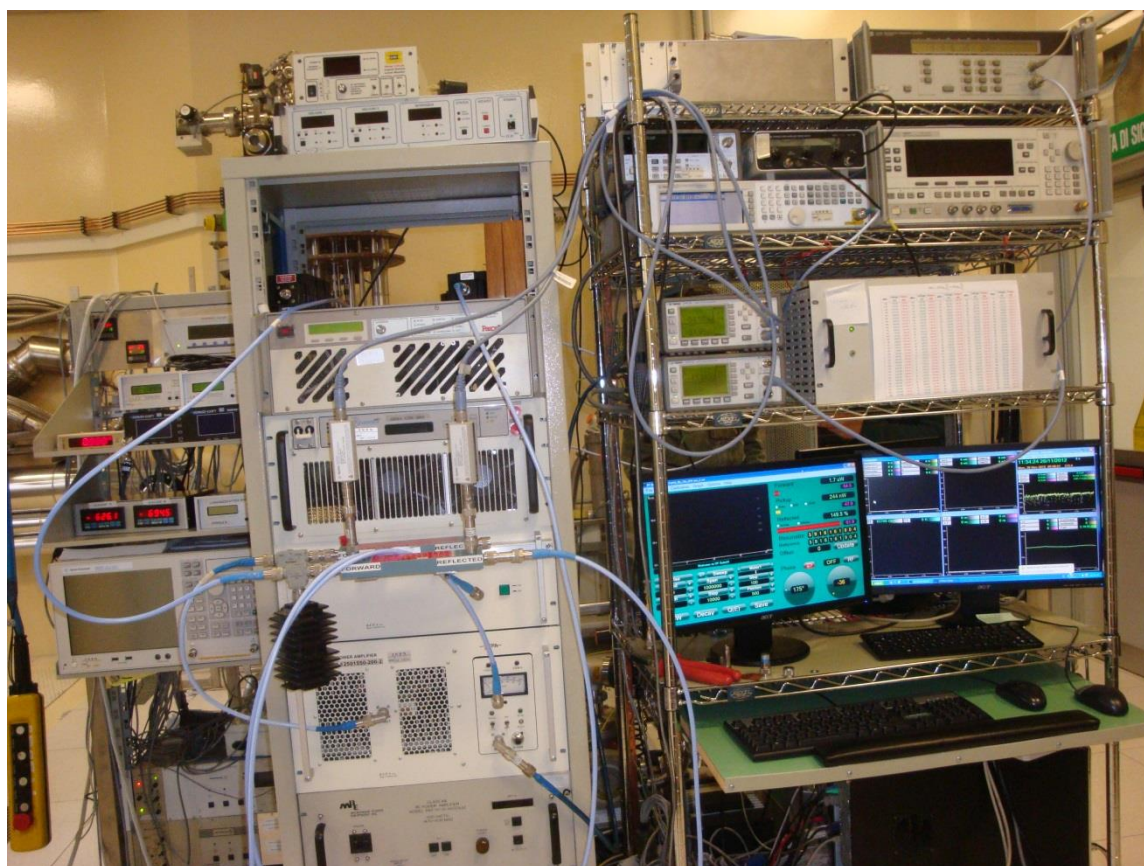


Figure 5.1: SRF cavity measurement system inside clean-room. This figure shows an image of the racks that consists set of instruments required to test an SRF cavity. This includes rf power heads, RF amplifier, RF generator, Frequency counter, dual directional coupler, rf box, oscilloscopes, DC amplifier, user interface, measuring computer etc.

This generator produces the signal frequency and amplitude, pulse width and repetition rate that will create the electromagnetic fields in the superconducting rf cavity that would accelerate particles in an accelerator. This signal is then split so the phase can be measured with respect to the phase of the forward power. If necessary, the RF signal is phase shifted

and amplified. The now shifted and amplified signal is sent through a directional coupler and into the cavity. A directional coupler is used to measure both the forward and reflected powers immediately at the input to the cavity because some of the power at input is reflected back. If one did not use a directional coupler, one could obtain interference between the forward and reflected powers. Some of the power is reflected back at the input coupler while most of the power is transmitted through the cavity to be detected on the other side. Each of the three powers: forward, reflected and transmitted, are then split enabling a scalar measurement to be made using a power meter.



Figure 5.2: **Left Fig.:** A picture of 6 GHz rf cavity mounted on test stand (before being lowered into the Cryostat) with pumping system for 4.2/1.8K test. **Middle Fig:** Cryostat (Blue) for single cavity test. **Right Fig** is the cryostat for triple cavity rf test inside clean-room is shown.

To actually test a cavity, the resonant frequency is excited in the cavity using an RF signal generator. During a vertical test of cavity, the cavity's resonant frequency cannot be changed except by external factors, such as temperature, so the rf input signal is adjusted to match that of the cavity under test. The RF signal frequency is recorded by the rf subs and rf guard (Courtesy: Dr. Sergey Stark, INFN/LNL). This frequency is changing throughout the test as a result of the changing temperature and power. These rf subs and rf guard also record the forward, reflected and transmitted powers, temperature and pressure of the helium cryostat and the decay time of the transmitted power. Using this data, the quality factor and the accelerating gradient of the cavity is obtained. In order to find the maximum accelerating gradient of the cavity, the helium pressure must be reduced to about 15 mbar. The reason for this is that at this pressure, a corresponding temperature of $\sim 1.8\text{K}$, liquid helium is below the superfluid lambda point of about 2.17K . Superfluid helium has better thermal conductivity

which eases the process of keeping a cavity cold. During the pump down to 15 mbar, the accelerating gradient doesn't fluctuate much. This is done by keeping a constant peak transmitted power. The reason for this is that as the temperature decreases, the power dissipated decreases and the quality factor increases. A review on measuring procedure of these rf cavity is given in next section in detail.

5.2 Preparation of cavity

Highest accelerator performance requires optimised production, surface treatments, materials testing, and diagnostics of the accelerating structures. The knowledge and mastering skills of these technologies become even more important since large scale production involves in industry. The accumulated know-how of several research institutes shall be exploited to further improve the quality of the SRF accelerator cavities by pushing further the detailed diagnostics tools and the surface treatment of the cavities.

In order to prepare the Nb cavities it is first treated either with centrifugal barrel polishing or vibrator then with fast BCP solution in order to remove residuals and polish the internal surface of cavity and finally rinsed with high pressure water. Thereafter, cavities are placed into inductor under the influence of the voltage, time, sample position, temperature, and pressure of pure ^4He and Ar gas used for protection. This induction technique at atmospheric pressure is developed in our laboratory.

Overall, required procedures for qualifying superconducting RF Cavities before RF test consists the following procedure, and is given below:

- ✚ Degreasing inner and outer surfaces to remove contaminates
- ✚ Removal of internal bulk damage layer of niobium from fabrication (200um)
- ✚ Chemical removal of internal surface for clean assembly (10-20um)
- ✚ Removal of hydrogen gas (absorbed during chemistry) from bulk Nb
- ✚ High Pressure Rinsing (HPR) to remove particulates from interior surfaces (incurred during chemistry and handling)
- ✚ Drying of cavity for assembly (i.e., to reduce risk of particulate adhesion and reduce wear on vacuum systems)
- ✚ Clean room (class 1000) assembly in the dust free atmosphere
- ✚ Clean evacuation

5.3 Clean room procedure

In this section clean room technique is explained step by step. In otherword, working process (ie, assebling tesla type cavity or samples) in clean room atmosphere for 6 GHz bulk-Nb and Nb coated Cu cavities and samples which are further treated and /or investigated inside UHV system or measured in cryogenic temperatures have been explained in detail.

At first, a cavity that is immediate high pressure rinsed (HPR) and dried with N_2 gas should be mounted (screwed) on bellow flange (one side of cavity toward forward antenna while other is toward pickup antenna using Kapton O-ring as a gasket and grease) inside clean room. It is shown in Figure 5.3 (Left hand side). Thereafter cavity should be connected to both pumping line of RF stand, and is shown in Figure 5.4 (Right hand side). And cavity must be pumped out nicely (4-6 hrs) to reach vacuum pressure approximately 10^{-6} - 10^{-8} mbar prior to cooling at LHe temperature. Most importantly, a great care must be taken to ensure that the vacuum system is throughly clean and dust free. The cavity itself is evacuated slowly to avoid turbulent flow and reduce risk of contaminants from the vacuum system reaching the cavity. At the same phase, it is essential to maintain dust free condition while attaching input and output couplers to the cavity.



Figure 5.3: Cavity mounting procedure on RF stand inside clean-room



Figure 5.4: Cavity screwed on forward power flange (top), and pick up flange (bottom). RHS figure: Cavity pumping lines are connected to RF stand (A complete RF insert)



Figure 5.5: Fig.A: classical Indium gasket above cavity flange. Fig.B: a new Kapton Gasket

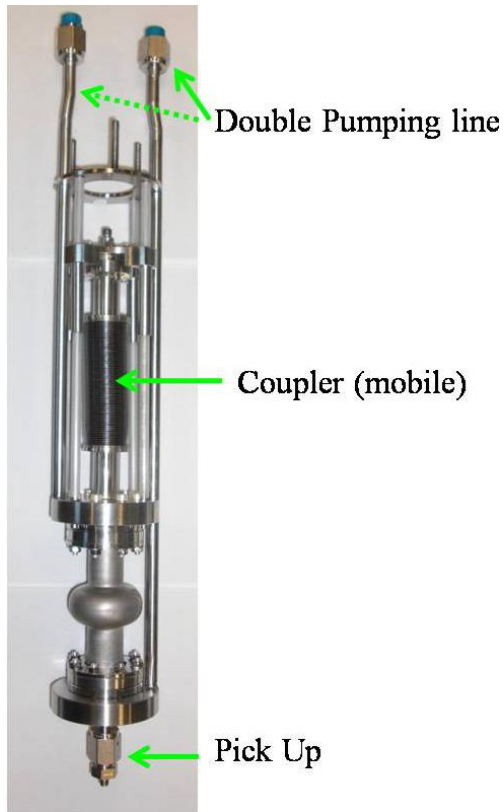


Figure 5.6: An RF insert after cavity is mounted inside clean room, and both pumping line are shown.

RF INSERT: Once the vacuum level inside cavity is achieved in the range of 10^{-6} - 10^{-8} mbar, install helium level guage (insert from top of RF stand flange down to pickup SMA connector) and thermometer (at bottom flange of bellow).

After high pressure rinsing the cavity is normally left drying for some minutes inside clean room. After drying, the cavity is mounted onto the RF test stand in the cleanroom class 100. Following assembly the pumping line to a roughing/turbo pump is connected, and cavity is pumped down to $2 \cdot 10^{-8}$ bar as indicated by cold cathode gauge on the pump. The initial pumping is done at a slow rate, so that the gas flow in the vacuum system stays laminar. Pumping down to the final pressure usually takes several hours (overnight is better). After the ultimate pressure is reached, the vacuum is leak-checked to ensure absence of leaks. Upon successful completion the cavity's vacuum, RF stand is slowly immersed inside cold cryostat for Cryogenic measurement.

5.4 Cryo cool down process for single cavity

Liquid Helium Transfer in Cryostat: A procedure

In order to measure Quality factor (Q_0) and hence surface resistivity of inner surface of cavity at low temperature liquid helium should be added inside Cryostat. In the existing Cryostat (Model: Precision Cryogenics Instrument USA) one should fill about 1000 mm (can be read at Helium depth indicator) liquid helium inside. Under assumption that Cryostat is at atmospheric pressure, the detail procedure is as follows:

- i. Connect fore-pump (roughing pump or scroll pump) to cryostat using KF flange (ie, metal clamper using viton O-ring) and start pumping to air for

- maximum 5 minutes. Stop pumping or better close valve (if installed) to cryostat.
- ii. Open 4He gas Valve to Cryostat. Flush cryostat with 4He gas upto 1 bar. For this purpose, a tube should be connected between Cryostat and 4He gas cylinder or 4He return line.
 - iii. Close 4He gas Valve to Cryostat. Again start pumping Cryostat to air for 2-5 minutes. Stop pumping cryostat or better close pumping valve (if installed)
 - iv. Repeat above process ii (ie, Open 4He gas Valve to Cryostat. Flush cryostat with pure 4He gas upto 1 bar then close 4He gas Valve to Cryostat).
 - v. Repeat above process iii (ie, Close 4He gas Valve to Cryostat. Again start pumping Cryostat for 2- 5 minutes. Stop pumping cryostat (close pumping valve to cryostat)
 - vi. Repeat (2nd time) above process ii (ie, Open 4He gas Valve to Cryostat. Flush cryostat with pure 4He gas upto 1 bar then close 4He gas Valve to Cryostat). Further, no need to pump Cryostat. Now need to fill liquid helium inside
 - vii. Connect Cryostat to return line using flexible bellow. Open the valve to return line
 - viii. Measure Liquid helium inside Helium Dewar (using level meter that will be inserted inside the Dewar up to the bottom). If helium is less than 40 liters then no need to fill empty Cryostat but could be added some amount like 20 liters only in case of semi-filled Cryostat (ie, at least 10 liters of liquid already existing inside cryostat)
 - ix. Insert one-end of syphon inside Dewar slowly and wait some minutes (say 2-5 minutes) then insert close to bottom surface (Syphon must be 5-10 mm above bottom surface of vessel). While other-end of syphone should be inserted inside Cryostat (Syphon must go down to the surface of cryostat as much as possible) if helium is transferring in cryostat at room temperature. Close both the knobs (at Cryostat and He Dewar) tightly in order to prevent leak during the transfer.
 - x. In case of helium transfer while Cryostat is cold: First insert syphone inside Dewar (as mentioned in para viii) and wait few minutes till other end of syphon begin to release cold gas. Once flow of cold gas started, insert other-end of syphon inside Cryostat slowly. Close both the transfer inlet knobs (at Cryostat and He Dewar) tightly in order to prevent leak during the transfer.
 - xi. Close the He Dewar return line valve.
 - xii. Connect He gas cylinder and He Dewar using tube. Apply pressure inside He Dewar (around 100-200 mbar). Rise of liquid helium level could be observed in Helium depth indicator after some minute.
 - xiii. It takes about an hour to fill liquid helium upto 1100mm inside cryostat. As soon as level is reached to 1000mm, one should stop applying pressure in He dewar, and slowly open return line valve to release over pressure.
 - xiv. After filling desired level of helium inside , stop transfer. Open transfer line carefully.
 - xv. Place the RF insert inside cryostate slowly (usually it takes about 20-30 minutes). Close nut-bolts of insert. Proceed RF calibration.

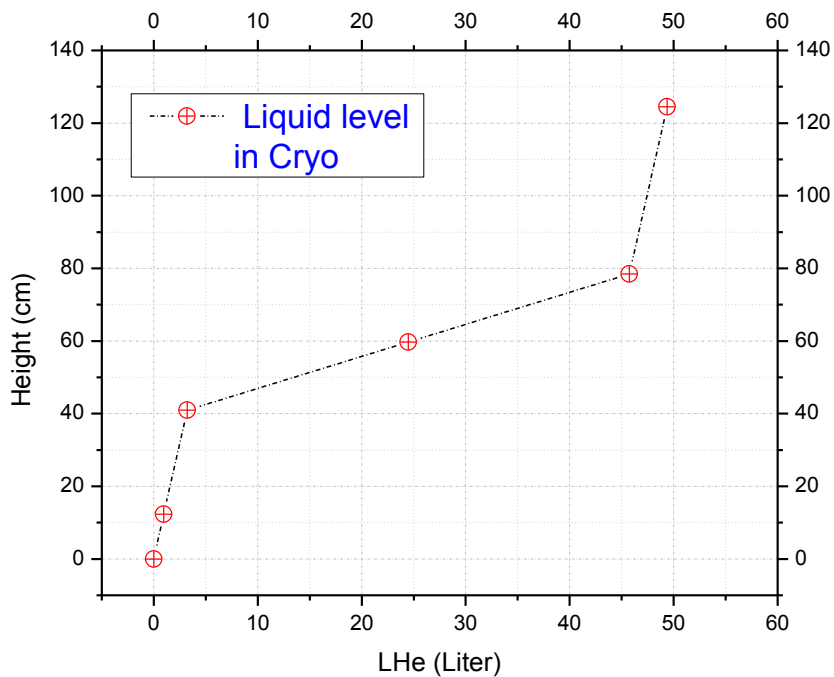


Figure5.7: Graph is plotted for height vs LHe level inside Blue cryostat. Over all required liquid to fill cryostat is shown without taking into account RF insert.

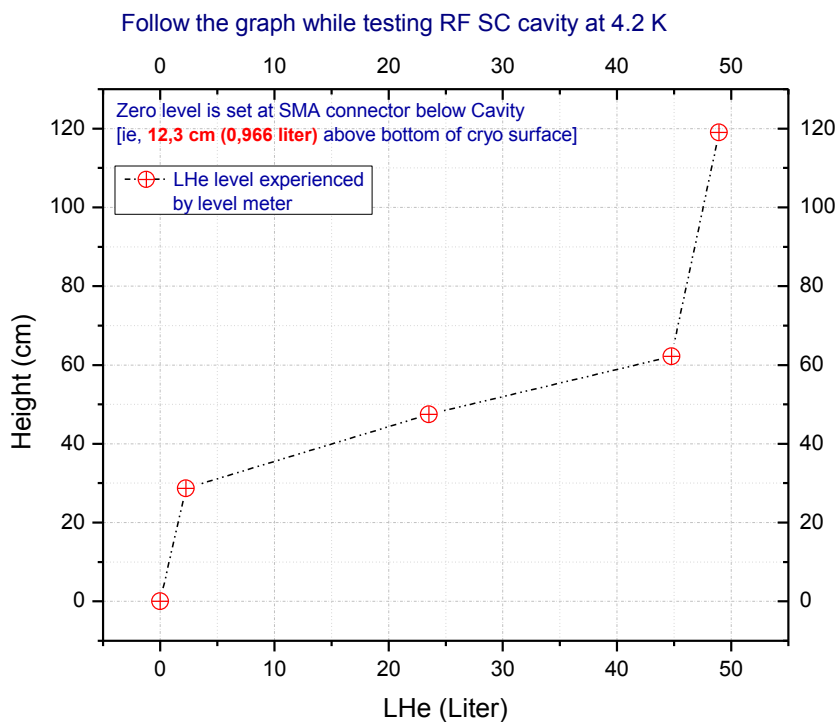


Figure5.8: Liquid helium level is shown while RF insert is inside Blue Cryostat. Here, liquid helium level is measure ZERO at pick up SMA connector.

5.5 RF cavity measurement system

A schematic diagram of RF measurement system used in our laboratory shown in Figure 5.9.

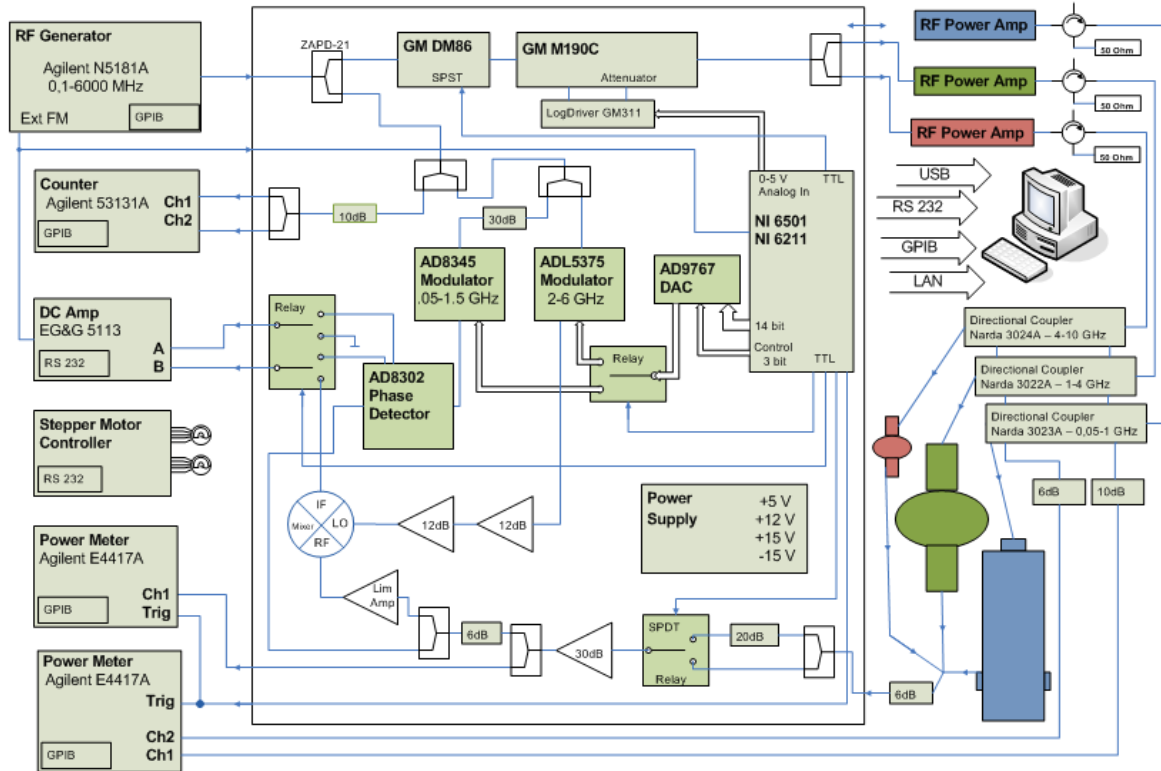


Figure 5.9: Schematic diagram of Rf measurement system of TESLA type cavity at INFN/LNL. The components which are needed to the incident, reflected and pickup power and feedback circuit are shown in diagram guard (Courtesy: Dr. Sergey Stark, INFN/LNL)..

Search for resonance frequency at room and $L^4\text{He}$ temperatures by Network Analyzer

It is essential to search for resonance frequency of cavity at room temperature. Hence need to connect *forward line of cavity* to the *Network analyser* (port 1) using coax cable. Move coupler-position using feed-through in scale around 44 mm for room temperature (finding resonance frequency at 4K coupler must go out from cavity, ie, in scale it should be less than the scale at room temperature). Then need to play (press) with push-button functions and touch-panel functions of Network analyser as follows:

- i. **PRESET** -> **OK** (Touch panel) -> **MARKER** -> **6** -> **GHz** -> **ENTER** (in this way freq is set to 6 GHz)
- ii. **SPAN** -> Turn circular **NAVIGATION KNOB** anti-clockwise (in the range of 10 MHz to get better resolution). Select a reasonable value for bandwidth and then move the markers which confine the bandwidth until they are at the beginning and at the end of the peak
- iii. **MARKER SEARCH** -> **MIN** (Touch panel)
- iv. **MARKER FCTN** -> **MARKER CENTER** (Touch panel)
- v. **Move coupler-position** using feed-through out and/or in cavity that correspondes to minimum-maximum (in scale) to find maximum attenuation (in dB) in signal and check resonance peak (negative) at Network analyser.

- Once the maximum resonance achieved (negative peak in -dB) go to next step (so that exact resonance frequency can be read)
- vi. **MARKER FCTN -> MARKER CENTER** (Touch panel). Here, one can get exact resonance frequency (in GHz) that can be read on top-left side of screen along with attenuation signal value (-dB). An example of a resonance frequency finding for a 6 GHz Nb-cavity (Nr 126) at room temperature is shown in figure 5.10.

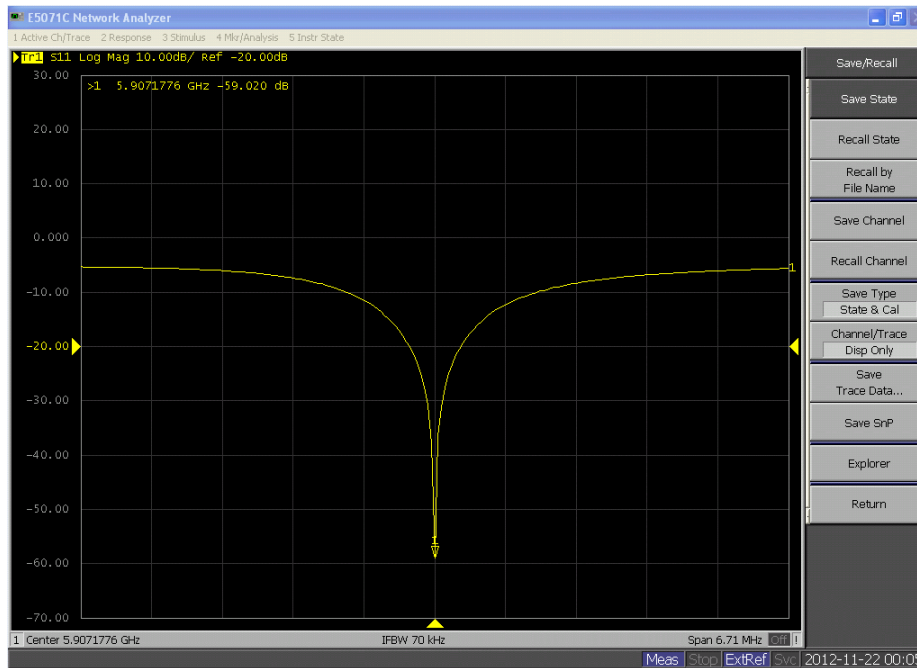


Figure5.10: Resonance frequency (maximum attenuation in signal) for a 6 GHz Nb-cavity at room temperature is shown. An exact value of frequency (GHz) can be read on top-left side of screen along with maximum attenuation signal value (-dB).

6GHz Cavity resonance

Table5.1: 6GHz tesla type cavity parameters. Temperatures and their corresponding frequencies and coupler position at feed-through scale are given.

T	f	Feedthrough level
Room ~300 K	5.85 – 5.95 GHz	41-45
4,2 K	+ 10 MHz	22-25

Moreover, Resonance frequency graph at low temperature (ie, 4.2K) will be changed. Summary of different parameters (eg, temperatures and their corresponding frequency along with coupler scale in mm) to find resonance frequency of tesla type 6 GHz cavity is given in table 1. For example, at room temperature cavity frequency range could be between 5.89 up to 5.95 GHz that corresponds to feed-through scale (coupler position in cavity) between 41-45 mm. And while at 4.2K frequency increases by 10 MHz, and couple must go out from cavity. Hence in feed through scale it will be around 25mm. At low temperature frequency increases due to the fact that material experiences stress and changes shape, and so wave squeezes in side cavity. That is seen (in table 1) in form of increase of 10 MHz frequency.

Power sensor heads Calibration

Objective of power sensor head calibration and cable (External and Internal cable) calibration are to reduce thermionic and other noise and hence reducing the error in RF measurement system.

i. Power sensor head Calibration

Calibration of all three power sensor head in sequence is necessary to reduce thermionic noise and hence reducing the error in RF measurement. All three power head must be calibrated while RF measurement software is closed, and just before starting experiment. First we begin to calibrate **Reflected power sensor head** (Fig. A-in red circle) then **Pick-up power sensor head** (Fig. B: It is connected to the back of RF box) and finally **Forward power sensor head** (Fig. A-Left hand side) will be calibrated using their respective power meter (Model: E4417A) instrument- [Fig. C: Red circle (top instrument) is for reflected and forward power sensor heads while below instrument is for pick up power sensor head. For this purpose, power sensors should be disconnected from dual directional coupler (Fig. A) and connected to the power meter on POWER REF plug (Fig C: red circle). Calibration can be done to the power sensor by pushing buttons in following manner:

- i. For reflected power sensor head: Press **Zero/Cal** -> **Zero + Cal** (on display)-> **Zero + Cal B** (on display)
- ii. For Pick-up power sensor head that is connected to the back of RF box (Fig. B), disconnect from back of RF box. Calibrate it and after that reconnect to the back of RF box.
- iii. For forward power sensor head: Press **Zero/Cal** -> **Zero + Cal** (on display)-> **Zero + Cal A** (on display)
- iv. Wait some seconds (less than a minute) for calibration process. Once calibration is finished disconnect the power sensor head and reconnect to their respective

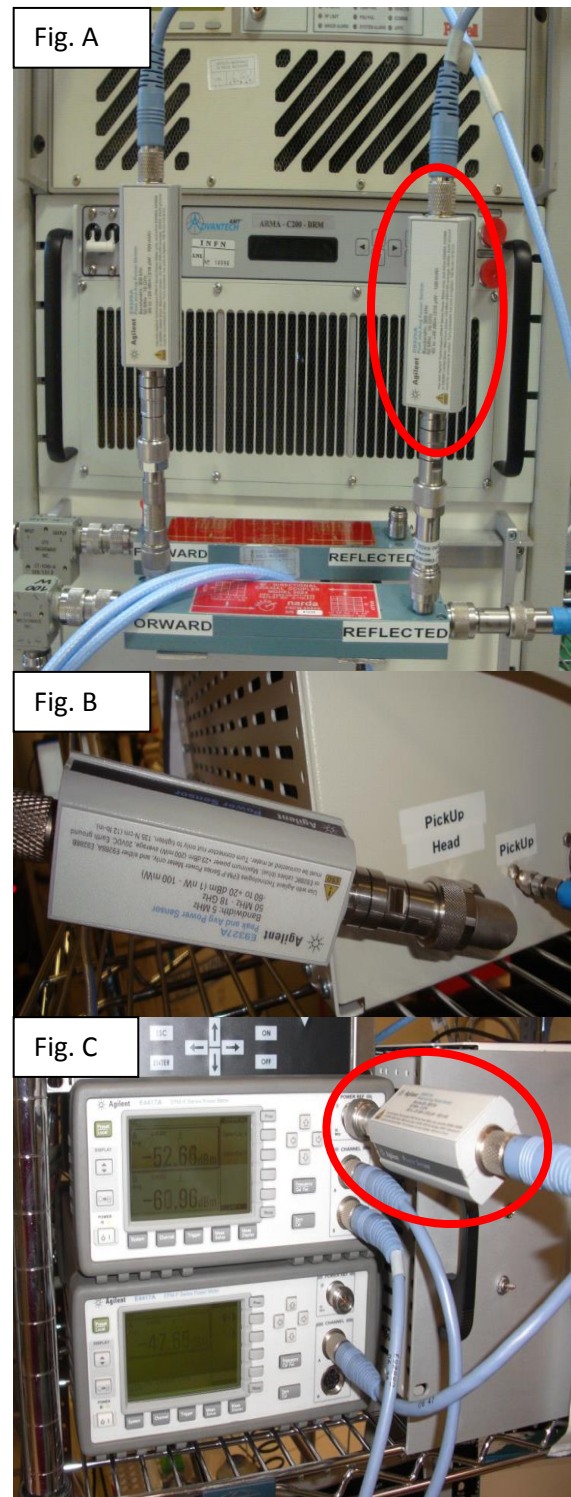


Figure 5.11: Power sensor heads and instruments. Fig A : reflected and forward sensors connected to dual directional coupler. Fig B: pick up power sensor head connected to the back of RF box. Fig C: calibration process in Power meter (Model: E4417A) instruments are shown.

dual directional coupler plug.

Now, start RF Programme at measurement Computer Isc_16. **Double click** on the icon **RF Subs_Net.exe** on the desktop shown in Figure 5.12. Fig A: Choose one of the last setup file-possibly a recent one, follow Fig B, and open it. This file needs to be updated with the calibration and whose utility is to give a comparison with the new calibration: new values should not be too different from the previous ones if the configuration of the system is the same.

But generally the separate set up for different cavity are used more parameters depends on Cavity.

Go at measurement software on monitor menu tab of *file* -> *save set up* with correct name.

GUARD:

A. External Cables calibration:

- i. **External circuit Calibration at room temperature** . Such calibration is independent of temperature. One can calibrate this part of the system either while cavity is at room temperature or at helium temperature.

Attention: Check the forward power. It can be read at forward bar. It should be at **minimum** or **switch off** before switching ON power amplifier. Minimum power can be set by rotating anti-clock wise on power (Knob) wheel (down-right side at measurement software on monitor).

- *Open forward and pick up cables from cryostat (if it is connected!).*
- Switch on the power amplifier. Click at **RF** (Power should be at minimum before switching power amplifier)
- Insert resonance frequency f_{res} (at reference field of frequency->*click*->*modify numbers* by pointing mouse and using mouse wheel) found at network analyzer
- Forward power should be set approximately ~15 mW. That could be read at forward bar (top-left at measurement software on monitor)

STEP 1:

- *Open the calibration tab of menu and go as: Calibration -> forward -> forward Calibrate* and follow the instructions. It will be as given below:
- *Connect 50 Ohm load to dual directional coupler port with attenuator of reflected power head port. Attention: In doubt put 30 dB attenuator on the forward cable and measure the actual power using reflected head.*

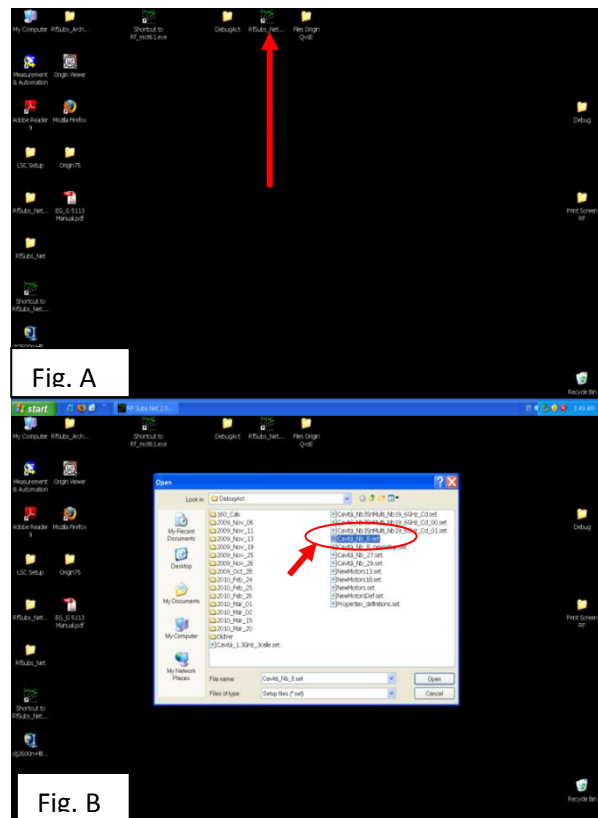


Figure 5.12. Fig A: Measurement computer Isc_16 desk top view. Fig B: last set up file shown in red circle

- Connect power head to forward cable using coaxial cable adaptor, a 4.4 cm long (power should be less than 50 mW otherwise power head will be burnt. Attention: 100mW is maximum power for the heads). Wait some seconds..! Follow the pop-up window message. There will be two dialogue pop-up appears. **1st** message concerning calibration result appears. If previous and current results are approximately similar then accept it, otherwise don't accept, and repeat the process again or try to find out problem. The **2nd** dialogue pop-up appears concerning further instruction that will lead to step 2 below.

STEP 2:

- Connect back *reflected power head port* to dual directional coupler port. And connect *short (mirror)* to forward power cable, and follow the instructions. There will be one dialogue pop-up concerning calibration result. If previous and current results are approximately similar then accept it, otherwise don't accept, and repeat the process again or try to find out problem.
- Go to File -> SAVE SET-UP

STEP 3:

- Again, **Forward power** should be at **minimum**
 - Connect **Forward** and **Pick up cable** together using coaxial cable adapter. Put the connected cable on ground. Attention: During the calibration process, cable should be kept at safe place. DO NOT MOVE or SHAKE cables. Otherwise calibration will be changed.
 - Select tick box (Radio button) **0 dB** then **Auto** in the **pickup bar** at measuring software program which makes an automatic change from high to low sensitivity for pickup values: high sensitivity = green numbers; low sensitivity = yellow numbers. Select "Auto" in the pickup bar at measuring software program
 - Now it is necessary to find from where the sensitivity switch starts working. It is necessary to find manually first, and then to do the automatic procedure to register it in the program: At the start of the procedure one should have high sensitivity (i.e., **GREEN COLOR** indicator pick up value or reading).
 - Change the *Forward* power slowly until switch is on (it is possible to hear a "tic" sound from the box without panels just above the computers: and in **YELLOW** color).
 - In order to find the switch automatically, write a value 1 to 2 dB under to the one just found in the pickup window **Calibration -> pickup -> pickup Calibration start** and wait. The procedure spans 5 dBm from the number given, increasing in power in 02 dB steps, so if the reading was -31 one should write -32 in pick up field.
 - **Calibration -> pickup -> pickup Calibrate.**
- WAIT!** Here the procedure takes time; one should check correction of previous value with new value before accepting calibrated data.
- Conditions for cancel?
- The switch changes the phase of the signal, so it is necessary to find this correction: select power at switching point "0 dB" in the pickup bar and minimize the error again.
 - Change the sensitivity to "-20 dB" and minimize the error again.

- The difference between these two phases is the correction that is to be given in *Calibration* -> *pickup* -> *phase correction*.
- TEST the RESULT (-20dB and 0 dB). The error should not change
- This last procedure is not necessary every time since the phase correction is saved in the setup loaded when starting the program and it only depends on the frequency of the cavity. SAVE SETUP
- Connect forward and pick-up cables to the respective cavity RF input of cryostat.
- Press SWEEP to observe cavity resonance at measuring software, if not found then reduce phase (ie, error). Even not found the cavity resonance then adjust coupler position in cavity by moving coupler feed-through Knob. The cavity resonance at measuring software is shown in Figure 5.13

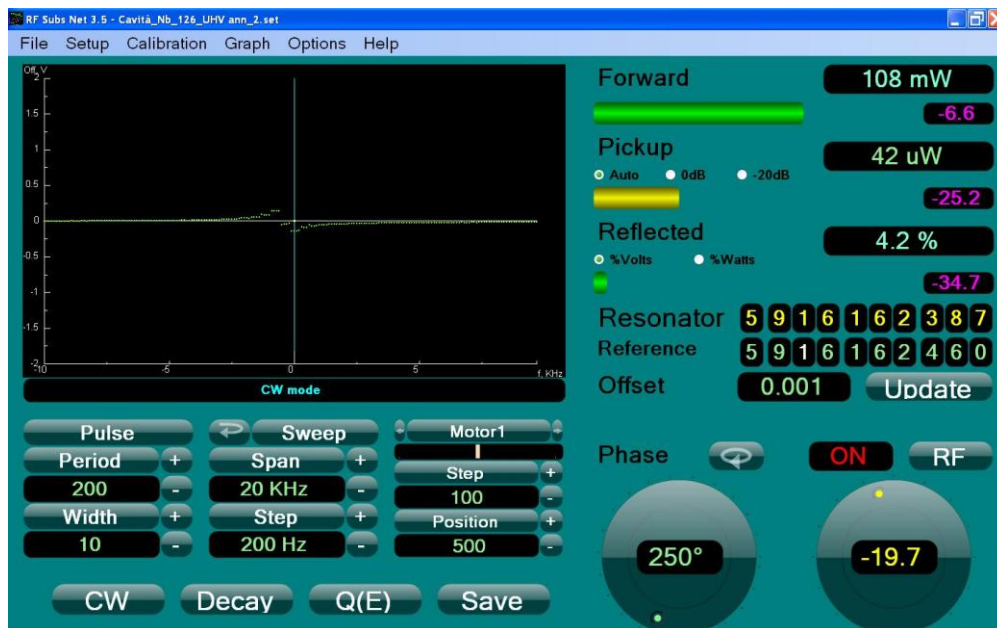


Figure 5.13: Cavity search at resonance frequency

- SAVE set-up.
- ii. Q_0 pick-up evaluation (through the decay time measurement)

Search of cavity inserting resonance frequency (in software of measurement computer) received at network analyzer at Room temperature or 4.2 K:

- Connect forward and pick up cables to the respective cavity input of cryostat. Go to *file* menu -> *save set up* with correct name.
- Set the gain to *Coarse 25* on the pre-amplifier (while at room temperature or in case of worse performance of Cavity at low temperature as well).
- Switch on the power amplifier. Click at **RF**
- Insert resonance frequency f_{res} found at network analyzer
Press-> SWEEP
- Change the coupler position with the Coupler feed-through Knob and adjust the phase form software in order to minimize the reflected wave up to 5% (voltage)
- Click *calibration* -> *Pickup* -> *Pickup Attenuator* (Insert -20 dBm software attenuation)

- Click **calibration** -> set decay time (between $1 \cdot 10^{-6}$ sec for warm cavity-0.0005 sec could be for cold cavity: It depends on Q_0 of Cavity)
- Set **forward power** to **3 W** (in case of room temperature)
- Adjust amplitude/power in W range (1 to 5 W) than click SWEEP and/ or change SPAN (ie, 10 KHz) to get resonance freq. of cavity at measuring computer. If resonance not found
- Again play with Amplitude and phase and then SWEEP or SPAN. Reflected power should be less than 5%. Play with Coupler feed-through (adjust coupler position inside cavity to get resonance frequency). If cavity resonance found (It is shown in figure 6). Actually it is phase signal from cavity. This means we put coupler at right position in cavity, ie, neither to far nor to close.
- Now, press DECAFY and note down Q values.
- Do a decay in order to see if Q_{pickup} has a reasonable value (It is the only important value from this measurement). The decay time is not important because it is used to calculate the Q value, so it is a redundant information.
- **Setup** -> **decay time range** $\sim 10^{-6}$ s, then push the **DECAFY** button and wait. Typical values at **Room Temperature** are:

Q_{cav}	Q_{pu}
5×10^3	$10^9 - 10^{10}$

The relation is, $Q_{pu} = Q_{cav} * 10$ (cavity at 1.8K)

These Q_{pu} values are the parameter which are expected to measure at 1.8K.

Now, **SAVE file** (Hence, resonance frequency of cavity along with other information will be saved)

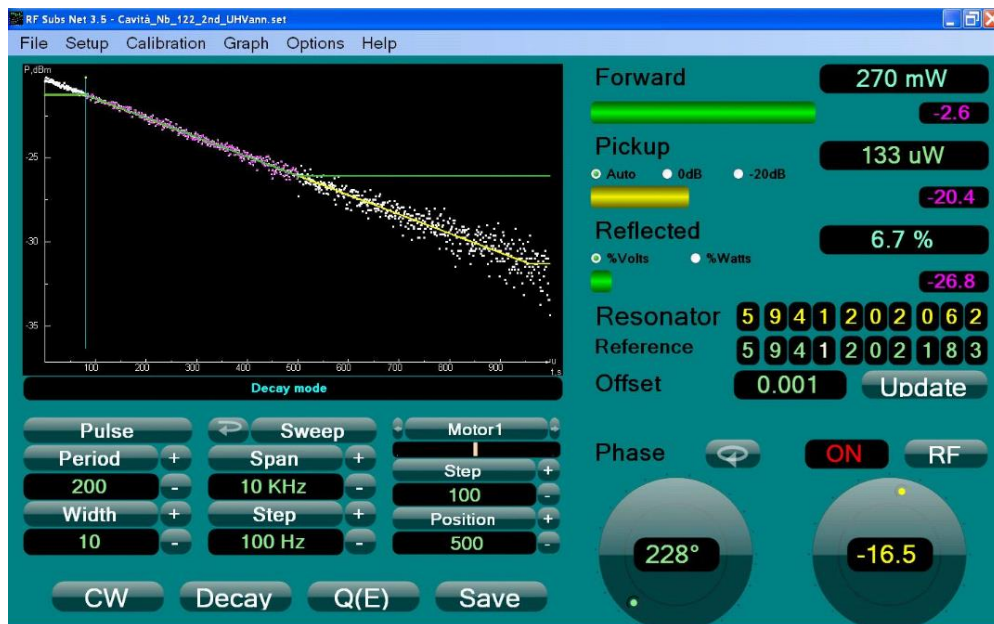


Figure 5.14: Decay time graph. The graph should show several points, a yellow line and a green one

- The graph should show several white points, a yellow line and a green one as shown in Figure 5.14.

- The points should form a line from the top left corner of the window (where they should be closer to the line they form) to the bottom right one (where they should be much more spread)
- The yellow line is a first data interpolation and considers all the data
- The green line is a more precise interpolation because it does not consider data with big errors (the ones in the bottom right corner in figure)
- Typically at room temperature it is only possible to do the interpolation with 4-5 points. So only **YELLOW line** is significant.

SAVE SETUP (with correct file name) and proceed measurement

All the previous test we have done at room temperature. At this time we need to cool down cavity at 4.2K.

Now start calibration of internal cables as given below.

B. Internal cables calibration at low temperature (4.2K)

- Insert 20 dB attenuator (If it is not already connected) in the pickup line and remove the software attenuation (Calibration->pick up->Pick up attenuator- put here 0 dB). Note: If 20 dB attenuator is not inserted in the pickup line in that case -20 dB should be added in software attenuation (ie, Calibration->pick up->Pick up attenuator- put here -20 dB)

FINDING THE CAVITY

- Set the gain to *Fine 1.0* on the pre-amplifier (MODEL: 5113 Princeton applied research instrument)
- Move out the coupler with the feed-through and adjust the phase. Press **UPDATE**

In order to calibrate the pickup internal cables it is necessary to **connect the forward cable to the pickup input line of the RF stand** (ie, Cryostat). And open **Calibration menu tab** and follow the instructions as given below.

- **Calibration -> forward -> forward cable loss** and change the value (by pressing ENTER) until there is **100%** of reflected wave and write that number in **Calibration -> pickup -> pickup cable loss**
- **Connect the forward cable to the coupler forward input and the pickup cable to the pickup input of the RF stand** (ie, Cryostat).
- Unlock cavity from software, set frequency difference from the resonance by 1 MHz higher at reference field of frequency bar *modify number* by pointing mouse (and using mouse wheel), and check the reflected wave is 100%.
- If it is not then **Calibration -> forward -> forward cable loss**, and modify the value until there is 100% reflection (same as earlier passage but now the forward internal cable is calibrated)
- Set back (Insert) the correct resonance frequency (Insert previous value that is 1 MHz less at reference field of frequency bar *modify number* by pointing mouse) and **lock the cavity**. It is shown in Figure 7.
- **Save set-up** with same file name

Decay time (Q_0 of cavity) measurement at 4.2K

Search of cavity inserting resonance frequency (in software of measurement computer) received at network analyzer at 4.2 K:

- Connect forward and pick up cables to the respective cavity input of cryostat. Open file and save set up with correct name.
- Set the gain to *Coarse 1.0* on the pre-amplifier
- Switch on the power amplifier. Click at **RF**
- Insert resonance frequency f_{res} found at network analyzer
- Change the coupler position with the feed-through circular know and adjust the phase form software in order to minimize the reflected wave up to 5% (voltage)
- Click **calibration** -> **Pickup** -> **Pickup Attenuator** (Insert -20 dB software attenuation)
- Click **calibration** -> set decay time (between 0.0002-0.0005)
- Set fwd power to -100 mW
- Adjust amplitude/power in W range (100 to 150 mW) than click SWEEP and/ or change SPAN (ie, 10 KHz) to get resonance freq. of cavity at measuring computer. If resonance not found again play with Amplitude and phase and then SWEEP or SPAN. Reflected power should be less than 5%. Play with freed through (adjust coupler position inside cavity to get resonance freq.). If found cavity resonance (It is shown in figure 6). Actually it is phase signal from cavity. This means we put coupler at right position in cavity, ie, neither to far nor to close.
- Now, press DECAF and note down Q values.
- Do a decay in order to see if Q_{pickup} has a reasonable value (It is the only important value from this measurement). The decay time is not important because it is used to calculate the Q value, so it is a redundant information.
- **Setup** -> **decay time range** $\sim 10^{-6}$ s, then push the **DECAF** button and wait. Typical values at room Temperature are:

Q_{cav}	Q_{pu}
5×10^3	$10^9 - 10^{10}$

These Q values are the parameter which are expected to measure at 1.8K.

Now, **SAVE file** (Hence, resonance frequency of cavity along with other information will be saved)

- The graph should show several points, a yellow line and a green one as shown in Figure 5.15.
- The points should form a line from the top left corner of the window (where they should be closer to the line they form) to the bottom right one (where they should be much more spread)
- The yellow line is a first data interpolation and considers all the data
- The green line is a more precise interpolation because it does not consider data with big errors (the ones in the bottom right corner in figure)
- Typically at room temperature it is only possible to do the interpolation with 4-5 points
- If the graph shown is not like the ones in the pictures it is necessary to adjust the decay time range (0.0001-0.0005 or set accordingly) until these graphs are obtained.

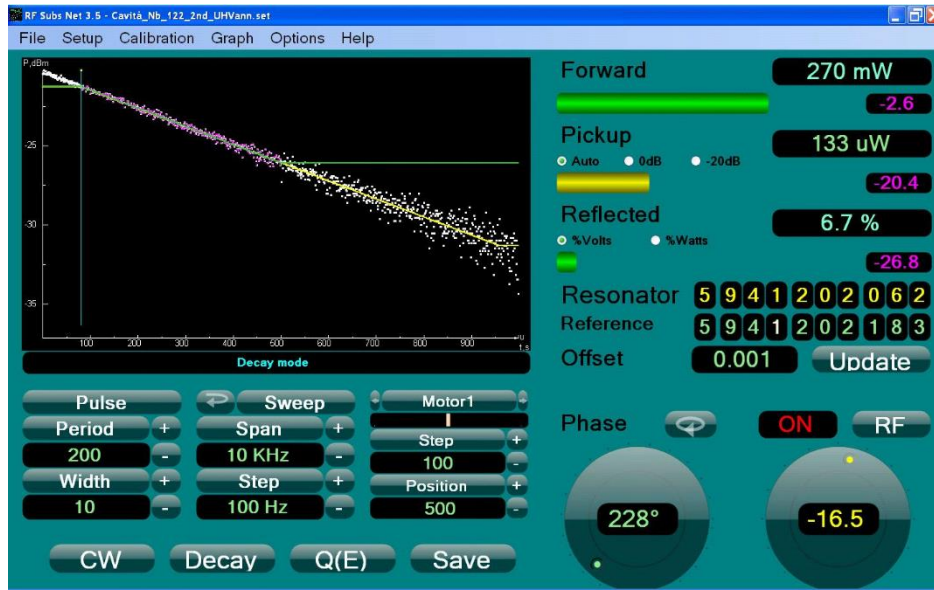


Figure 5.15: Decay time graph. The graph should show several points, a yellow line and a green one

Decay time:

- Set fwd power until there is -20 dBm on the pickup power head for good precision
- Setup -> decay time range ~0,0002s for 6 GHz or 0,02 for 1,3 GHz and then press DECAY button. Typical values @ 4,2 K:

• Q_{cav}	Q_{pu}
$10^6 - 10^7$	$10^9 - 10^{11}$

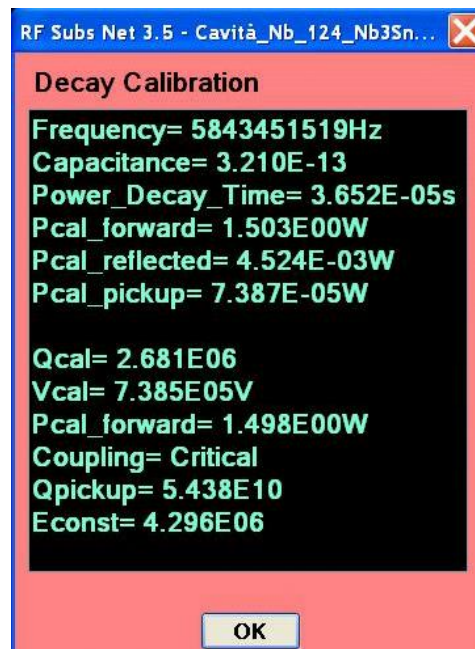


Figure 5.16: Decay calibration graph showing Q value alongwith other important values as mentioned in figure.

SAVE SETUP (with correct file name) and proceed measurement

Now it is possible to start the measurements by pressing the button Q(E). For that, follow the subheading 5. Measurements of Q_0 vs E_{acc} , and onward.

Measurements of Q_0 vs E_{acc}

Now start measurement. Increase power by rotating mouse wheel than reduce reflected power less than 5% --Press SAVE button-OK. The same process will go on till the maximum power available (in case of 6 GHZ cavity, $P= 15W$ and $E_{acc}=10$ MV/m- approximately)

i. Data point (Q_0 vs E_{acc}) measurement at 4.2K

Increase power by rotating mouse wheel while cursor is on power circle (RHS-down at PC software) then reduce reflected power less than 5% -> SAVE button-> OK. Measured data points are shown in figure lower curve (indicating $Q_0 4*10^7$ vs $E_{acc} 7$ MV/m).

Here, reflected power should be reduced by two ways. First, by rotating mouse wheel while cursor is at Phase wheel of monitor-software. If reflected power cant reduce up to 5% then apply second method, ie, press UPDATE, and slowly rotate coupler feed-through (going out of cavity) and watching at PC software. As soon as reflected power approaches minimum less then 5% stop rotating feed through and rotate mouse wheel while cursor is at Phase wheel of monitor-software for further reduction of reflected power (if required), then press SAVE -> OK.

The same process will go on till the maximum power available (in case of 6 GHZ cavity, $P= 15W$ and $E_{acc}=10$ MV/m- approximately).



Figure 5.17: Measured data points are shown at 4.2K. Such data points are measured by increasing power then reducing reflected power below 5%.

After finishing the measurement, go back to minimum power (preferably at $E_{acc}=2$ MV/m). And now connect cryostate recovery line to pumping line. For that follow the procedure as:

- a) Close recovery valve and then open bellow connector
- b) Connect to pumping line and open pumping wheel
- c) Switch on power of big pumping panel
- d) Open switch V4 of pumping system return line to helium ballon
- e) Switch on pump P4 (RHS-top white know)

f) Reduce pressure at 990 mbar (by pushing down button pumping line controle panel). And wait till set prtessure will be stabilized with corresponding temperature.

ii. Data point (Q_0 vs E_{acc}) measurement from temperatures 4.2-1.8 K at fixed E_{acc} or power input ($P=100$ mW)

PUMPING CRYOSTAT (COOLING PROCEDURE): In order to measure points at decreasing temperatures we need to pump Cryostat. For that purpose four pumps are employed. Once set temperature is stabilized, measure the data point as follows;

- Set accelerating field at $E_{acc}=2$ MV/m (preferably) by rotating mouse wheel while curser is on power circle (RHS-down at PC software) then reduce reflected power less than 5% -> SAVE button-> OK.

Again, reflected power should be reduced by two ways (detail is mentioned above in 5.i). Measured data points are shown in figure (at two different parameters, at constant power ($P=100$ mW) and at constant accelerating field $E_{acc} = 2$ MV/m. Indicating Q_0 $4 \cdot 10^7$ up to $4 \cdot 10^9$).

- Set He pressure (eg, 669 mbar) at main panel, and wait (usually it takes 4-6 minutes to stabilize at corresponding temperature). Then measure data point as above mentioned procedure temperature till 1.8 K.



Figure 5.18: Here lower curve at 4.2 K. After that begin to pump cryostate to reduce temperatures and measurements of data have been done at fixed power and fixed accelerating field while reducing temperatures from 4.2K-1.8K are shown.

iii. Data point (Q_0 vs E_{acc}) measurement at 1.8K

Here, follow the exactly same measurement procedure as mentioned above in 5.i.

- Increase power by rotating mouse wheel while curser is on power circle (RHS-down at PC software).
- Then reduce reflected power less than 5% --Press SAVE button-OK.

- While taking data at increasing power cavity will heat up and hence temperature will slowly go up. Hence in order to keep temperature stable at 1.8K during the measurement it is required to reduce pressure slowly.

The same process will go on till the maximum power and accelerating field are available [in case of 6 GHz cavity, P= 5W and E_{acc} =22 MV/m (approximately)]. Measured data points are shown in figure upper curve (indicating Q_o = 4*10⁹ vs E_{acc} =17 MV/m). In this figure, all measured data are shown in detail. For example, curve at 4.2 K, then measurements of data at fixed power and fixed accelerating field while reducing temperatures from 4.2K-1.8K, and curve at 1.8 K are shown clearly.

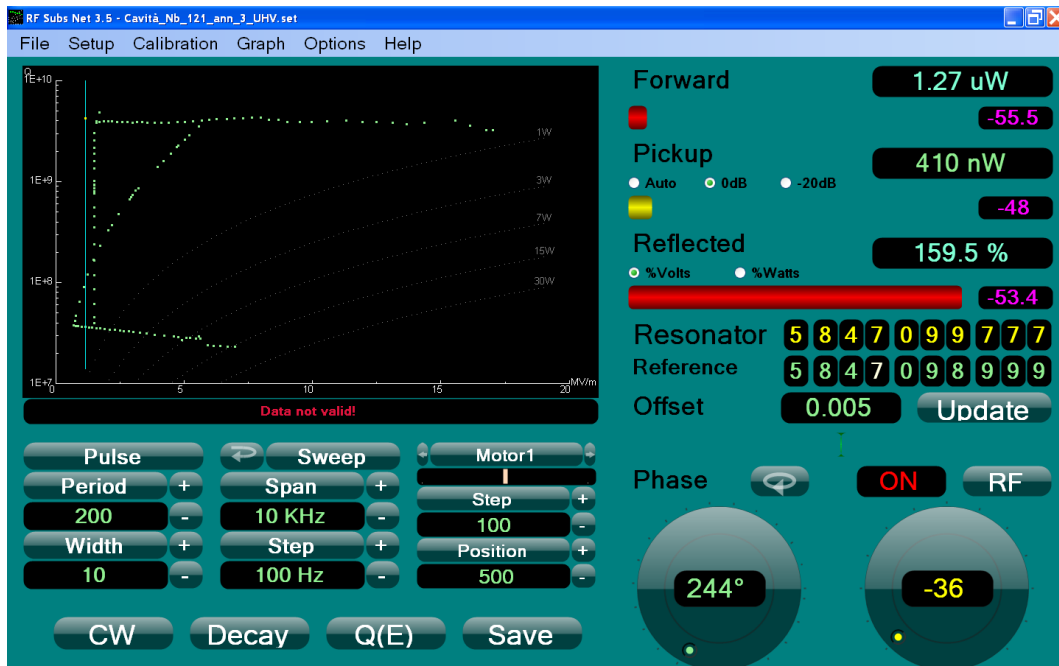


Figure 5.19: Finally we measured data points at 1.8K (upper curve). Such data points are measured by increasing power then reducing reflected power below 5%.

After finishing the measurement, switch OFF **RF power** (by clicking at **RF**). It is at RHS-down at PC software). Then switch off RF power machine. Print a copy of measurement for record. Analyse measured data of Q_o as a function of temperature to calculate surface resistivity of the materials (in this case 6 GHz cavity).

RF System: Correction factors

In this section we give detail information in context of different correction factors. For example, cable calibration (forward, reflected and pick-up cable calibration with low and high sensitivity), and wave function decay calculation that are responsible for calculation of Quality Factor (Q₀).

i. Corrections in cable calibrations

(A) Forward Calibration

$$P_f^{Cavity} = P_f^{Measured} * K_f^{Correction} = \text{forward power @ cavity coupler port} = [W]$$

$$P_f^{Measured} = \text{forward power read by power meter} = [W]$$

$$K_f^{Correction} = \text{forward correction factor}$$

$$K_f^{Correction} = 10^{\left(\frac{Forward\ Attenuator - Forward\ Internal\ Cable\ Attenuation + Forward\ Network\ Attenuation}{10}\right)}$$

Forward Attenuator = [dB] = generally not present

Forward Internal Cable Attenuator = [dB]

Forward Network Attenuation = [dB]

(B) Reflected Calibration

$$P_r^{Cavity} = P_r^{Measured} * K_r^{Correction} = \text{reflected power @ cavity coupler port} = [W]$$

$P_r^{Measured}$ = reflected power read by power meter = [W]

$K_r^{Correction}$ = reflected correction factor

$$K_r^{Correction} = 10^{\left(\frac{Reflected\ Attenuator + Reflected\ Internal\ Cable\ Attenuation + Reflected\ Network\ Attenuation}{10}\right)}$$

Reflected Attenuator = [dB] = generally not present

Reflected Internal Cable Attenuator = [dB]

Reflected Network Attenuation = [dB]

(C) Pickup Calibration with two sensitivities

Low Sensitivity

$$P_{pk}^{Cavity}(LS) = P_{pk}^{Measured} * K_{pk}^{Correction}(LS) = \text{forward power @ cavity pickup port_Low Sensitivity line} = [W]$$

$P_{pk}^{Measured}$ = forward pickup power read by power meter = [W]

$K_{pk}^{Correction}(LS)$ = low sensitivity pickup correction factor

$$K_{pk}^{Correction}(LS) = 10^{\left(\frac{Pickup\ Attenuator + Pickup\ Internal\ Cable\ Attenuation + LS\ Forward\ Pickup\ Network\ Attenuation}{10}\right)}$$

Pickup Attenuator = [dB] = generally present

Pickup Internal Cable Attenuation = [dB]

LS Forward Pickup Network Attenuation = [dB]

High Sensitivity

$$P_{pk}^{Cavity}(HS) = P_{pk}^{Measured} * K_{pk}^{Correction}(HS) = \text{forward power @ cavity pickup port_High Sensitivity line} = [W]$$

$P_{pk}^{Measured}$ = forward pickup power read by power meter = [W]

$K_{pk}^{Correction}(HS)$ = high sensitivity pickup correction factor

$$K_{pk}^{Correction}(HS) = 10^{\left(\frac{Pickup\ Attenuator + Pickup\ Internal\ Cable\ Attenuation + HS\ Forward\ Pickup\ Network\ Attenuation}{10}\right)}$$

Pickup Attenuator = [dB] = generally present

Pickup Internal Cable Attenuation = [dB]

HS Forward Pickup Network Attenuation = [dB]

ii. Corrections in Decay calculation

f = Frequency = [Hz]

*CR = Capacitance = $0,321 * 10^{-12}$ for 6 GHz cavities*

P_f^{Cavity} = forward power @ cavity port = [W]

P_r^{Cavity} = reflected power @ cavity port = [W]

P_{pk}^{Cavity} = Pickup power @ cavity port = [W]

*$V_f^{Cavity} = \sqrt{P_f^{Cavity} * 400}$ = forward voltage = [V] Forward voltage*

*$V_r^{Cavity} = \sqrt{P_r^{Cavity} * 400}$ = reflected voltage = [V] Reflected voltage*

*$V_{pk}^{Cavity} = \sqrt{P_{pk}^{Cavity} * 400}$ = pickup voltage = [V] Pickup voltage*

L = Gap Length = [m] = 0,025 for 6 GHz cavities

$$\Gamma = \sqrt{\frac{P_r^{Cavity}}{P_f^{Cavity}}}$$

$$VSWR = \frac{(\Gamma + 1)}{(1 - \Gamma)}$$

If coupling = "Crit" then swr = 1

If coupling = "over" than swr = VSWR

If coupling = "under" than swr = 1/VSWR

$$P_{diss} = P_f^{Cavity} - P_r^{Cavity} - P_{pk}^{Cavity}$$

$$\beta_{pk} = \frac{P_{pk}^{Cavity}}{P_{diss}}$$

$$\beta_{cp} = swr$$

$$\omega = 2 * 3,141593 * f$$

$$Q_L = \omega * \tau$$

$$U_{st} = \frac{Q_L * (1 + \beta_{cp} + \beta_{pk}) * P_{diss}}{\omega}$$

$$Q_{pk} = \frac{\omega * U_{st}}{P_{pk}^{Cavity}}$$

$$Q_0 = Q_L * (1 + \beta_{cp} + \beta_{pk})$$

$$E_{Acc} = \frac{\sqrt{\frac{U_{st}}{CR}}}{L}$$

$$K_e = \frac{E_{Acc}}{V_{pk}^{Cavity}}$$

$$Q_{point} = \omega * (E_{Acc} * L)^2 * \frac{CR}{P_{diss}}$$

Single Point Calculation

$$P_{diss} = P_f^{Cavity} - P_r^{Cavity} - P_{pk}^{Cavity}$$

$$E_{Acc} = K_e * \sqrt{P_{pk}^{Cavity} * 400}$$

$$Q_{point} = \omega * (E_{Acc} * L)^2 * \frac{CR}{P_{diss}}$$

Summuary

we have explained systematically RF measurement process of 6 GHz bulk-Nb and Nb coated Cu cavities from room temperature down to 1.8K. Also correction factors of RF system have been explained in detail. Step-by-step measurement process of tesla type Cavity has been demonstrated starting from the search of cavity resonance at room temperatute, cable calibrations (internal and external) at different temperatures (room temperature and helium temperature,ie, 4.2K) and three set of Data point (Q_o vs E_{acc}) measurement from temperatures 4.2-1.8 K at increasing power (firstly at 4.2K then at 1.8K)and at fixed accelerating electric field (while measuring at decreasing temperature scale, ie, 4.2-1.8K) along with RF system correction factors have been explained indetail .

-----*****-----

Chapter 6

RF cavity results

The research work reported in this dissertation carried out on 6GHz monocell Nb cavities which are fabricated using spining technique to create seamless structure. Details in context of various steps of surface treatments are given in chapters 3 and 4 respectively. Bulk Nb sheets of 3mm thickness is used for the purpose. These cavities are purified using induction heating method. The Nb cavities were tumbled, chemically and thermally treated, ultrasonic degreased for 1 hour and finally High Pressure Rinsed (HPR) for 10-15 minutes.

A short overview of the rf measurement system: After HPR with DI water, cavities are dried in clean room for 10 minutes and then RF antennas were assembled carefully on the cavity flanges with Kapton^R gaskets. The cavity is equipped with input and pickup antennas and vacuum sealed in a clean-room (class 1000), then evacuated to approximately 10^{-8} mbar and transferred to the cryostat for vertical test. A layout of the cryostat is given in chapter 5 (Figure 5.2). The input antenna is connected through a flexible metallic bellow to the cavity, so that the distance between antenna tip and cavity can be changed. The coupling strength of the input coupler can be varied by several orders of magnitude by moving the center piece of the input coupler by a few centimeters. In the vertical test cryostats, the external coupling of the input antenna can be varied from about $Q_{\text{ext}} = 2 \cdot 10^6$ up to $Q_{\text{ext}} = 5 \cdot 10^9$ so that a matched coupling ($Q_{\text{ext}} = Q_0$) can be achieved in the temperature range from 4.2 K to 1.6 K. The second antenna is used as a pickup probe with a much higher $Q_{\text{ext}} = 5 \cdot 10^{10}$ for monitoring the cavity field which is proportional to the square root of the power coupled out by the antenna. As the SC cavities have a very high quality factor the width of the resonance curve is extremely small (say, between 1 to 10 Hz). Small changes in the helium pressure of the cryostat cause changes of the resonance frequency of the cavity. Therefore the frequency generator has to be controlled with a phase-locked loop (PLL), where the phase difference between the input signal, taken from a directional coupler, and the pickup signal are compared. As a temperature sensor, Cernox thermometer and a carbon resistor are used. To ensure thermal contact with the resonators, the resistors are glued and screwed gently at the upper surface of cavity flange, which have high heat conductivity at helium temperature.

Once the resonator is mounted in the cryostat, it will be first cooled at 4.2 K (atmospheric pressure) while cooling down to 1.8 K is achieved via pumping down the helium pressure approximately 16 mbar.

Quality factor: In principle, the quality factor of the cavity is measured when the incident power is switched off, leading to the exponential decays of the field excited in the cavity. It is given by the differential equation,

$$P_{\text{tot}} = -\frac{dU}{dt} \quad (6.1)$$

Where, $P_{\text{total}} = P_{\text{diss}} + P_{\text{ext}} + P_t$

where P_{diss} is the power dissipated in the cavity, P_{ext} the power coupled out through the input antenna and P_t the power coupled out from the pickup probe. Usually, the pickup probe is very weakly coupled, therefore, P_t can be neglected.

The external quality factor Q_{ext} and loaded quality factor Q_L are given as:

$$Q_{ext} = \frac{\omega U}{P_{ext}} \quad (6.2)$$

And,

$$Q_L = \frac{\omega U}{P_{tot}} \quad (6.3)$$

After co-relating both equations, we have,

$$\frac{1}{Q_L} = \frac{1}{Q_0} + \frac{1}{Q_{ext}} \quad (6.4)$$

Integrating the differential equation gives,

$$U(t) = U_0 * \exp\left(-\frac{t}{\tau_L}\right) \quad (6.5)$$

Here, τ_L is $\frac{Q_L}{\omega}$

Therefore from measuring the decay time, τ the loaded quality factor, Q_L can be determined.

Here, the required surface treatment procedures of cavity preparation and RF test sequences that are summarized as given below.

- i. Centrifugal tumbling of more than 40 hours: removed ≥ 3 grams of defected inner materials.
- ii. Degreasing surfaces to remove contaminations: Ultrasonic cleaning for 1 hour then rinsed with ultra-clean DI water and drying with nitrogen in class 100 clean room.
- iii. BCP Static, 5minutes: removed $d \geq 200\mu\text{m}$ of inner thickness.
- iv. BCP flux, 5hours: removed $d \geq 200\mu\text{m}$ of inner thickness.
Or,
EP flux, 5 hours: removed $d \geq 400 \mu\text{m}$ of inner thickness
- v. High Pressure Rinse (HPR) with ultra-clean DI water and drying with nitrogen in class 1000 clean room to remove particulates from interior surfaces that incurred during the chemistry and handling.
- vi. RF test at temperatures between 4.2-1.8K
- vii. Atmospheric pressure high temperature treatment $\geq 2000^\circ\text{C}$ inside clean quartz tube under cover of 4He gas for 2 to 7 minutes
- viii. High Pressure Rinse (HPR) with ultra-clean DI water and drying with nitrogen in class 1000 clean room
- ix. RF test at temperatures between 4.2-1.8K
- x. Low temperature UHV baking ($\sim 135^\circ\text{C}$) for 60hours. High temperature heat treatment inside UHV chamber for 2 to 7 minutes
- xi. High Pressure Rinse (HPR) with ultra-clean DI water and drying with nitrogen in class 1000 clean room
- xii. Clean room assembly
- xiii. RF test at temperatures between 4.2-1.8°K

6.1 Purification

We have studied several Nb cavities with different parameters. i.e., some cavities are thermally treated under atmospheric pressure in an induction heating and later on at UHV system as well, while some cavities are annealed at UHV system to compare RF test performance as shown later section.

6.1.1 Atmospheric pressure treatment

6.1.1.1 Thermal treatments and RF test results

RF test: The vertical test has been done to measure Quality Factor vs accelerating field (MV/m). Here, we have done three sets of measurements. At first set, we collected data, i.e., datum points (Q_o vs E_{acc}) at 4.2 K. It was done while increasing power then by reducing reflected power that should be less than 5% then collected datum (saved datum point). The same process was repeated until the maximum power available (in case of 6 GHz cavity, approximate power, $P=15W$ and $E_{acc}=10$ MV/m). After finishing the measurement, power was reduced (preferably at $E_{acc}=2$ MV/m). In second set of measurement, data were collected at different fixed power ($P=100$ mW) and/or at different fixed accelerating field (e.g., $E_{acc}=2$ MV/m) while reducing bath temperatures from 4.2 K-1.8 K. Mostly, two different R_s curve have been measured. One is at constant power (i.e., 100 mW) while other is at constant field (i.e., 0.7 or 2 MV/m). It was difficult to measure at low constant field while approaching at low temperatures. Since very low power corresponds to high field gradient if the cavity has high performance, i.e., high Q value and hence very low R_s . In order to measure datum points at decreasing temperatures we actively pumped 4Helium bath. Once desired temperature is stabilized, we measured the datum point as follows: set accelerating field at $E_{acc}=2$ MV/m (preferably) then reduced reflected power less than 5% and collected datum (saved datum point). The same process was repeated until the minimum temperature achieved (i.e., 1.8K). In third set of measurement, we collected datum points (Q_o vs E_{acc}) at 1.8K. Datum points were taken as explained in first set (i.e., at 4.2K). In this way, there was several (about 200 points) measurement data have been recorded along with the temperatures of the bath (between 4.2K and 1.8K) of the outer surface of cavities, and cross-checked.

We have done series of RF tests after several combinations of surface treatment (i.e., successive removal of inner materials of cavities by BCP and/or EP, HPR and combination of low and high temperature heat treatments). The cavity have been either flux BCPed or EP and HPR treated to remove damaged inner layer, then RF tests performed before and after high temperature annealing between temperatures 1980-2230 °C are shown in various Figure for almost all cavities which subjected to induction heating (cavity no.121-132). We have plotted quality factor vs accelerating field. Surface resistivity vs inverse of temperature is calculated from the Q measurement and theoretically fitted over experimental data (red solid line). The measured data are fitted using BCS theory to extract R_{res} for all cavities using equation (6.9). The overall formula is given below,

$$R_s = R_{BCS} + R_{res} \quad (6.6)$$

$$R_s = \frac{A}{T} * \frac{\exp\left(-\frac{ST_c}{2T}\right)}{1 + \exp\left(-\frac{ST_c}{2T}\right)} + R_{res} \quad (6.7)$$

Where,

$$R_s = y * \frac{1}{T} = x \quad (6.8)$$

$$y = A * x * \frac{\exp^{-Bx}}{(1+\exp^{-Bx})^2} + C \quad (6.9)$$

Where, $B = \frac{S}{2}T_c$, is induction voltage.

S is strong coupling factor, and is = 4.07 at 9.3K, while 4.12 at 9.2K. T_c is critical temperature, and C is constant.

After that cavity was subjected either to atmospheric pressure heat treatment or UHV treatment, quickly followed by HPR then RF test have been done which are shown in various Figures, also surface treatments procedure history is mentioned for each cavity. Explanation of some most important achievements alongwith the impact of different procedures have been given at the end of all the graphical representation.

Nb 121 (History):

Surf. Treat. procedure	Total wt. lost (g)	Total thickness removed (um)	Total thickness removed (%)	Time	6GHz inner surf. (cm ²)	Remarks
Tumbling(CBP)	1.353g	17.94	0.77%.	56Hrs	88	Mandrel scatches still visible.
Fast BCP	3.362g	19.61	1.95%.	5min	200	
Flux BCP	37.809 g	501.34	22.33%.	2.5Hrs	88	
EP	NA	NA	NA	NA		NA

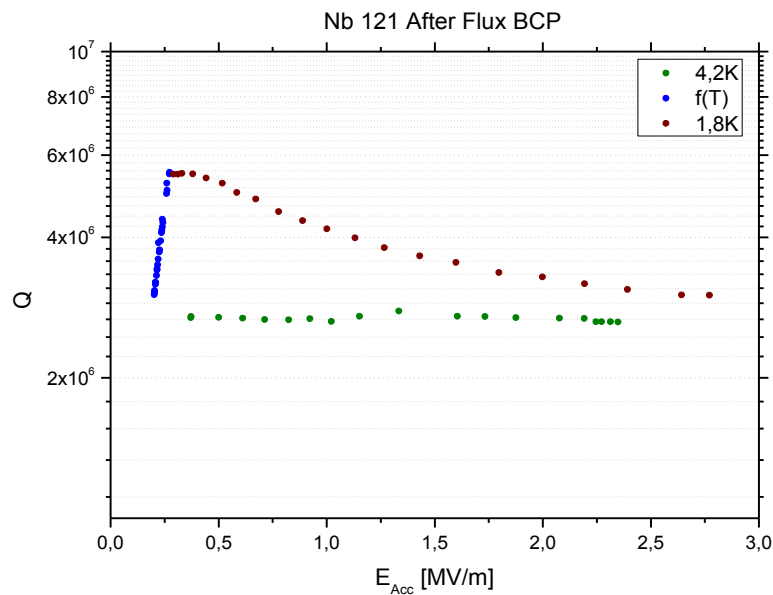


Figure 6.1: Measurement of quality factor vs accelerating field (RF test after Flux EP) is shown.

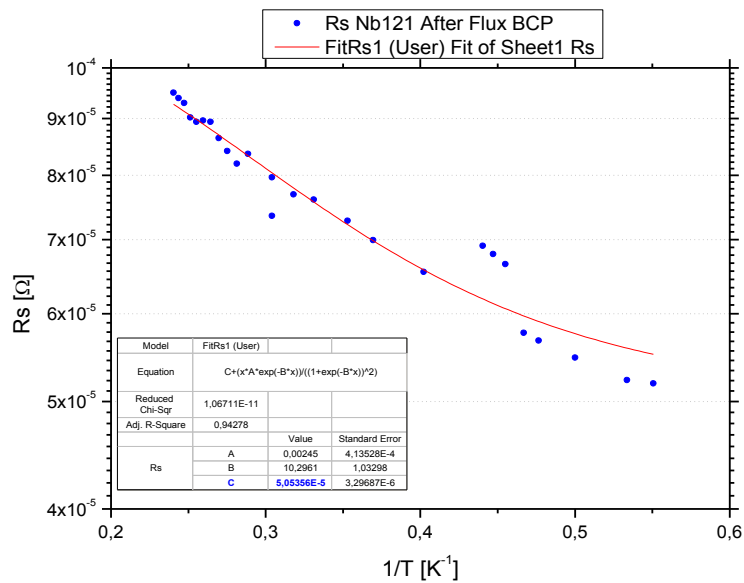


Figure 6.2: Shows surface resistivity (calculated from Figure 6.1) vs inverse of temperature and theoretically fitted using equation (6.9).

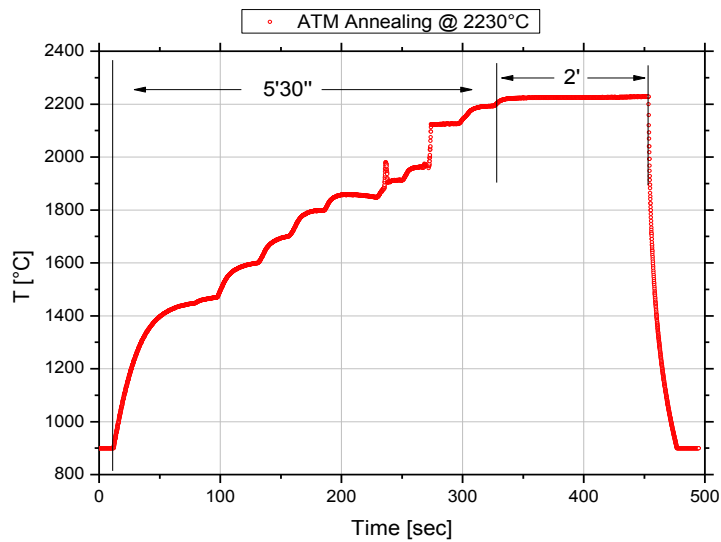


Figure 6.3: Induction heating at atmospheric pressure under He gas atmosphere (2 bar)

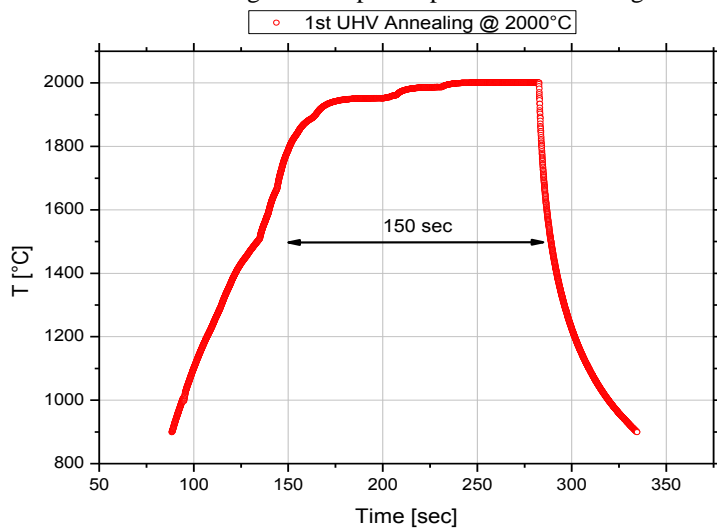


Figure 6.4: Induction heating in UHV chamber has been done to the same cavity (number 121). The purpose is to observe difference from atmospheric treatment

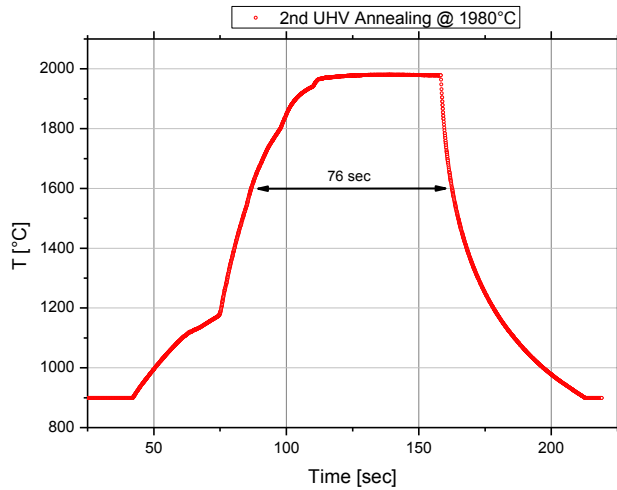


Figure 6.5: Second annealing at UHV system has been done to the same cavity (number 121). The purpose is to observe difference from first UHV annealing

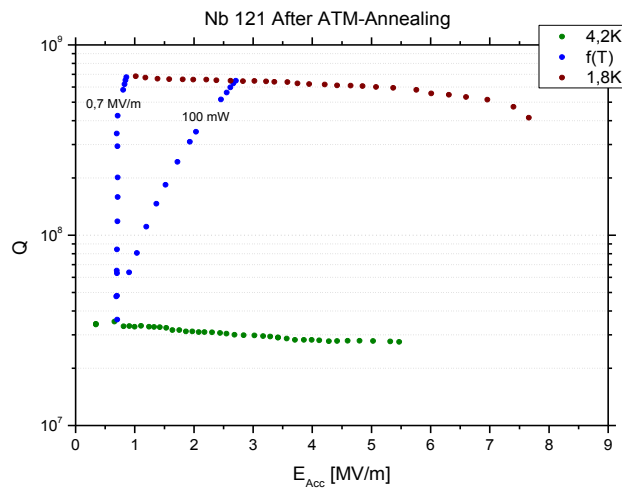


Figure 6.6: RF tests data after high temperature annealing is shown. value Quality (Q_0) factor vs accelerating field (RF test after Flux BCP of cavity 121). Q_0 is measured at fixed power and also at fixed accelerating field, as shown.

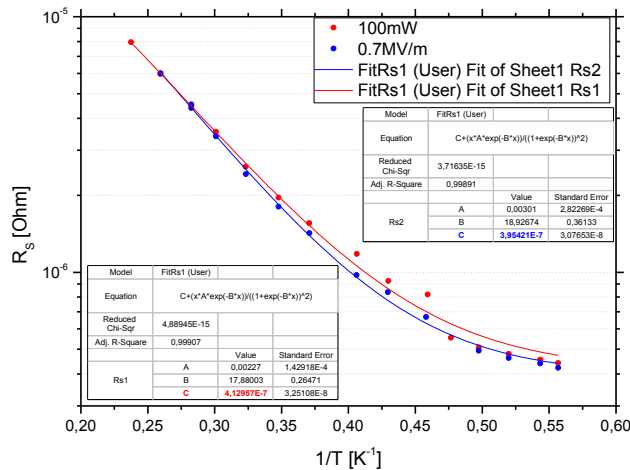


Figure 6.7: Surface resistivity vs inverse of temperature calculated from Fig 6.6, and theoretical fit using equation (6.9).

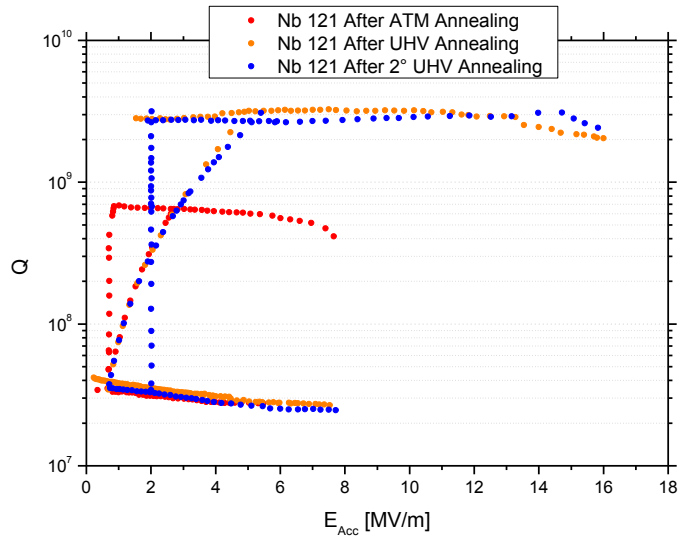


Figure 6.8: A comparison of RF tests at 3 stages is shown. After atmospheric pressure annealing, and first and second annealing at UHV system to the same cavity has been done

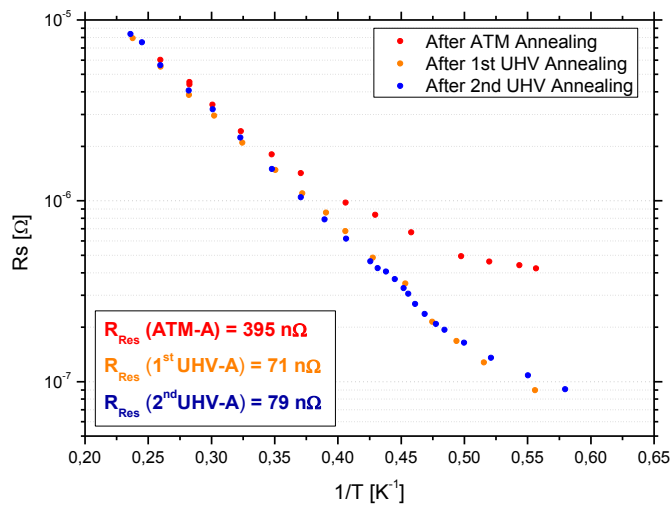


Figure 6.9: Comparison of surface resistivity vs inverse of temperature (calculated from Fig.6.8) is mentioned.

Nb 122: History

Surf. Treat. procedure	Total wt. lost (g)	Total thickness removed (um)	Total thickness removed (%)	Time	6GHz inner surf. (cm ²)	Remarks
Tumbling(CBP)	1.388g	18.40	0.77%.	60 hrs	88	Mandrel scratches still visible.
Fast BCP	18.488g	107.86	10.27%.	5 min	200	
Flux BCP						NA
EP	13.419	184		2.5 hrs	60	NA

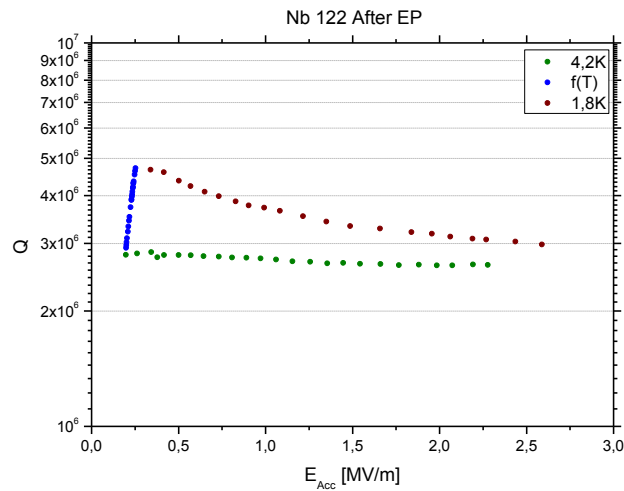


Figure 6.10: RF tests data after EP is shown. Quality (Q_0) factor vs accelerating field (RF test after EP of cavity 122) is shown.

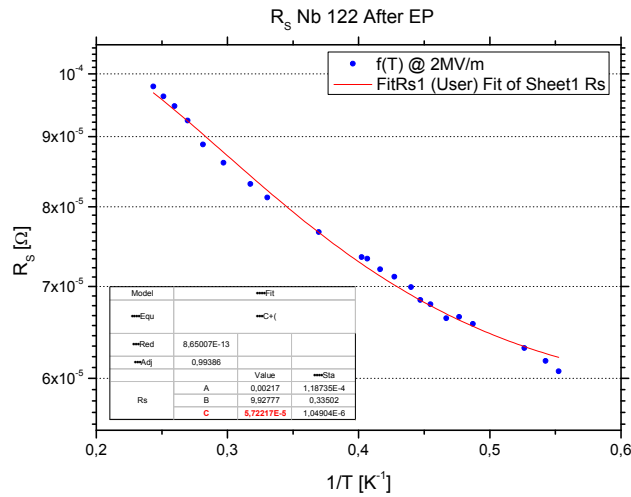


Figure 6.11: Surface resistivity vs inverse of temperature calculated from Fig 6.10, and theoretical fit using equation (6.9).

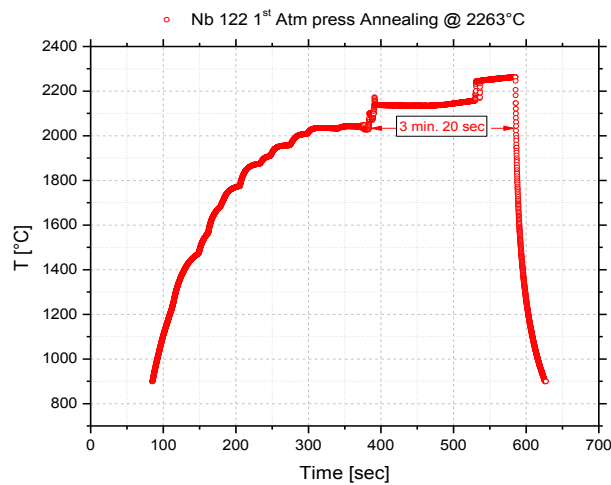


Figure 6.12: Graph shows temperature vs time of 1st atmospheric pressure annealing

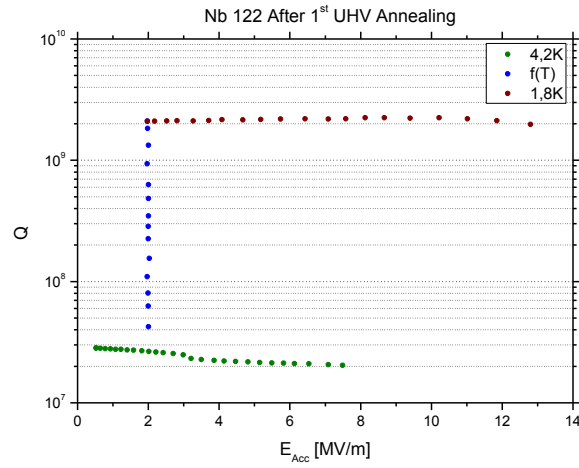


Figure 6.16: RF tests data after annealing is shown. Quality (Q_0) factor vs accelerating field (RF test after EP of cavity 122) is shown.

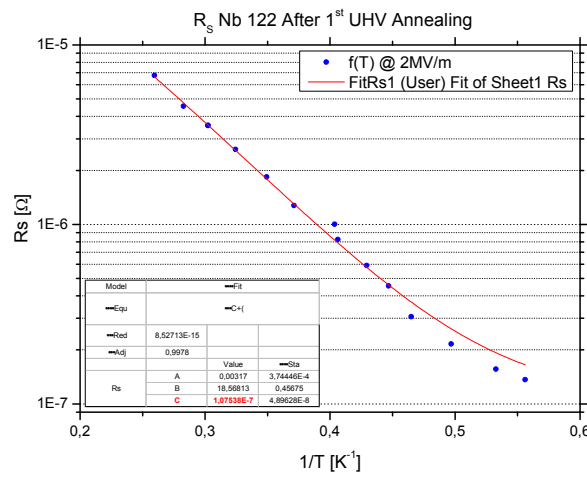


Figure 6.17: Surface resistivity vs inverse of temperature calculated from Fig 6.16, and theoretical fit using equation (6.9)

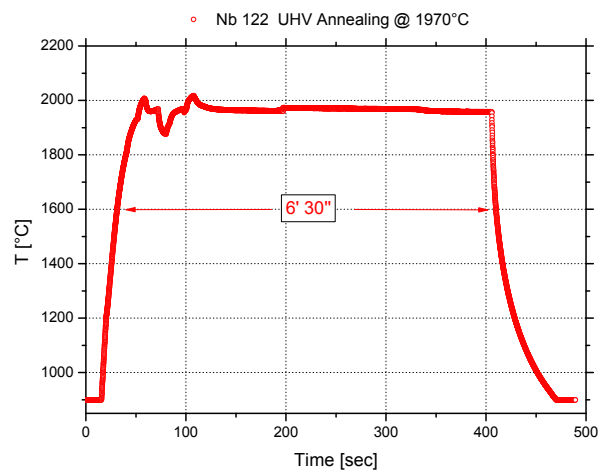


Figure 6.18: 2nd UHV annealing at 1970 C for 6'30" at max. temperature. This is, altogether 3rd annealing done to the same cavity .

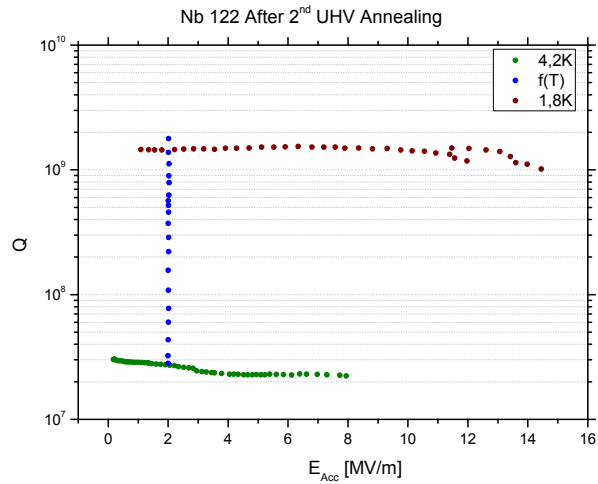


Figure 6.19: RF tests data after annealing is shown. Quality (Q_0) factor vs accelerating field (RF test after 2nd UHV annealing of cavity 122) is shown.

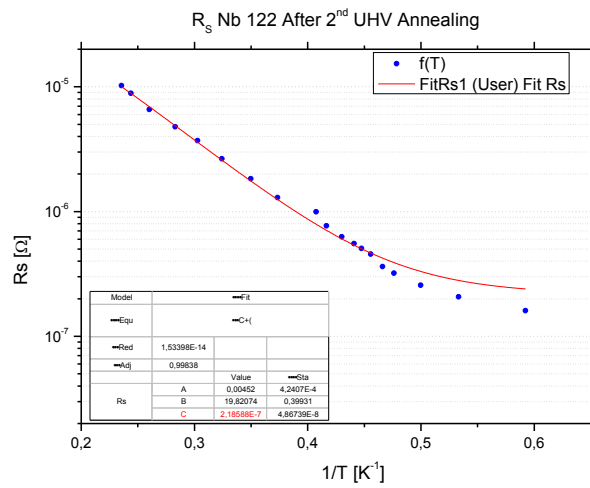


Figure 6.20: Surface resistivity vs inverse of temperature calculated from Fig 6.19, and theoretical fit using equation (6.9)

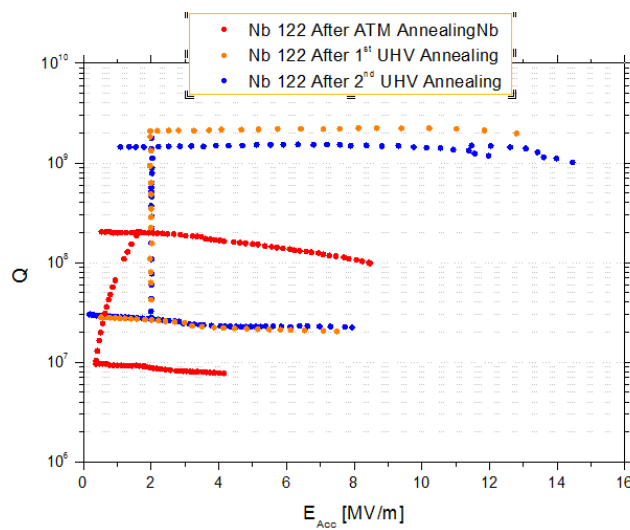


Figure 6.21: A comparison of RF tests at 3 stages is shown. After atmospheric pressure annealing, and first and second annealing at UHV system to the same cavity has been done

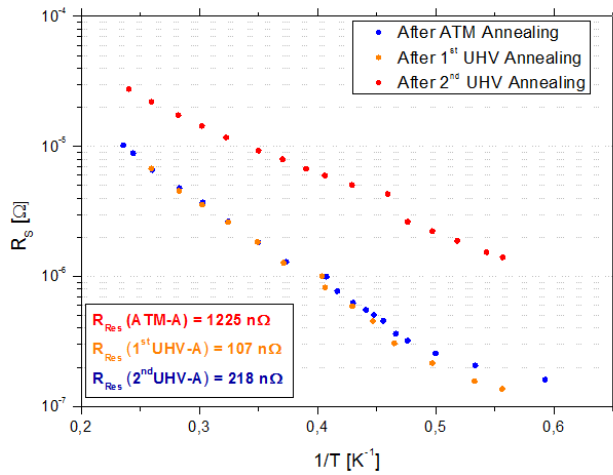


Figure 6.22: Comparison of surface resistivity vs inverse of temperature (calculated from Fig.6.21) is mentioned.

Nb 125: History

Surf. Treat. procedure	Total wt. lost (g)	Total thickness removed (um)	Total thickness removed (%)	Time	6GHz inner surf. (cm ²)	Remarks
Tumbling(CBP)	1.388g	18.40	0.77%.	60 hrs	88	Mandrel scratches still visible.
Fast BCP	7.033g	41.03	3.91%.	4 min	200	
Flux BCP						NA
EP	13.894	184.23	8.04%	5 hrs	60	

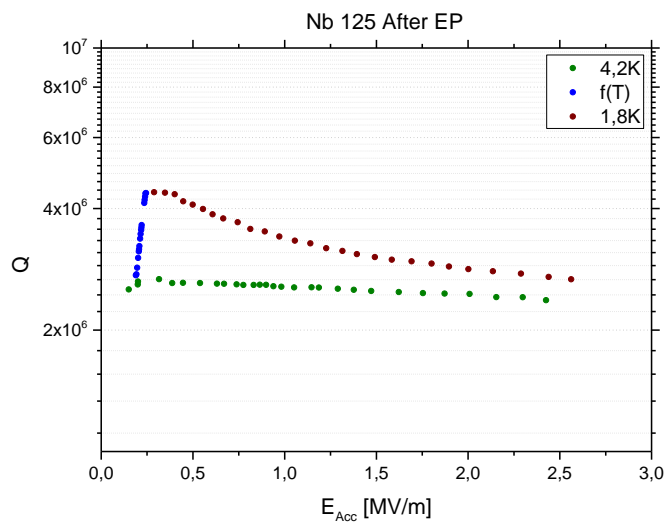


Figure 6.23: RF tests data after annealing is shown. Quality (Q_0) factor vs accelerating field (RF test after 2nd UHV annealing of cavity 125) is shown.

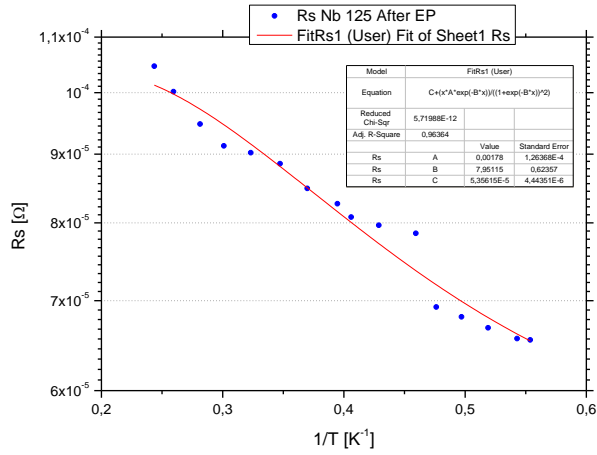


Figure 6.24: Surface resistivity vs inverse of temperature calculated from Fig 6.23, and theoretically fitted (leaving some points at lemdu transition) using equation (6.9)

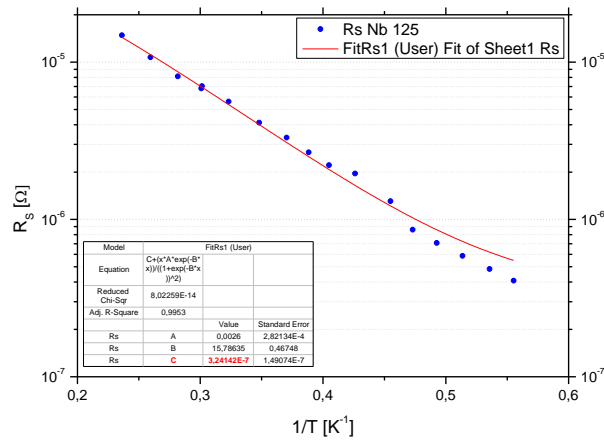


Figure 6.25: Surface resistivity vs inverse of temperature calculated from Fig 6.22, and theoretical fitted (including points measured at lemdu transition) using equation (6.9)

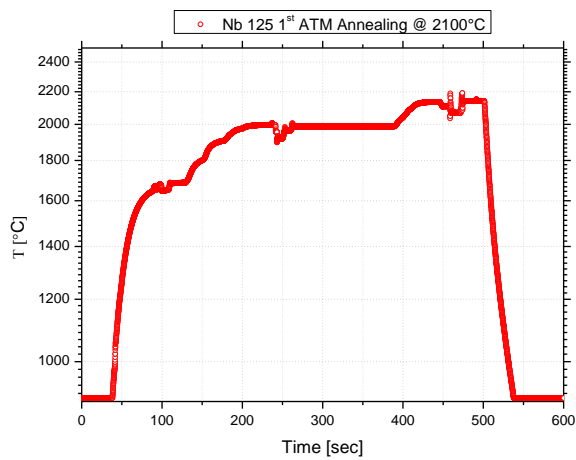


Figure 6.26: Graphical representation of 1st Atmospheric pressure annealing at 2100 C.

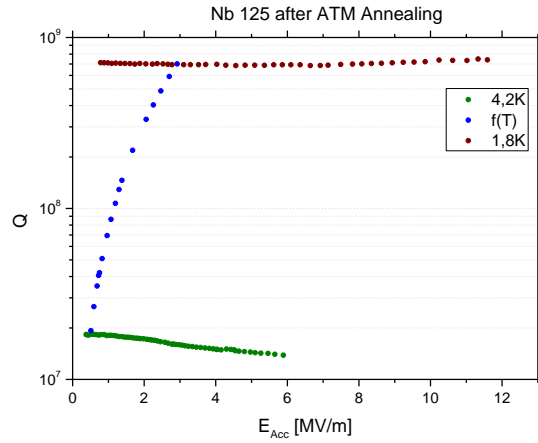


Figure 6.27: RF tests data after ATM. annealing is shown. Quality (Q_0) factor vs accelerating field (RF test after annealing of cavity 125) is shown.

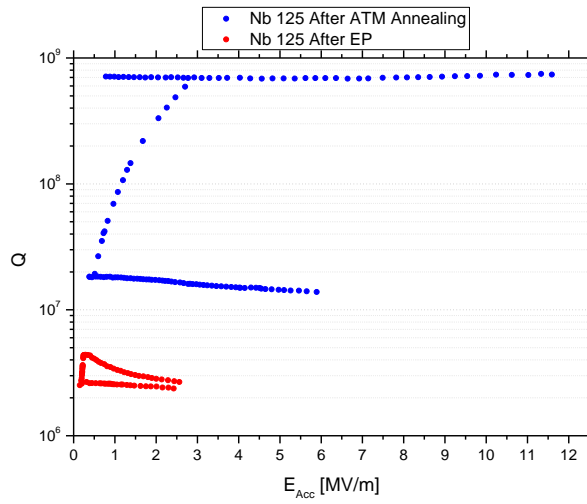


Figure 6.28: A comparison is done for RF tests data after both type of annealing is shown.

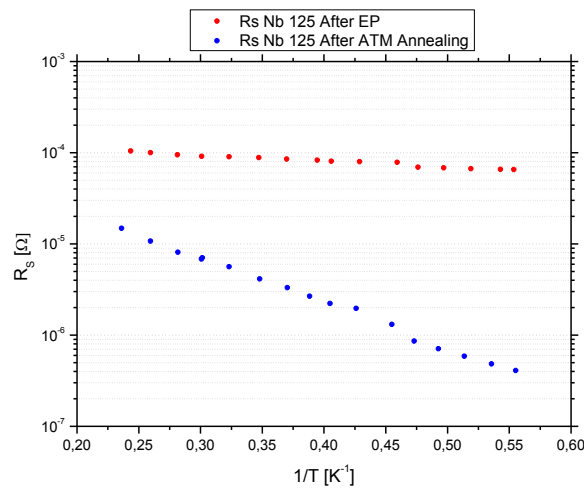


Figure 6.29: A comparison (R_s vs inverse of temperature) is done for RF tests data after both type of annealing is shown.

Altogether, RF tests have been done inside transparent quartz tube under ^4He gas atmosphere (2 bar) to three cavities (Identity number 121 BCP treated, 122 and 125 were EP treated) before and after high temperature annealing at atmospheric pressure. Surface resistivity that was calculated from measured Quality (Q_0) factor vs inverse of temperature is summarized, are shown in Figure 6.30.

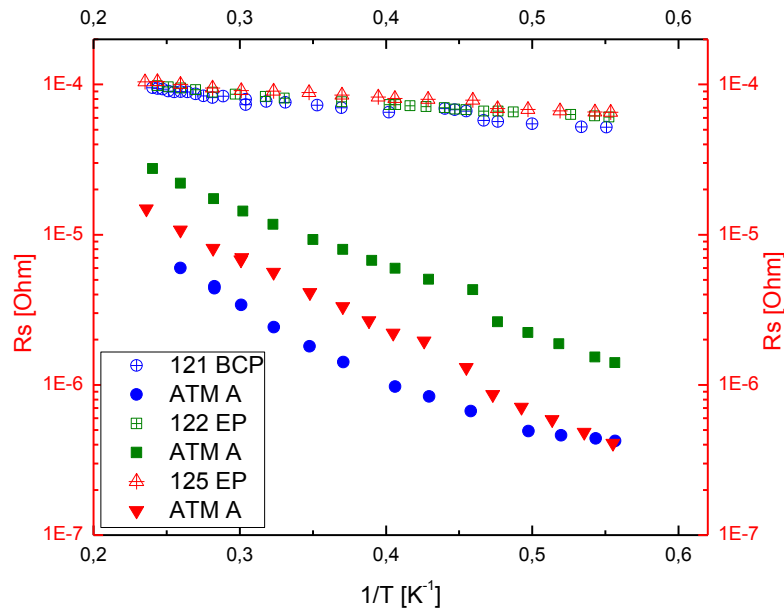


Figure 6.30: A summarized surface resistivity [calculated from measured Quality (Q_0) factor] vs inverse of temperature shown in this figure. Reduction of surface resistivity by atmospheric pressure annealing that has been done inside quartz tube under ^4He gas atmosphere. RF tests are done before and after high temperature annealing at atmospheric pressure are shown.

6.1.2 UHV treatment

6.1.2.1 Thermal treatment and RF test results

RF tests data before and after high temperature annealing at UHV system for several cavities (cavity identity number 123, 124, 126, 127, 129, 131, 132) have been done in order to compare cavity performances which were annealed at atmospheric pressure under cover of He-gas (for example, cavity number 121, 122 and 125). Measurements of quality (Q_0) factor vs accelerating field (RF test after Flux BCP and/or EP) have been performed. Surface resistivity is calculated from measurements of quality (Q_0) factor, which is plotted vs inverse of temperature and are theoretical fitted using equation (6.9). All measured data are shown in various Figures for individual cavity (in increasing identity number of cavity).

Nb 123:History

Surf. Treat. procedure	Total wt. lost (g)	Total thickness removed (um)	Total thickness removed (%)	Time	6GHz inner surf. (cm ²)	Remarks
Tumbling(CBP)				hrs		
Fast BCP	3.36g	23.09		5 min	200	
Flux BCP	-	-	-	-	-	
EP	6.73	92.5	%	2.5 hrs	60	
Inner EP	7.52	206.61		2.5 hrs	60	
Inner EP	2.44	66.93		30 min	60	289 um removed during 3 cycles of EP

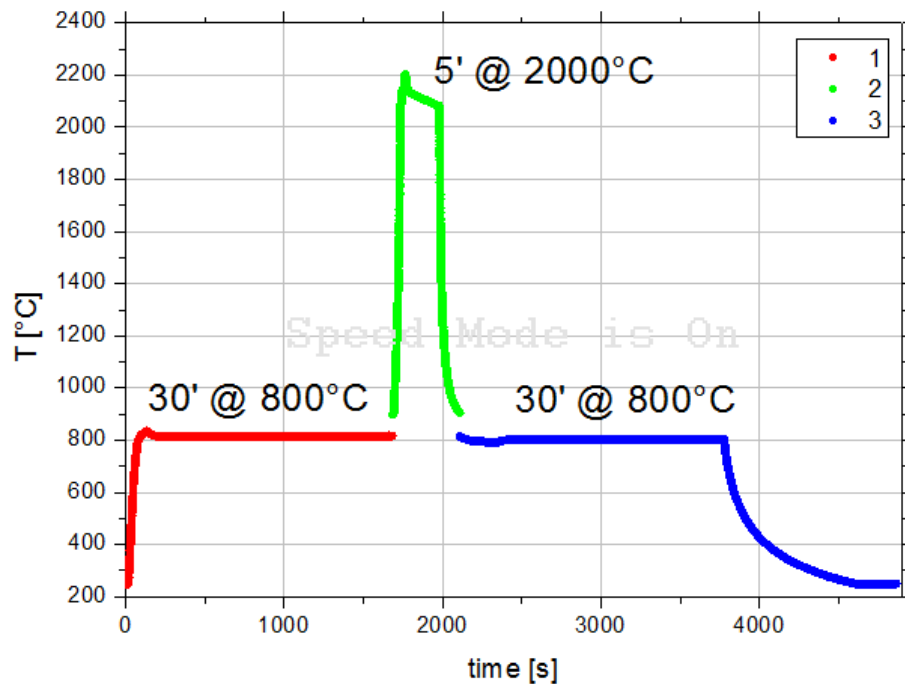


Figure 6.31: Low temperature backing at 800 C has been done before and after high temperature treatment under UHV condition. The maximum annealing temperature is 2000 C for 5 min is shown in between low backing duration.

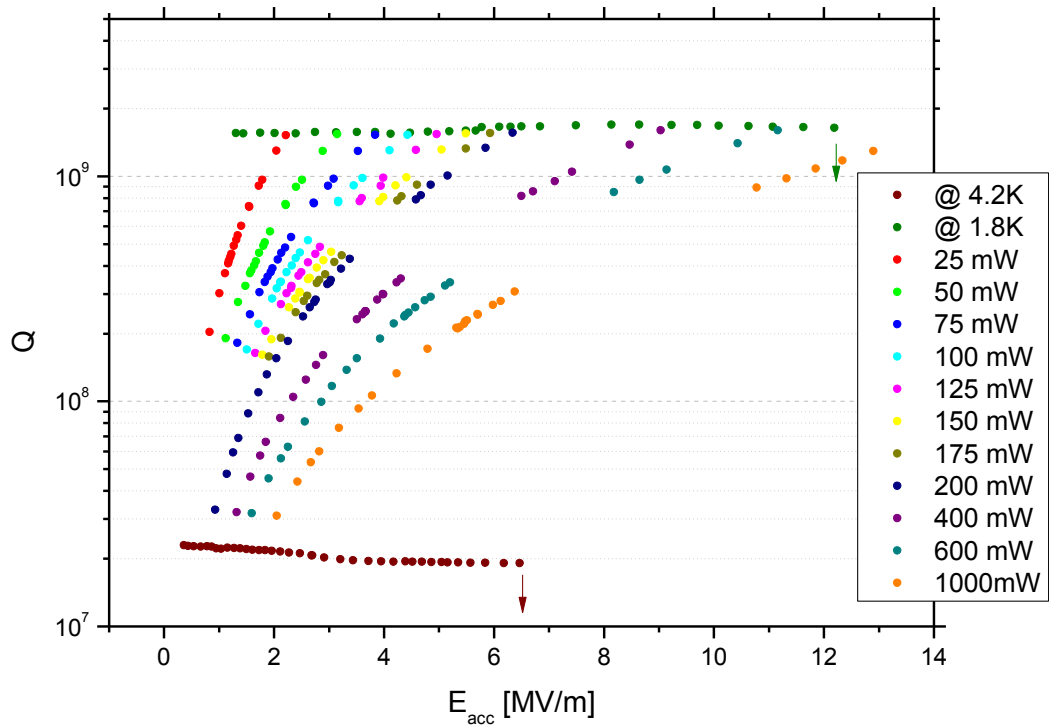


Figure 6.32: RF tests data after annealing is shown. Quality (Q_0) factor vs accelerating field (RF test after UHV annealing of cavity 123) is shown for various power input.

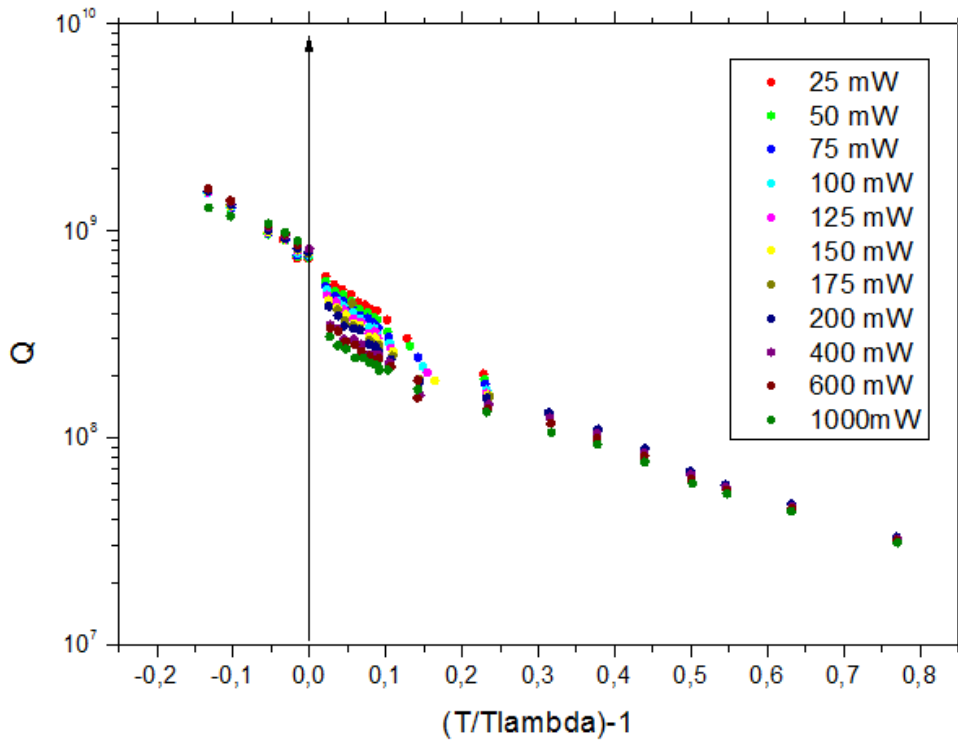


Figure 6.33: RF tests data after annealing is shown. Quality (Q_0) factor vs inverse of T/T_{lamda} temperature (RF test after UHV annealing of cavity 123) is shown.

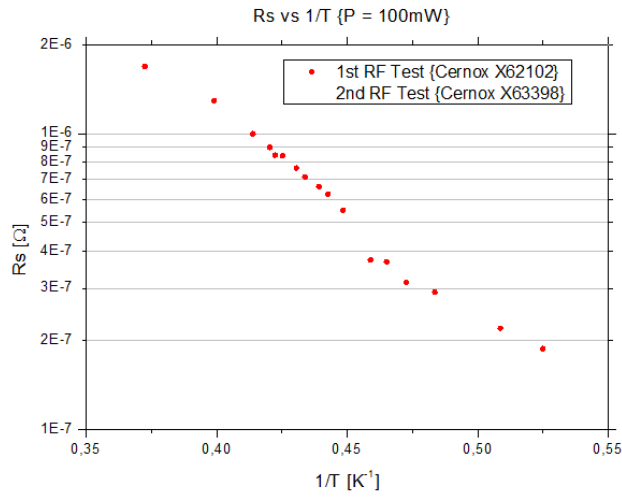


Figure 6.34: Surface resistivity vs inverse of temperature calculated for fixed input power using two thermometers.

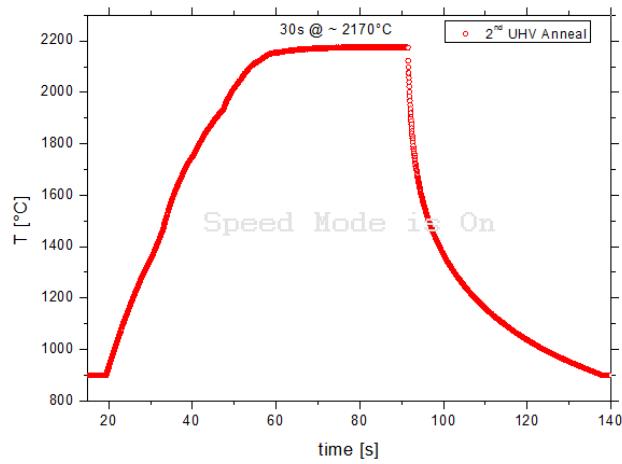


Figure 6.35: 2nd UHV annealing at 2170 C for 30 seconds at maximum temperature. Graph shows temperature vs time.

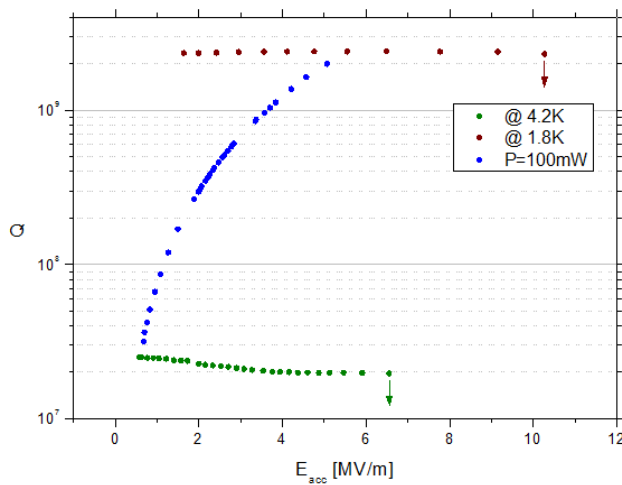


Figure 6.36: 3rd RF tests data after annealing is shown at fixed input power. Quality (Q_0) factor vs accelerating field (RF test after 2nd UHV annealing of cavity 123) is shown.

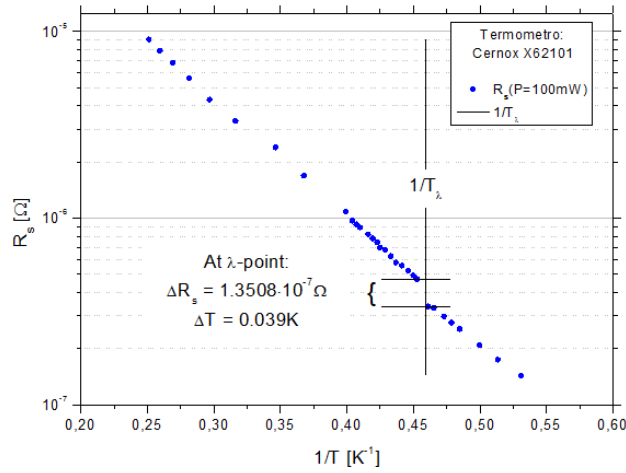


Figure 6.37: Surface resistivity vs inverse of temperature calculated, and theoretically fitted using equation (6.9)

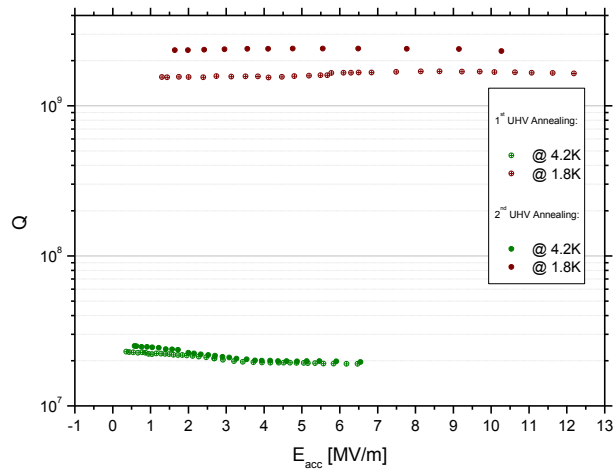


Figure 6.38: A comparison is done for RF tests data after both UHV annealing are shown.

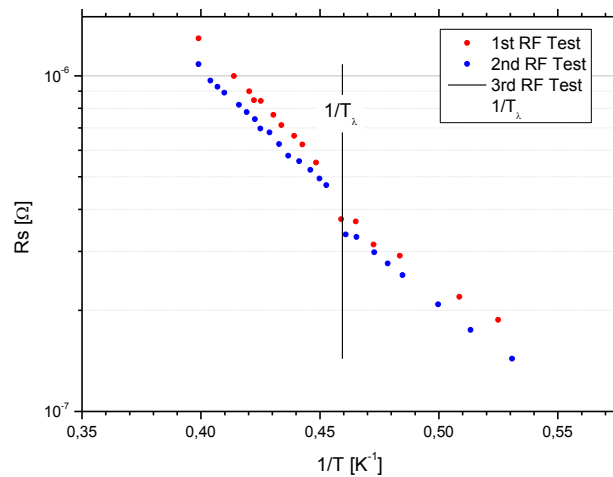


Figure 6.39: A comparison (R_s vs inverse of temperature) is done for RF tests data after both type of annealing is shown.

Nb 124: History

Surf. Treat. procedure	Total wt. lost (g)	Total thickness removed (um)	Total thickness removed (%)	Time	6GHz inner surf. (cm ²)	Remarks
Tumbling(CBP)	3.28	43.49	1.84	60 hrs	88	
Fast BCP	4.173	24.35	2.38	5 min	200	
Flux BCP inner	25.195	334.09	14.74	2.5 hrs	88	

- No rf test has been done prior to annealing, since all cavities shows approximately similar quality factor values.

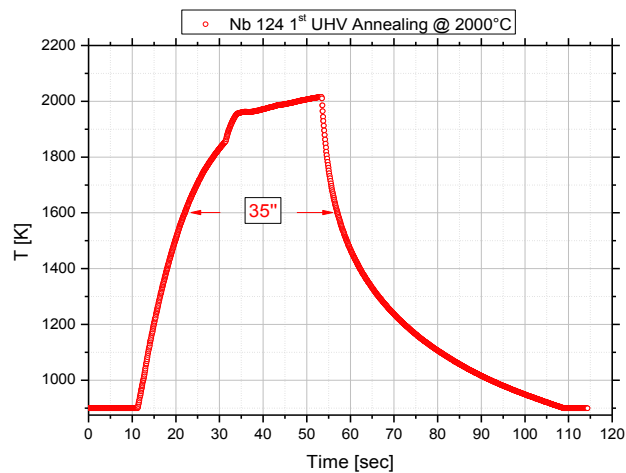


Figure 6.40: 1st UHV annealing at 2000 C for 35 seconds at maximum temperature.

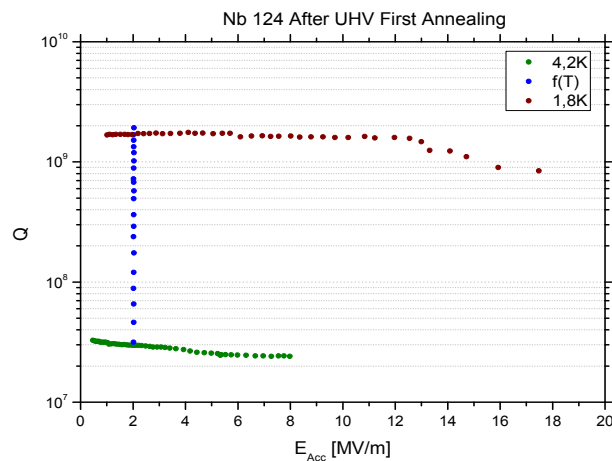


Figure 6.41: RF tests data after annealing is shown. Quality (Q_0) factor vs accelerating field (RF test after 2nd UHV annealing) is shown.

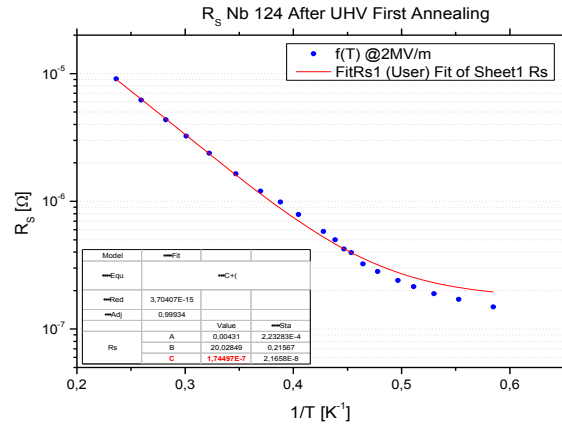


Figure 6.42: Surface resistivity vs inverse of temperature calculated from Fig 6.41, and theoretical fit using equation (6.9)

Nb 126:

Surf. Treat. procedure	Total wt. lost (g)	Total thickness removed (um)	Total thickness removed (%)	Time	6GHz inner surf. (cm ²)	Remarks
Tumbling (CBP+ Vibrator)	2.73	36.20	1.45	56 hrs	88	
Fast BCP	7.134	41.62	3.85	4 min	88	
Flux BCP inner						
Internal EP	8.221	109.01	4.63	5 hrs		
Internal EP	9.179	121.71 (230.72)	5.42	5 hrs		

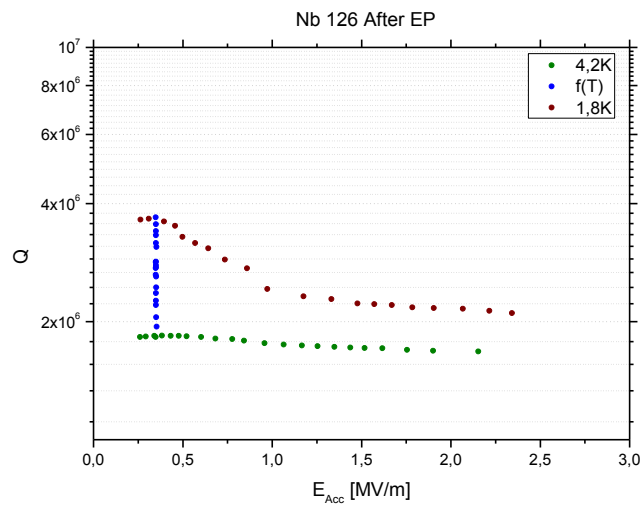


Figure 6.43. RF tests data before and after high temperature annealing at UHV system are shown for one cavity. Quality (Q₀) factor vs accelerating field (RF test **after Flux EP** of cavity 126) is shown.

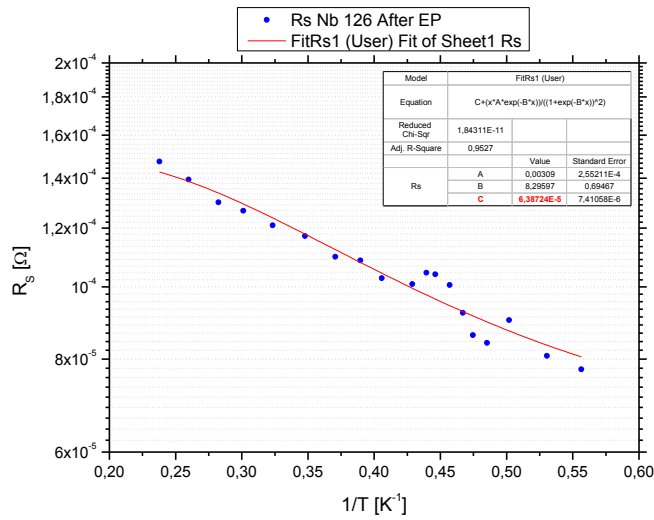


Figure 6.44: Surface resistivity vs inverse of temperature calculated from Fig 6.43, and theoretical fit using equation (6.9)

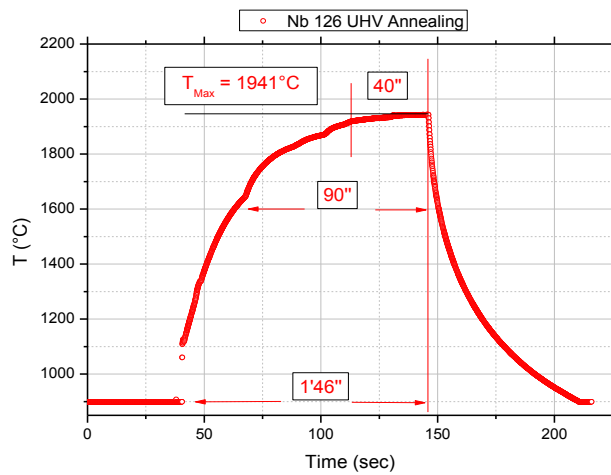


Figure 6.45: UHV annealing at 1941 C for 40 seconds at maximum temperature. Graph shows temperature vs time

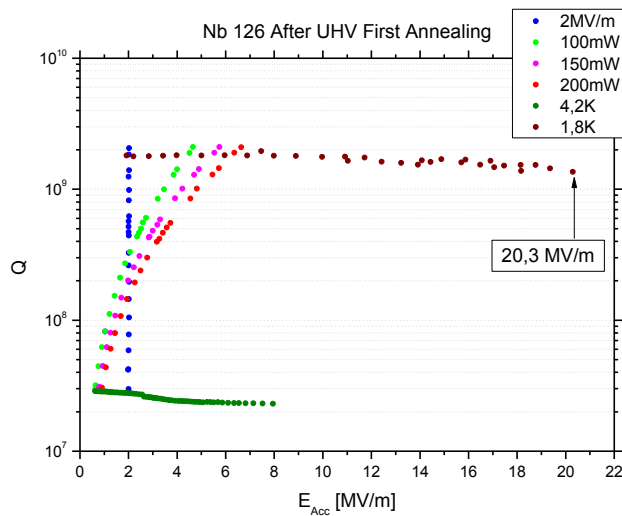


Figure 6.46: RF test data at different fixed power after annealing is shown. Quality (Q_0) factor vs accelerating field (RF test after UHV annealing) is shown.

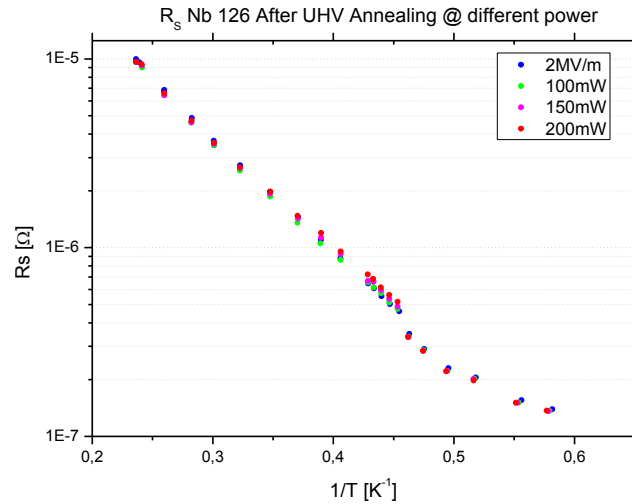


Figure 6.47: Surface resistivity vs inverse of temperature calculated from Fig 6.46. A comparison of surface resistivity at fixed E_{acc} and fixed different power input is illustrated. These data are measured while temperature was decreasing from 4.2-1.8K).

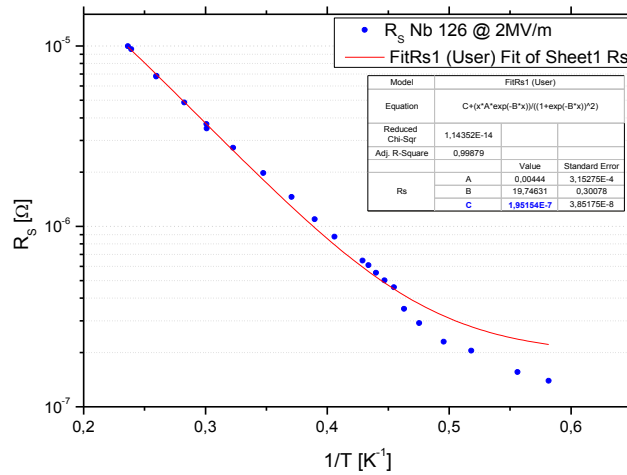


Figure 6.48: Surface resistivity (at fixed $E_{acc}=2$ MV/m) vs inverse of temperature calculated from Fig 6.46, and theoretical fit using equation (6.9) for surface resistivity

Nb 127: History

Surf. Treat. procedure	Total wt. lost (g)	Total thickness removed (um)	Total thickness removed (%)	Time	6GHz inner surf. (cm ²)	Remarks
Tumbling (Vibrator)	10.306	144.284		305 hrs	88	
Fast BCP	3.362	19.61	1.95	5 min	200	
Internal Flux BCP	37.809	501.34	22.33	2.5 hrs	88	

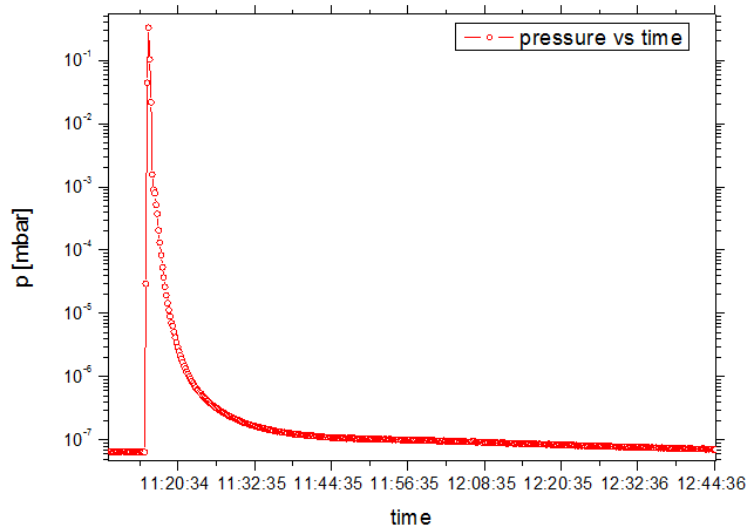


Figure 6.49: Picture illustrates pressure vs time during/after UHV annealing.

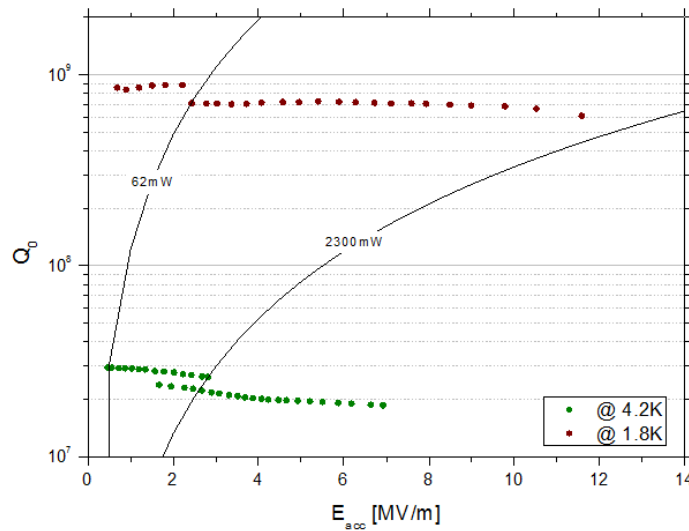


Figure 6.50: RF tests data after annealing is shown. Quality (Q_0) factor vs accelerating field (RF test after UHV annealing) is shown.

Nb 129:

Surf. Treat. procedure	Total wt. lost (g)	Total thickness removed (um)	Total thickness removed (%)	Time	6GHz inner surf. (cm ²)	Remarks
Tumbling (Vibrator)	10.10	141		353 hrs	88	
Fast BCP	11.74	80.65		4 min		
Internal Flux EP	6.79	186.47		2:20 hrs	88	
Internal EP	4.35	119.41	-	1:30 hrs	-	$T_{wt}=22.88$ 387 um

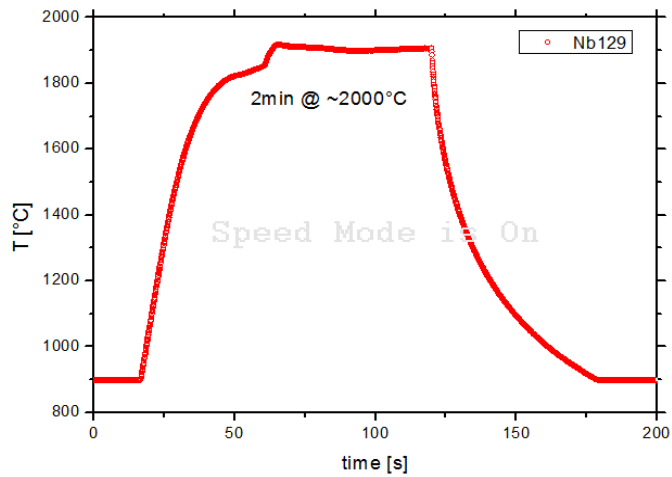


Figure 6.51: UHV annealing at 2000 C for 2 minutes at maximum temperature. Graph shows temperature vs time profile.

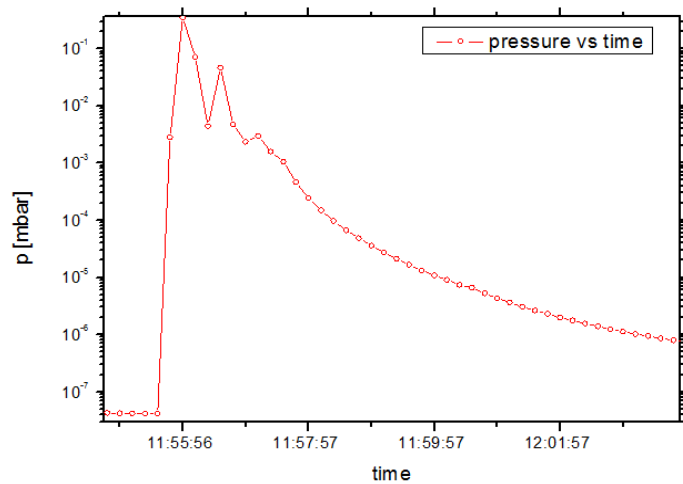


Figure 6.52: In this graphical representation, the thermal process illustrated during UHV annealing. Pressure vs time is shown for one cycle of thermal process.

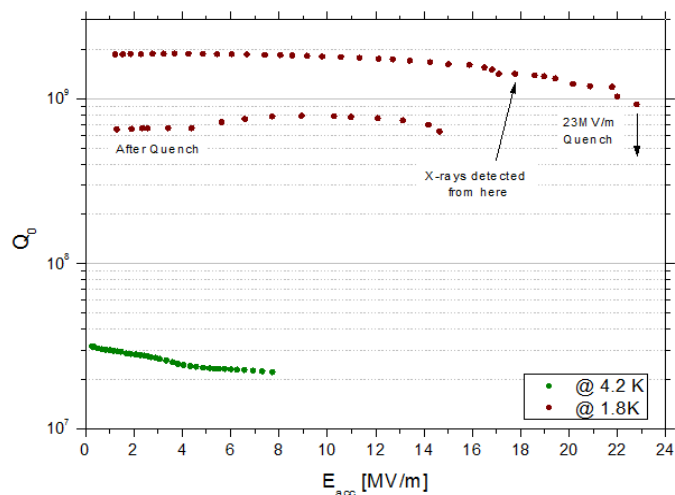


Figure 6.53: RF tests data is shown. Quality (Q_0) factor vs accelerating field (RF test after UHV annealing) is shown. With this cavity we have obtained maximum accelerating field, though x-ray detected during the measurement at high field.

Nb 131:

Surf. Treat. procedure	Total wt. lost (g)	Total thickness removed (um)	Total thickness removed (%)	Time	6GHz inner surf. (cm ²)	Remarks
Tumbling (Vibrator)	10.126	98.53		59.6 hrs	88	
Fast BCP	9.26	66.05		4 min	200	
Internal EP	13.51	185.57			88	
Internal EP	5.09	139.96	-	2 hrs	-	
Internal EP	3.16	86.77		1.5 hrs		

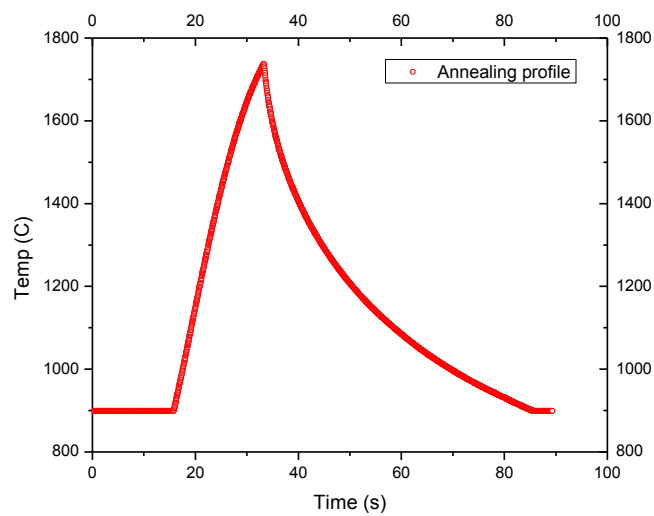


Figure 6.54: Graph shows very short firing duration of cavity. Temperature vs time during UHV annealing is shown.

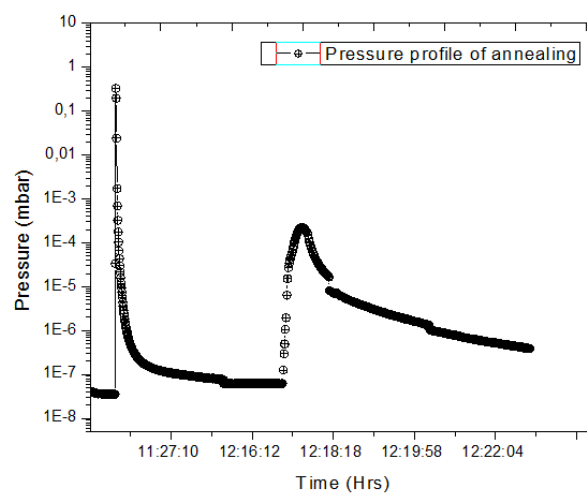


Figure 6.55: Pressure profile vs time is shown for 1st and 2nd cycles of UHV annealing.

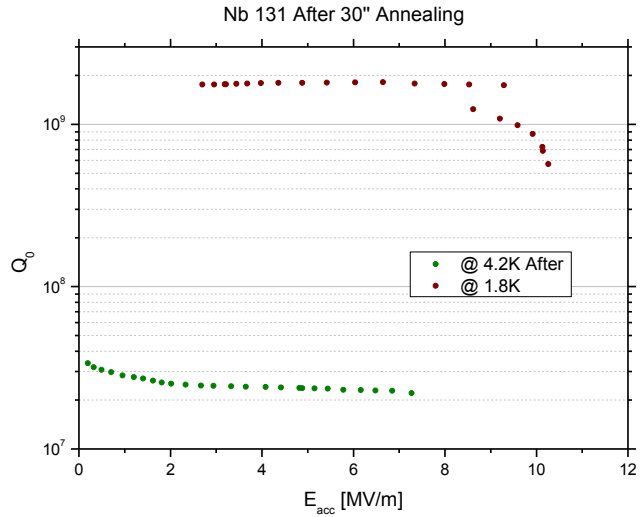


Figure 6.56: RF tests data after annealing is shown. Quality (Q_0) factor vs accelerating field (RF test after UHV annealing) is shown.

Nb 132:

Surf. Treat. procedure	Total wt. lost (g)	Total thickness removed (um)	Total thickness removed (%)	Time	6GHz inner surf. (cm ²)	Remarks
Tumbling (Vibrator)	10.07	141			88	T _{wt} removed 26.21g
Fast BCP	5.76	39.53		6 min	200	
Internal EP	4.05	111.16		2 hrs	88	
Internal EP	6.34	174.11	325+141 um	3:30 hrs	-	

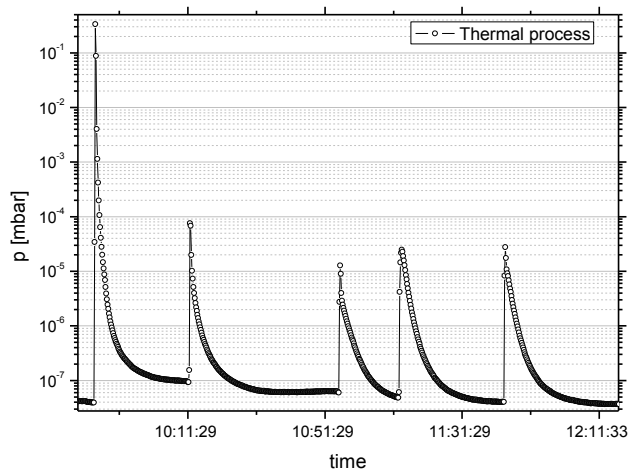


Figure 6.57: Some cycles of thermal process illustrated during UHV annealing. Pressure vs time is shown for 5 different cycles (in 5 peaks) of thermal processes.

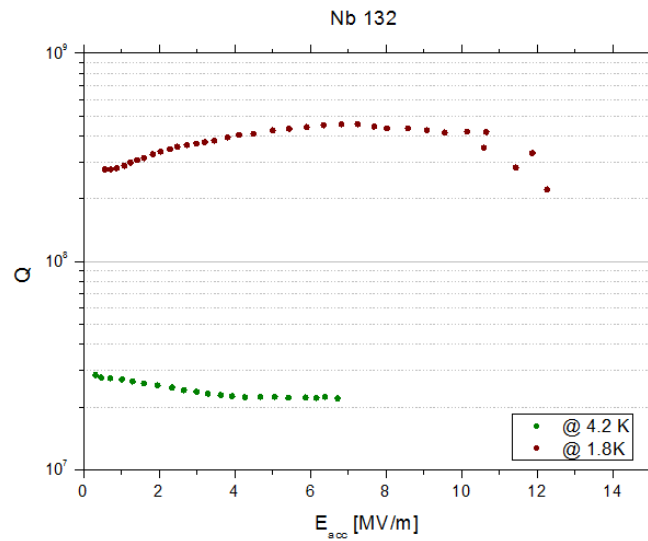


Figure 6.58: RF tests data after annealing is shown. Quality (Q_0) factor vs accelerating field (RF test after UHV annealing) is shown.

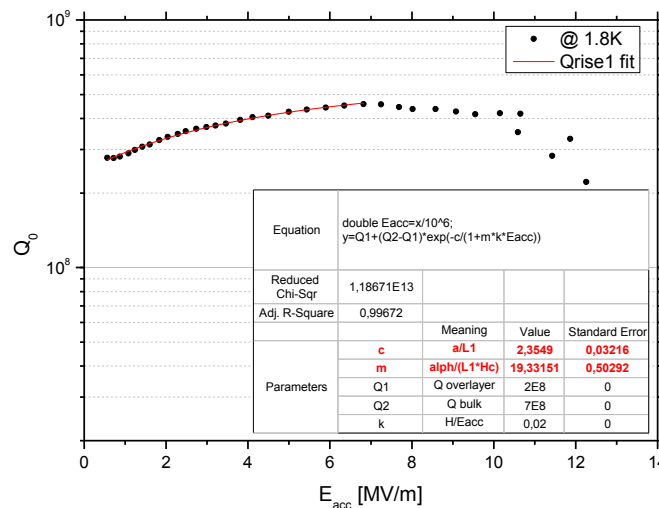


Figure 6.59: RF tests data after annealing is shown. Quality (Q_0) factor vs accelerating field (RF test after UHV annealing) is shown.

6.1.3 Comparison: ATM vs UHV

Atmospheric pressure heating performance: Several seamless mono cell cavities are measured (cavity numbers 122, 125 and 126). RF test have been done to BCPed and electro-polished. The surfaces of BCP treated cavities were very much different, say, rough and fish scale appearance. However, inner surfaces of EP treated cavities were very smooth and mirror like shiny. Naturally, there is a difference in the reaction of BCP chemicals and EP process at different crystal orientations [67]. RF tests were done to three cavities (number 121 BCP treated, 122 and 125 were EP treated) before and after high temperature annealing at atmospheric pressure that has been done inside quartz tube under 4He gas atmosphere.

Table 6.2 Summary of the RF test results before and after atmospheric pressure annealing that have been done inside quartz tube under ⁴He gas atmosphere and UHV annealing are shown in this table.

Cavity Nr.	RF test performance at temperature, T~1.8K								
	After Flux BCP/EP			After Atmospheric pressure annealing and/or annealing at UHV system			After 1 st and 2 nd annealing at UHV system (<i>cavities with only UHV ann.</i>)		
	Q ₀	R _{res} (Ω)	E _{acc} (MV/m)	Q ₀	R _{res} (Ω)	E _{acc} (MV/m)	Q ₀	R _{res} (Ω)	E _{acc} (MV/m)
121(BCP)	5.8*10 ⁶	5.053*10 ⁻⁵	2.8	7*10 ⁸	3.954*10 ⁻⁷	7.7	3.26*10 ⁹ 3*10 ⁹	7.1*10 ⁻⁸ 7.9*10 ⁻⁸	16 15.9
122(EP)	4.8*10 ⁶	5.72*10 ⁻⁵	2.8	2.05*10 ⁸	1.22*10 ⁻⁶	8.55	2.1*10 ⁹ 1.7*10 ⁹	1.07*10 ⁻⁷ 2.18*10 ⁻⁷	12.45 14.8
123(EP)	NA	NA	NA				1.7*10 ⁹ 2*10 ⁹	4*10 ⁻⁷ 8*10 ⁻⁷	12 10
124(BCP)	NA	NA	NA	NA	NA	NA	1.8*10 ⁹	1.74*10 ⁻⁷	17.6
125(EP)	4.4*10 ⁶	5.35*10 ⁻⁵	2.6	7.1*10 ⁸	3.24*10 ⁻⁷	11.7	NA	NA	NA
126(EP)	3.9*10 ⁶	6.38*10 ⁻⁵	2.3	NA	NA	NA	2*10 ⁹	1.95*10 ⁻⁷	20.3
127(BCP)	NA	NA	NA	NA	NA	NA	7*10 ⁸		12
129(EP)	NA	NA	NA	NA	NA	NA	2*10 ⁹		23
131(EP)	NA	NA	NA	NA	NA	NA	1.8*10 ⁹		10
132(EP)	NA	NA	NA	NA	NA	NA	4.5*10 ⁸		12

Summarized surface resistivity that was calculated from measured Quality (Q₀) factor vs inverse of temperature are shown in previous Figures (particularly in Fig.6.30). A Summary of RF test results are given in Table 6.2. Cavity 125 (EP treated) has exhibited best performance in terms of Q₀ vs E_{acc} at 1.8 K among all other cavities that were annealed at atmospheric pressure. After the atmospheric pressure heat treatment the low field Q₀ was increased from 4.4*10⁶ up to 7.1*10⁸ before it quenched. This value of Q₀ is the highest ever measured in an SRF niobium cavity of 6 GHz at 1.8K hence the surface resistivity was calculated 3.24*10⁻⁷Ω using geometrical factors 286 for our cavity. We have achieved Q₀=7.1*10⁸, R_s= 3.24*10⁻⁷ Ω, E_{acc} =11.7 MV/m after huge amount of materials removed by surface treatments (such as, centrifugal tumbling, BCP and EP processes) and high temperature heating at 2100°C for 5 minutes under cover of helium gas at pressure 2 bar. While cavity 122 (EP treated) has exhibited rather poor performance. The Q₀ at low accelerating field begin to drop intriguingly at increased field inside the cavity. That could be seen as a heating of the inner surface due to the tiny spot impurities. Nevertheless, such behaviour is not yet well understood while as all

other seamless large grain Nb cavities that were manufactured from the same material batch have performed well. In this context, we suspect that scratches, impurities or other manufacturing defects are limiting the cavity performance. RF tested BCP and EP treated cavities are compared. From the result, it is clear that the BCP does not smooth out the grain boundaries as well as EP. The average roughness of chemically etched niobium surfaces is in the order of $R_a = 1\mu\text{m}$ [68,69]. The step height on etched surfaces at grain boundaries can be even in the order of a few μm . The roughness on the EP surface is typically one order of magnitude lower than that of an etched sample on length scales larger than $10\mu\text{m}$. The performances after electropolishing show that the average gradient of the batch of electropolished cavities is about 8-12 MV/m. Therefore, it is very clear that electropolishing leads to higher gradients. The smoother surface offers less defects and is easier to clean from chemical residues as it is discussed in chapter 3.

UHV heating performance: The long-term stability of superconducting cavities in particle accelerators is an important issue. In the next step the cavity was heated (IH) in a high vacuum condition above 2000°C to remove the hydrogen and other contaminations, impurities from the bulk material. The cavity is also tested after fast cool-down and showed a normal residual resistance. After keeping the cavity at 100 K for several hours, no change in the behaviour was observed. This indicates that Q-disease was cured by the high temperature treatment. After the heat treatment at 2000°C , the average high field behaviour was improved during the treatment. The results of several cavities before and after the heat treatment above 2000°C are shown.

However, UHV heat treated cavities produced higher accelerating field. Particular cavity 129 showed best performance. It is EP treated, and IH has been done at UHV system for 2 minutes. It showed highest accelerating field, $\geq 22\text{ MV/m}$ with Quality factor of $\approx 2 \times 10^9$ among all measured cavities, though X-ray was detected after 18 MV/m. It is shown in Figure 6.53. The average gradient is 8-12 MV/m before and 18-23 MV/m after the induction heat treatment at UHV system. With the discovery of the high temperature effect, there is some concern that a long exposure of the surface to air might destroy the effect of the high temperature effect. The suspicion was that the benefit of heating either comes from the desorption of water from the surface or the reduction of oxides on the surface. An electropolished cavity was baked out in UHV chamber for 60 hrs at 140°C . The rf test has been done and gradients are plotted. After the test the cavity was exposed to clean air for some time intervals. Before the measurement HPR has been done to avoid a particle contamination. Within the rf measurement errors no significant change in the cavity behaviour was observed even after exposure to air for a month. Hence, further work on surface treatment at large scale is required to understand the material behaviour and to improve the efficiency of cavity in terms of quality factor and accelerating field measurements at low temperature.

6.2 Conclusion

Considering the application of SRF resonators for particle accelerators, the accelerating field level inside the resonators should be as high as possible in order to most efficiently accelerate the beam passing through it. The Quality (Q_o) Factor value tends to degrade as the fields increase, which is shown in several curve of Q_o vs E_{acc} curve. Ideally, the cavity Q_o would remain constant as the accelerating field is increased up to the point of a magnetic quench field (H_{c2}), but in reality, is quenching before due to impurities, and a rough surface finish etc. [70]. While Hydrogen contamination leads to lower Quality (Q_o) values.

Mostly, we have measured two different R_s curves for the same cavity. One is at constant power input (i.e., 100 mW or other values mentioned in respective graph) while other is at constant field (i.e., 0.7 or 2MV/m or other values mentioned in respective graph). It was

difficult to measure at low constant field while approaching at low temperatures. Since very low power input corresponds to high field gradient if the cavity has high performance, i.e., high Q value and hence very low R_s .

A model of an atmospheric pressure purification technique of 6GHz cavities along with different surface treatment processes have been explained systematically. Several cavities were purified to corroborate this technique. It was found that the defect less and pure Nb Bulk cavity RF measurement shows high Q value at low accelerating field. At low temperature, ie, 1.8K, RF test confirmed that the cavities obtained after the different surface treatment procedure especially under atmospheric pressure annealing above 2000°C for few minutes, Quality (Q_o) factor values up to three orders of magnitude have been improved. Summarizing residual surface resistivity, for cavity no 121, about $50\mu\Omega$ has been measured before thermal treatment which reduced up to $325n\Omega$ at 1.8K after the high temperature heat treatment. Results of purification technique are one of the most promising for the cavities of high performance that could be used for the investigations in particle accelerators. However, UHV heat treated cavities produced higher accelerating field. Particular cavity 129 showed highest accelerating field, ≥ 23 MV/m with Quality factor of $\approx 2 \times 10^9$, and surface resistivity reduced up to $70n\Omega$ at 1.8K after the high temperature heat treatment among all measured cavities, though X-ray was detected after 18 MV/m. It is shown in Figure 6.53. It is worth mentioning that testing a SRF cavity is a very much complex process. A well characterized system requires for rf testing. A large component of this system is the power cables. Before each test, calibration (internal-external at room and cryogenic temperatures) of the power cables must be done. Incorrect calibration will give the wrong quality factor and accelerating gradient data. Another component of the testing system is the cryo-system itself. Sometimes, during the cavity test, cryo-system instabilities occurred. Due to this, the resulting graphs for the quality factor vs accelerating gradient were different from expected. The reason for this is that different pressures correspond to different temperatures. Since the pressure increased from the desired ~ 15 mbar ($\sim 1.78K$), the surface resistance of the cavity increased and the quality factor therefore decreased. The quality factor data graph might have been better If the pressure remained constant. Nevertheless, further work at large scale is required to understand the material behaviour and to improve the efficiency of cavity in terms of achieving higher accelerating field and lowest surface resistivity at $\sim 1.6K$.

-----*****-----

Chapter 7

Summary and Future outlook

The ultimate goal for an ideal accelerating cavities are achieving very high quality factor value hence lowest possible surface resistivity and higher accelerating field. These two are the paramount considerations in Accelerator technology. Therefore, further improvement in the surface treatments of superconducting cavities are required. In this frame work, two techniques have been discovered, Mechanical polishing and atmospheric pressure annealing at high temperature. A new technique for mechanical polishing using vibrator, and another new technique for purification by means of high temperature treatment of SRF cavities have been developed in order to optimize RF resonators for accelerator technology. Purification has been accomplished either under cover of He or Ar gas (inert gas) atmosphere for protection of inner and outer surface of cavity, and also under UHV system. These are the most important achievements of the research work reported in this dissertation.

Mechanical polishing performance: Several Nb, Cu and Fe seamless cavities have been studied with different parameters to achieve best tumbling result so far. Series of tumbling process to successive removal of inner materials of cavities using two different mechanical polishing techniques, CBP and vibrator have been done. However, mechanical finishing is going on for several Nb, Cu cavities. Before starting tumbling an inner surface picture has been taken to compare surface smoothness after final set of tumbling. The primary goal is to remove about 10 grams of inner materials (polish inner surface) using vibrator. Cavities are cleaned and optically inspected inner surface prior to mechanical polishing, and after removing 10 grams again optically inspected to ensure best soomthness of inner surface. It is learnt that inner surface is defect less, all manufacturing scratches, mandrel lines, surface roughness and most probable contaminations are removed. Hence, provides very smooth inner surface. One cavity has been omitted from the statistics, because the cavity has been broken during the mechanical treatment, just before the final cycle. However, mechanical treatment of this cavity was almost finished, about 9 grams of inner materials was removed, only one grame was left to reach the goal. The cavity was broken from the neck-flange though the optical inspection showed very smooth inner surface.

Previously CBP has been used for mechanical finishing of cavities, which is heavy, expensive and dangerous as well. So the CBP has been substituted by Vibrator-tumbling technique. In this technique, all required process steps need not more than a week per cavity. Hence, this technique is simple, cost effective and fast. Results obtained from vibrator indicate that this technique has considerable improvement to increase removal rate of defected inner materials and contaminations of the cavity hence reduces the chemical process.

(Electro-)chemical performance: After etching and electropolishing (before heat treatment) shows that the average gradient of the batch of electropolished cavities are between 8-12 MV/m, and 18-23 MV/m after the Induction heat treatment. Therefore it is well understood that electropolishing leads to higher gradients. The smoother surface offers less defects and is easier to clean from chemical residues. Moreover, by comparing BCP and EP treated niobium cavities, it is concluded that the BCP does not smooth out the grain boundaries as well as EP. The average roughness of chemically etched niobium surfaces is in the order of $R_a = 1\mu\text{m}$ [98]. The step height on etched surfaces at grain boundaries can be even in the order of a few μm . It is well-known that surface roughness can lead to an geometric field enhancement and therefore

to a local breakdown of superconductivity at lower field [99]. The roughness on the EP surface is typically one order of magnitude lower than that of an etched sample on length scales larger than 10 μm . The main difference between EP and etching is the smoothing of the grain boundaries. An important question for electropolishing is of course how much material has to be removed to achieve a smooth surface. In EP treated sample (removes 150 μm of inner material) the total roughness drops below 1 μm .

Induction heating performance: In the next step the cavity was heated (IH) at atmospheric pressure inside quartz tube and also in a high vacuum condition above 2000°C to remove the hydrogen and other contaminations, impurities from the bulk material. A short HPR of about 10 minutes has been done to clean the surface from dirt which might have been introduced during the furnace treatment and handling. Again the cavity is tested after fast cooldown and showed a normal residual resistance. After the heat treatment at 2000°C, the average high field behaviour was improved during the treatment. The average gradient is 08-12 MV/m before and 18-23 MV/m after the Induction heat treatment.

A model of an atmospheric pressure purification technique of 6GHz Nb and Cu cavities along with different surface treatment processes have been studied systematically. Several cavities were purified to corroborate this technique. It was found that the defect less and pure Nb Bulk cavity RF measurement shows high Q value at low accelerating field. At low temperature, ie, 1.8K, RF test confirmed that the cavities obtained after the different surface treatment procedure especially under atmospheric pressure annealing above 2000°C for few minutes, Quality (Q_0) factor values up to three orders of magnitude have been improved. Summarizing residual surface resistivity, for cavity no 121, about 50 $\mu\Omega$ has been measured before thermal treatment which reduced up to 325n Ω after the heat treatment at 1.8K.

The excitation curves of the electropolished cavities exhibit a strong degradation in quality factor at high field. Field emission (in few cavities) and quench are observed. For most of measurements, no signs of X-rays were detected and also the electron pick-up antennas did not show signals. Also, multipacting, thermal breakdown like phenomena did not observed during the measurement of 6GHz cavities.,

The behaviour at low surface fields (below 10 MV/m) of niobium cavities after chemistry can be understood with a reduction of the dielectric oxide layer due to the diffusion of oxygen into a surface layer of 200 - 300 nm. The increased impurity content of this layer reduces the mean free path of the electrons thus reducing the BCS surface resistance. The oxygen diffusion also can explain slight a increase in the residual resistance. The high field behaviour is not yet fully understood. Several models have been proposed so far to describe the degradation of the quality factor. A more detailed analysis (X-ray) of the niobium surface is needed. Also, cavity measurements on anodized cavities open the possibility to investigate the behaviour of niobium surface which is heavily loaded with oxygen. The thickness of the Nb₂O₅ layer is well defined by the applied voltage. Baking of such a cavity would not lead to a complete dissolution of the dielectric Nb₂O₅, so that it should be possible to distinguish whether the Nb₂O₅ layer has an effect on the high field behaviour or not. So far some measurements have been done at LNL with out a big success, though the resaerch is going on and hopefully some good result will revel few unknown phenomena. Also, by eliminating many disturbing effects like field emission of electrons or magnetic field enhancement due to the surface roughness, electropolishing combined with the precise clean-room handling might allow to drive SRF cavities close to the physical limit of the superconductor.

RF results from all set of cavities indicate that atmospheric pressure technique has considerable improvement to increase cavity quality factor and hence reduce the surface resistance. The Quality (Q_0) Factor value tends to degrade as the fields increase. Ideally, the cavity Q_0 would remain constant as the accelerating field is increased up to the point of a

magnetic quench field (H_{c2}), but in reality, is quenching before due to impurities, and a rough surface finish etc [70]. While Hydrogen contamination leads to lower Quality values. Results of purification technique are one of the most promising for the cavities of high performance that could be used for the investigations in particle accelerators. Nevertheless, how to improve accelerating field while maintaining constant high Q_0 would be the focus of further research.

All required process steps for surface treatments and materials investigation for mechanical polishing, (electro-) chemical processes, and thermal treatment need not more than a month. Such a UHV absent technique is simple, cost effective and fast. Therefore, the main advantages of using 6 GHz bulk-Nb cavities are saving time, cost, and materials. One can fabricate 4-6 cavities out of the rest Nb sheet material which was used to prepare 1 big cavity. And collecting statistics of treatments like mechanical tumbling, chemical, electro-chemical process, heat treatment, and RF test in simple way and in short time. A big cavity, about one meter long requires several months to collect same experimental statistics. So, what we developed 6 GHz bulk-Nb cavity that after all the above mentioned treatments in a week like such a short time duration we get about 3 order of magnitude improvement in terms of Q-factor, and hence reduction of surface resistivity.

Future Outlook

Fundamental properties of NbN, NbC and Nb₃Sn are on further investigation in to seamless Nb cavity which are either thermally diffused or mechanically tumbled. The idea is to create layers of Nitrides, Carbides and Tin on inner surface of Nb cavity. Thermally diffused NbN where thickness of nitride depends on Nitrogen pressure, temperature and nitration time. In Nb₃Sn (powder & pieces are tumbled several hours to create layer) the Sn layer thickness depends on tumbling mechanism, such as tumbling duration and Sn powder and pieces. These transition metals (Nitrides and Carbides) have critical temperatures higher than Niobium. Altogether, layers of Nitrides, Carbides and Tin on inner surface of Nb cavity under certain process allow increasing Q-value up to several factors. All these investigation need careful attention and investigation.

-----*****-----

References

1. R. Russenschuck, G. Vandoni. "Superconductivity and Cryogenics for accelerators and detectors". CERN Accelerator School. (2004)
2. V. Palmieri, Seamless cavities: the most creative topic in RF superconductivity, Proceedings of the 8th workshop on RF superconductivity (1997), vol. 3, P.553
3. J.M.Pierce et al., In Proceedings of the 9th Inter Conf on Low Temp. Physics, Vol.A. Plenum, New York, p.36 (1965)
4. H. Kamerlingh Onnes, "Communications from the Physical Laboratory at the University of Leiden by Prof. Dr. H. Kamerlingh Onnes", 108, 1908.
5. H. Kamerlingh Onnes, "Communications from the Physical Laboratory at the University of Leiden by Prof. Dr. H. Kamerlingh Onnes", 124c, 1911. H. Kamerlingh Onnes, "Communications from the Physical Laboratory at the University of Leiden by Prof. Dr. H. Kamerlingh Onnes", 119, 1908.
6. W. Meissner and R.Ochsenfeld, "Ein neuer Effekt bei Eintritt der Supraleitfähigkeit", Naturwiss.,21, 787, 1933.
7. C.J.Gorter and H.Casimir,"Zur Thermodynamik des supraleitenden Zustandes", Zeitschr.f.techn.Physik, 15, 539, 1934.
8. J. Bardeen, L. Cooper, J. R. Schrieffer, Theory of superconductivity, Physical Review 108 (1957) 1175.
9. French, R.A., Cryogenics 8, 301, 1968.
10. Alekseevskii, N.E. et al., Phys. Met. Metallogr. USSR, 37, 53, 1974.
11. H. Padamsee, J. Knobloch, T. Hays, RF Superconductivity for Accelerators, John Wiley and Sons, 1998.
12. A. Pippard, Proc . Roy. Soc A203 (1953) 98.
13. J. Waldram, Surface Impedance of Superconductors, Adv. Phys. 13.
14. D.C. Mattis, J. Bardeen, Phys. Rev. 111, 412 (1958)
15. I. Ben-Zvi and J.M. Brennan, "The quarter wave resonator", Nucl. Inst. and Meth. 212 p. 73, 1983
16. W. Singer, A. Brinkmann, D. Proch, and X. Singer, Quality requirements and control of high purity niobium for superconducting RF cavities, Physica C 386, 379 (2003)
17. Saito K and Kneisel P 1992 Proc. 3rd EPAC (Berlin) vol 2 (Gif-sur-Yvette: Editions Frontieres) p 1231
18. B. Aune et al., "Superconducting TESLA cavities", Phys. Rev. ST Accel. Beams 3, 092001 (2000). A thorough presentation of the many aspects of an SRF cavity
19. Yogi T, Dick G J and Mercereau J E 1977 Phys. Rev. Lett. 39 826
20. Klein U and Proch D 1979 Proc. Conf. Future Possibilities for Electron Accelerators (Charlottesville, VA) ed. J S McCarthy and R R Whitney N1-N17
21. K. Schulze, The metallurgical society of AIME, 1981, P.163
22. Gladun et al, Journal of Low Temperature Physics, 27 (1977) P873].
23. W. Meissner and H. Franz, Messungen mit Hilfe von flüssigen Helium. VIII.Supraleitfähigkeit von Niobium, Physikalisch-Technische Reichsanstalt, Mitteilung: 558-559, 1930.
24. A. Inoue et al., J. Phys., Colloque-8. 41, 758, 1980.
25. V. Novotny et al., J. Low Temp. Phys. 18, 147, 1975.
26. W. Meissner and R.Ochsenfeld, "Ein neuer Effekt bei Eintritt der Supraleitfähigkeit", Naturwiss.,21, 787, 1933.
27. Bednorz J G and Mueller K A 1986 Z. Phys B 64 189
28. Weingarten W 1996 Particle Accelerators 53/54 199–215

29. Hein A M 1996 Particle Accelerators 53/54 135
30. The Fourth International Workshop on Thin Films and New Ideas for Pushing the Limits of RF Superconductivity, Padua, Italy, (2010)
31. Kneisel P and Lewis B 1996 Particle Accelerators. 53 97–121,
D. Proch, W. Singer, and H. M. Wen, Some Results about RRR Distribution in Nb of Superconducting Cavities for the TESLA Test Facility, TESLA Report TESLA 98-02, DESY, 1998.
32. Singer W, Proch D and Brinkmann A 1997 Proc. 8th SRF Workshop on Particle Accelerators
33. A. Dacca, G. Gemme, L. Mattera, and R. Parodi, XPS analysis of the surface composition of niobium for superconducting RF cavities, Appl. Surf. Sci., 126:219 , 1998.
34. Gmelin, Handbuch der anorganischen Chemie, volume 49(Nb), Springer Verlag Berlin, 1970. 34
35. J. Guerin, Etude du bain de polissage chimique de niobium, Technical Report TE/LC/157/89, CERN, October 1989. 34
36. B. Hillenbrand, N. Krause, K. Schmitzke, and Y. Uzel, Abschlussbericht- Supraleitende Resonatoren, Technical Report NT 20247, Siemens AG, Dezember 1982, BMBF Forschungsbericht.
37. R. Russenschuck, G. Vandoni. "Superconductivity and Cryogenics for accelerators and detectors". CERN Accelerator School. (2004).
38. S. Turner. "Superconductivity in Particles Accelerators". CERN Accelerator School. (1996).
39. B. Hillenbrand, N. Krause, K. Schmitzke, and Y. Uzel, Abschlussbericht- Supraleitende Resonatoren, Technical Report NT 20247, Siemens AG, Dezember 1982, BMBF Forschungsbericht
40. H. Padamsee, Cornell University, (Private communication), 2013
41. H. Diepers, O. Schmidt, H. Martens, and F. Sun, A new method of electropolishing niobium, Physics Letters, 37A:139, 1971. 36, 42
42. K. Saito et al., Electropolishing of L-Band cavities, In Proceedings of the 4th Workshop on RF Superconductivity [Kojima 1990], pp. 635– 695, KEK Report 89-21. 36, 42, 60
43. P. Kneisel, R. Roth, and H.-G. Kurschner, Results from a nearly "Defect-Free" Niobium Cavity, In Proceedings of the 7th Workshop on RF Superconductivity [1995]. 33, 35, 85
44. L. Ponto and M. Hein, Elektropolitur von Niob, Technical Report WUP 86-17, Bergische Universität at Wuppertal, 1986. 35, 37
45. A. Citron, G. Dammertz, M. Grundner, L. Husson, R. Lehm, and H. Lengeler, The Karlsruhe-CERN superconducting RF separator, Nucl. Inst. Meth., 164:31 , 1979. 36, 37
46. B. Aune et al., "Superconducting TESLA cavities", Phys. Rev. ST Accel. Beams 3, 092001 (2000).
47. E. Kako et al., Improvement Of Cavity Performance In The Saclay/Cornell/Desy's Sc Cavities, In Proceedings of the 9th Workshop on RF Superconductivity [Krawczyk 1999], TUP011. 33, 38,63, 65
48. L. Ponto and M. Hein, Elektropolitur von Niob, Technical Report, WUP 86-17, Bergische Universität at Wuppertal, 1986. 35, 37
49. F. Stivanello, INFN/LNL, EP samples, Private communication, 2013
50. W. Meissner and B. Voigt, Ann. Phys. Leipzig, 7, 892 (1930)
51. H. H. Potter, Proc. Phys. Soc. (London) 53, 695 (1941)

52. G.K White and S.B. Woods, Phil. Trans. Royal Society of London Ser. A251, 273 (1959)
53. G. W. Webb, B.T. Matthias, Science 155, 191 (1967),
54. G.W. Webb, Bull. Of Am. Phys. Soc. 12, 519 (1967); G.W Webb, Phys. Rev. 181, 3, 1127-1135 (1969)
55. G.W. Webb, Solid State Communication. 6, 33 (1968)
56. D.K. Finnemore, F.T. Stromberg, and C.A. Swenson, Phys. Rev.149, 231 (1966)
57. H. Suhl, B. T. Matthias, and L. R. Walker, Phys. Rev. Letters 3, 552 (1953)
58. L. Y.L. Shen, N. M. Senozan, and N. E. Phillips, Phys. Rev. Letters 14, 1025 (1965).
59. J. Bardeen, G. Rickayzen and L. Tewordt, Phys. Rev., 113(4) (1959) 982.
60. Good-Sun Choi, Jae-Won Lim, N. R. Munirathnam, Il-Ho Kim, Purification of niobium by multiple electron beam melting for superconducting RF cavities, Metals and Materials International, June 2009, Vol. 15, Issue 3, pp 385-390
61. Alfred Koethe and Jens Ingolf Moench, Preparation of ultra-high purity Niobium, Materials Transactions, JIM, Vol.41, No.1, 7-16 (2000)
62. Hernane R. Salles Moura and Lourenço de Moura, Melting And Purification Of Niobium, AIP Conf. Proc. 927, 165 (2007); doi: 10.1063/1.2770689
63. M Hörmann, Production of high thermal conductivity niobium on a technical scale for high-frequency superconductivity, Journal of the Less-Common Metals, Volume 139, Issue 1, (1988), Pages 1–14. [http://dx.doi.org/10.1016/0022-5088\(88\)90324-4](http://dx.doi.org/10.1016/0022-5088(88)90324-4)
64. H. Padamsee, IEEE Trans. Magn., Z (2) (1985) 1007. P. Kneisel, Use of the titanium solid state gettering process for the improvement of the performance of superconducting r.f. cavities, J. Less-Common Metals, 139 (1988) 179.
65. H. Safa, D. Moffat, B. Bonin, F. Koechlin, Advances in the purification of Nb by solid state gettering with Ti, J. Alloys and Compounds 232 (1996) 281–288.
66. W. Singer, A. Brinkmann, D. Proch, and X. Singer, Quality requirements and control of high purity niobium for superconducting RF cavities, *Physica C* **386**, 379 (2003)
67. D. Baars et al., “Crystal orientation effects during fabrication of single or multi-crystal Nb SRF cavities”, SRF07, Beijing, October 2007, TH102. <Http://www.pku.edu.cn/academic/srf2007/proceeding.html>
68. C. Z. Antoine et al., Alternative Approaches for Surface treatment of Nb superconducting cavities, In Proceedings of the 9th Workshop on RF Superconductivity, Krawcyk 1999. 35, 38, 40
- 69 M. Kl'aui and L. Lilje, Surface roughness of niobium for different surface treatments, 2001. 39, 40
- 70 Wilfried Rockenbauer, “Production of Niobium Metal and Compounds from Tantalite” in Niobium - Proceedings of the International Symposium, ed. by H. Stuart (Warrendale,PA, The Metallurgical Society of AIME, 1984), 133-152.

-----*****-----

Acronyms

BCP- Buffered chemical polishing
Cu- Copper
DI water- Di ionized water
 E_{acc} - Accelerating electric field
EP- Electro-polished
FG - Function generator
FLASH - Free Electron Laser in Hamburg
HF- Hydrofluoric acid
 HNO_3 - Nitric acid
 H_3PO_4 - Phosphoric Acid
 H_2SO_4 - Sulphuric Acid
HPR - High Pressure Rinsing
IH- Induction heating
ILC - International Linear Collider,
LCR - An electrical circuit consisting of an inductor (L),
a capacitor (C), and a resistor (R)
LHC - Large Hadron Collider
MI- Magnetic induction
Nb- Niobium
NC - Normal Conducting
 O_2 -Oxygen
OFHC- Oxygen free high conducting copper
PLL- Phase-locked loop
PZT - A Piezoelectric material, which contains lead zirconium titanate
 Q_L - Loaded quality factor
 Q_0 - Unloaded quality factor
RRR - Residual Resistivity Ratio
SRF- Superconducting Radio-Frequency
SSG - Solid state gettering
SiC -Silicon Carbide
SASE - Self amplified spontaneous emission
SC - Superconducting

TCE - Temperature coefficient of expansion,
TESLA - Tera-eV Superconducting Linear Accelerator,
TTF - TESLA Test Facility,
UHP- Ultra high pure
UHV- Ultra-High Vacuum
 V_{acc} - Accelerating voltage
VUV-FEL - Vacuum Ultra-Violet Free Electron Laser,
X-FEL - X-Ray Free Electron Laser,
ZrO₂-Y - Ytria stabilized Zirconium oxide

Acknowledgements

I extend thanks to Prof V. Palmieri for introducing this research field, and being supportive with constructive comments in context of superconductivity and surface treatments activities. Working with Antonio A. Rossi is a fun...stress less and much pleasant experience...many thanks for helpful discussion and constructing comments. S. Stark for helpful discussions. F. Stivanello for (electro-) chemical polishing of all cavities, untiring support and valuable suggestions.

I would like to thank the entire superconductivity-team. Working with enthusiastic team is a pleasant experience, energetic and memorable forever! In particular, I thank G.Kopple, C. Pira, Oscar and S. Martin alongwith all master students for priving general support throughout.